

**Deposition and Characterization of AlN and GaN Thin Films by
Plasma-Enhanced Atomic Layer Deposition**

by

Pooyan Motamedi

A thesis submitted in partial fulfillment of the requirements for the degree of

Doctor of Philosophy
in
Materials Engineering

Department of Chemical and Materials Engineering
University of Alberta

© Pooyan Motamedi, 2015

Abstract

III-nitride semiconductors have a combination of structural characteristics and engineering properties that give them a unique place among semiconductors. The fact that they have the same crystal structure makes it possible to deposit alloys with fine-tuned band gaps from infrared to ultraviolet wavelengths. Such alloys have applications in general lighting, UV detectors, and laser diodes. In addition, piezoelectric sensors and actuators are an attractive area of application for AlN. GaN has a high breakdown field and carrier mobility, which make it a promising choice for high power/high frequency applications.

While metal-organic chemical vapor deposition and reactive sputtering have been successfully used for deposition of micron-thick III-N films, they are not suitable for deposition on high aspect ratio surface features, or when thickness control at the atomic level is required. Atomic layer deposition (ALD) offers the perfect solution for such applications. Plasma-enhanced ALD makes it possible to deposit crystalline films at lower temperatures. Employing this method for deposition of crystalline AlN and GaN thin films at low temperatures is the subject of this thesis.

AlN and GaN films were deposited on various substrates using nitrogen plasma and metal-organic precursors. Comprehensive experiments were carried out to optimize the deposition parameters. Both AlN and GaN films were found to be structurally comparable to the films deposited at much higher temperatures using conventional methods. GaN films deposited on sapphire have the desirable (001) preferential

orientation, high mass density, high electron mobility, and optical properties close to the bulk values.

In addition to deposition of AlN and GaN, several interesting phenomena were observed and investigated to varying degrees, in light of the available means. Substrate temperature was found to have a profound role in determination of the structure and properties of GaN films. A likely change in the growth mechanism was observed at higher growth temperatures. It was found that the growth of GaN starts epitaxially, but a shift to the three-dimensional growth occurs afterwards. In-situ ellipsometry was employed to investigate the evolution of optical properties of the films during growth, and the results are in good agreement with structural observations.

Preface

This thesis is based on an original research project by Pouyan Motamedi. The document has been prepared according to “Thesis Requirement and Preparation” guideline, published by University of Alberta Faculty of Graduate Studies and Research, under the category of “*Paper-based theses*”. According to the aforementioned guideline, in a Paper-based thesis, the following constitutes the body of the text:

“ ...

Body of Text:

- *Introductory chapter (Introduction) to the entire thesis with its own bibliography*
- *Each subsequent chapter is presented in a paper format without an abstract, but with its own bibliography*
- *Final chapter (General Discussion and Conclusions), to relate the separate studies to each other and to a relevant discipline or field of study. This section has its own bibliography.”¹*

1

<http://www.gradstudies.ualberta.ca/degreesuperv/thesis/~media/Faculty%20of%20Graduate%20Studies/degreesuperv/thesis/thesispecs.pdf>

Adhering to this format, this thesis is composed of six chapters. Chapter One includes a general introduction to the subject, a brief survey of the current status of the related scientific literature, and a statement of the basic motivations behind this research. Chapters Two to Five include manuscripts of four research articles submitted for publication in various scientific journals. Unless stated otherwise in the text, the author of this thesis has been responsible for preparation of the research materials, collection and analysis of the research data, and composition of the articles. Chapter Six summarizes the conclusions, describes the contributions of this research to related fields of knowledge, and discusses potential future research based on the results of this work.

Dedication

I dedicate this thesis to my dear parents.

*Your lifetime of wholehearted support and enthusiastic encouragement
made this possible.*

Acknowledgment

I would like to express my deep gratitude to my PhD supervisor, Professor Kenneth Cadien, for his continued help and support throughout the program. The completion of this work would not be possible without Dr. Cadien's insight and expertise at certain critical points. His enthusiasm and dedication to work has been a great source of inspiration for me, guiding me through my professional, as well as personal life.

I would also like to thank Dr. Douglas Barlage for sharing his wealth of knowledge and experience in this field, and offering promising advice. I also learned a great deal through cooperation with the members of his research group. I would also like to thank the other esteemed member of my supervisory committee, Dr. Douglas Ivey. I thank Steve Launspach from National Institute of Nanotechnology for his help with XRD measurements and analyses. I also express my appreciation for all the support I received from my friends and family who were always there for me at the hardest times.

Table of Contents

1. INTRODUCTION.....	1
1.1 Introduction to III-Nitride Materials.....	2
1.1.1 Crystal structure.....	2
1.1.2 Properties and applications.....	4
1.1.3 Potential substrates.....	9
1.1.4 Conventional deposition methods.....	14
1.2 Atomic Layer Deposition.....	18
1.2.1 General principles of ALD.....	18
1.2.2 Plasma-Enhanced ALD (PEALD).....	21
1.2.3 Potential Application of ALD.....	21
1.2.4 ALD of Various Types of Materials.....	22
1.3 The objective and structure of this thesis.....	23
References.....	26
2. STRUCTURAL AND OPTICAL CHARACTERIZATION OF LOW- TEMPERATURE ALD CRYSTALLINE ALN.....	33
2.1. Introduction.....	34
2.2. Experimental Procedure.....	35
2.3 Results and Discussion.....	37
2.3.1 Structure.....	37
2.3.2 Composition.....	41
2.3.3. Optical Performance.....	46
2.4 Conclusions.....	53
References.....	53
3. XPS ANALYSIS OF ALN THIN FILMS DEPOSITED BY PLASMA- ENHANCED ATOMIC LAYER DEPOSITION.....	65
3.1. Introduction.....	66

3.2. Experimental Procedure	68
3.3. Results and Discussion.....	69
3.4. Conclusion	83
References.....	83
4. AS DEPOSITED P-TYPE (002) GAN ON SAPPHIRE GROWN BY ATOMIC LAYER DEPOSITION.....	89
4.1 Introduction.....	90
4.2. Experimental Procedure	91
4.3. Results and discussion	93
4.3.1. Composition	93
4.3.2 Structure	96
4.3.3 Growth mechanism.....	101
4.3.4. Electrical and Optical Properties	107
4.4. Conclusion	111
References.....	112
5. THE CRITICAL EFFECT OF GROWTH TEMPERATURE ON THE STRUCTURE AND PROPERTIES OF GAN DEPOSITED BY ALD	119
5.1 Introduction.....	120
5.2 Experimental.....	122
5.3 Results and Discussion.....	123
5.3.1 Deposition parameters	123
5.3.2 Crystal structure.....	124
5.3.3 Growth rate and mechanism.....	132
5.3.4 Structure and normalized density	138
5.3.5 Electrical and optical properties	141
5.4 Conclusions.....	145
References.....	147
Chapter Six.....	154

6. CONCLUSIONS, CONTRIBUTIONS TO KNOWLEDGE, AND FUTURE WORK.....	154
6.1 Conclusions and Contribution to Knowledge.....	155
6.1.1 ALD of AlN.....	155
6.1.2 ALD of GaN.....	156
6.2 Future Work.....	157

List of Tables

Table 1.1: Prominent physical and optical properties of wurtzite III-N materials ²	5
Table 1.2: Comparison of the essential electrical properties for four different candidate semiconductors for high-power electronics ¹⁴	7
Table 1.3: Comparison of the main relevant properties for the potential candidate substrates for deposition of GaN; data after Ref ²²	13
Table 2.1: Relative XRD peak intensities for AlN thin films grown on various substrates, as compared to the standard powder diffraction pattern	40
Table 3.1: Chemical composition of the samples at various depths, as determined by high-resolution scans	71
Table 3.2: The observed atomic bonding at various sample depths and their corresponding electron subshell energies; the reported values in the literature have been offered for comparison	75
Table 4.1: Elemental composition of the GaN films, as determined by XPS.....	95

List of Figures

Figure 1.1: Schematics of wurtzite crystal structure of GaN, cut along a: (111) and b: (100) crystallographic planes.....	2
Figure 1.2: Schematic of zincblende structure in III-N crystal, cut parallel to a: (111) and b: (100) crystallographic planes.	3
Figure 1.3: Illustration of the values of the optical band gap for different III-N semiconductors.	5
Figure 1.4: Comparison of the combined figure of merit (CFOM) for four different semiconductors, based on the values presented in Table 1.2.....	8
Figure 1.5: History and forecast for the GaN-based semiconductor device market size, according to data published by Yole Development ¹⁵	9
Figure 1.6: Schematic diagrams of a: three-dimensional lattice structure, b: (100) plane, and c: (111) planes of sapphire.	10
Figure 1.7: Schematic diagrams of a: three-dimensional lattice structure, b: (100) plane, and c: (111) planes of silicon.	13
Figure 1.8: The total number of publications in Web of Science database, in which the terms “ALD” or “ <i>atomic layer deposition</i> ” have been mentioned as topics; the numbers include journal publications, as well as patents.	18
Figure 1.9: Schematic showing the four phases that constitute a single deposition cycle in ALD process; the red and blue species represent the two types of precursors.....	20
Figure 2.1: a) X-ray reflectometry spectra for AlN thin films b) determination of the critical angle.....	37
Figure 2.2: Kiessig fringes in AlN XRR spectrum; dotted and solid lines illustrate experimental and fitted data, respectively.	38
Figure 2.3: Grazing incidence X-ray diffraction spectra of AlN thin films deposited on different substrates; notations mark various AlN crystallographic planes.	39

Figure 2.4: Atomic force microscopy image of a 40-nm AlN thin film.	41
Figure 2.5: High-resolution XPS spectra of Al 2p, N 1s, and O 1s peaks; the corresponding peaks and subpeaks have been connected by lines. The intensities are adjusted for the purpose of illustration in a single diagram.	43
Figure 2.6: Fourier-transformed infrared spectrum of an AlN film deposited on Si (111) substrate taken in reflectance mode, b) Deconvolution of the peak centered at 672 cm^{-1}	44
Figure 2.7: Variations of real and imaginary parts of the dielectric function in the wavelength range of 200-600 nm.	47
Figure 2.8: The derived values of refractive index and absorption coefficient. ...	48
Figure 2.9: Variations of refractive index of AlN as a function of wavelength, for different numbers of deposition cycles.	49
Figure 2.10: Values of the refractive index at three representative wavelengths, as a function of the film thickness; the region with a stable refractive index has been marked.....	50
Figure 2.11: Demonstration of applying Tauc method for extraction of the optical band gap for films of different thicknesses.	51
Figure 2.12: Plot of optical band gap vs. thickness for AlN; the region with a stable optical band gap has been marked.	52
Figure 3.1: Survey scan of the uncoated sample a) before etching; b) after 20 minutes of etching.....	70
Figure 3.2: Comparison of the high resolution Al 2p peaks of the uncoated sample before and after 20 minutes of etching.	72
Figure 3.3: High resolution XPS AL 2p spectra of the Al-coated thin films a) before etching; b) after 1 minute of etching; c) after 20 minutes of etching.	74
Figure 3.4: High resolution XPS N 1s spectra of the Al-coated thin films a) before etching; b) after 1 minute of etching; c) after 20 minutes of etching.	79

Figure 3.5: High resolution XPS O 1s spectra of the Al-coated thin films a) before etching; b) after 1 minute of etch; c) after 20 minutes of etch.....	82
Figure 4.1: XPS survey spectrum of the GaN film after ion etch cleaning.	94
Figure 4.2: X-ray reflectometry spectra of a 1000-cycle ALD GaN film showing a) the critical angle and b) the method used to extract the critical angle.....	95
Figure 4.3: Characteristic Kiessig fringes in GaN XRR spectra.	97
Figure 4.4: Coupled scan XRD spectrum of GaN on sapphire.....	98
Figure 4.5: The schematic illustration of the geometrical parameters of the XRD tests.	99
Figure 4.6: A two dimensional XRD frame of GaN on sapphire with the accompanying integration of the intensity along the χ axis.....	100
Figure 4.7: Superimposed azimuthal scans of sapphire (006) and GaN (002) XRD peaks.	101
Figure 4.8: High resolution transmission electron micrographs of GaN-sapphire interface.....	103
Figure 4.9: Convergent beam electron diffraction pattern of the epitaxial layer at the interface.....	104
Figure 4.10: a) Phase image atomic force micrograph of the surface of the GaN films b) a three-dimensional reconstruction of the surface contour, extracted from the AFM height sensor data.	106
Figure 4.11: Variations of the refractive index and extinction coefficient, extracted from spectroscopic ellipsometry data.	107
Figure 4.12: The evolution of the refractive index of GaN at 632 nm during the growth process.	109
Figure 4.13: Transmission spectrophotometry data for GaN films on sapphire.	110
Figure 4.14: comparison of the optical band gap extracted from spectrophotometry and ellipsometry data.	111

Figure 5.1: ALD saturation curves for the two precursors; the deposition temperature and plasma power were 275°C and 600W, respectively.	124
Figure 5.2: Schematic illustrating the geometric variables of XRD test.	125
Figure 5.3: Two-dimensional XRD frames of 1000-cycle GaN films deposited at a) 150°C b) 200°C c) 240°C d) 275°C e) 325°C f) 360°C g) 425°C.....	126
Figure 5.4: Integration of the diffraction intensity as a function of 2θ for GaN films deposited at various substrate temperatures.....	128
Figure 5.5: Integration of the diffraction intensity as a function of χ for GaN films deposited at various substrate temperatures.....	128
Figure 5.6: The azimuthal scans of sapphire (006) and GaN (002) deposited at 325°C.	130
Figure 5.7: Evolution of XRD rocking curves of the GaN (002) peak with increasing substrate temperature.....	132
Figure 5.8: Growth rate of GaN as a function of growth temperature.....	133
Figure 5.9: Variations of GaN surface roughness vs. deposition temperature. ..	135
Figure 5.10: AFM images of 1000 cycle-grown GaN films with the substrate temperature of a) 150°C b) 325°C c) 425°C.....	137
Figure 5.11: Schematic illustrating the effect of substrate temperature on lateral and longitudinal growth rates of GaN hillocks; blue and red arrows indicate lower and higher temperature, respectively.....	138
Figure 5.12: X-ray reflectometry spectra of GaN films deposited at various temperatures.....	139
Figure 5.13: Variations of the mass density as a function of the growth temperature. The numbers are normalized to the maximum observed density.	141
Figure 5.14: The dependence of resistivity and carrier mobility on the substrate temperature.	142

Figure 5.15: The in-situ observation of the evolution of refractive index at 632 nm, plotted at two representative temperatures. 143

Figure 5.16: The in-situ observation of the evolution of refractive index at 632 nm, plotted at two representative temperatures b) The dependence of refractive index on the growth temperature, plotted at three different representative wavelengths; three different zone have been designated based on the behavior of the refractive index..... 144

List of Abbreviations:

ALD: Atomic Layer Deposition

PEALD: Plasma-enhanced Atomic Layer Deposition

CVD: Chemical Vapor Deposition

MBE: Molecular Beam Epitaxy

GPC: Growth per Cycle

TMA: Trimethylaluminum

TEG: Triethylgallium

XRD: X-ray Diffraction

GIXRD: Grazing Incidence X-ray Diffraction

XRR: X-ray Reflectometry (Reflectivity)

XPS: X-ray Photoelectron Spectroscopy

FTIR: Fourier-Transformed Infrared Spectroscopy

AFM: Atomic Force Microscopy

TEM: Transmission Electron Microscopy

HRTEM: High-Resolution TEM

Chapter One

Introduction

1.1 Introduction to III-Nitride Materials

In this section, a brief review of III-nitride materials has been presented. This review includes their crystal structure, properties and applications, potential substrates, and common deposition methods.

1.1.1 Crystal structure

Generally, III-nitrides may exist in the form of three distinct crystallographic structures. The most common form, wurtzite, is composed of alternating layers of atoms, where each layer consists of two close-packed sub-layers of Ga and N atoms standing directly on top of each other. The wurtzite structure may also be pictured as two interpenetrating hexagonal close packed lattices, each comprised of single-type atoms, while one lattice is transferred $5/8$ of lattice parameter in the direction of c-axis from the other ¹. A schematic of the wurtzite structure is depicted in Fig. 1.1.

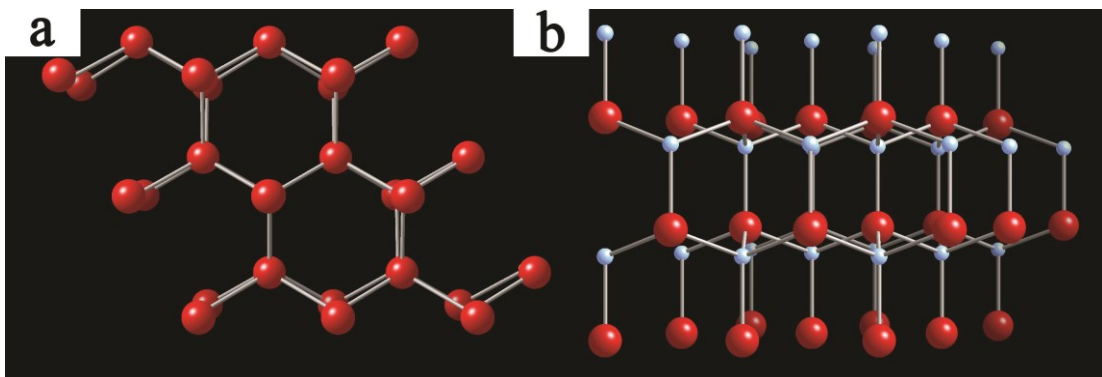


Figure 1.1: Schematics of wurtzite crystal structure of GaN, cut along a: (111) and b: (100) crystallographic planes.

A second possible crystal structure for III-nitrides is the zinc-blende structure, in which close-packed layers of anions are placed in ABCABC... sequence, therefore forming an FCC structure, while cations are placed in octahedral positions. Alternatively, this structure may be viewed as two inter-penetrating cubic close-packed structures, one offset by one quarter of the diagonal length, along the unit cell diagonal. A schematic of this crystal structure may be seen in Fig. 1.2.

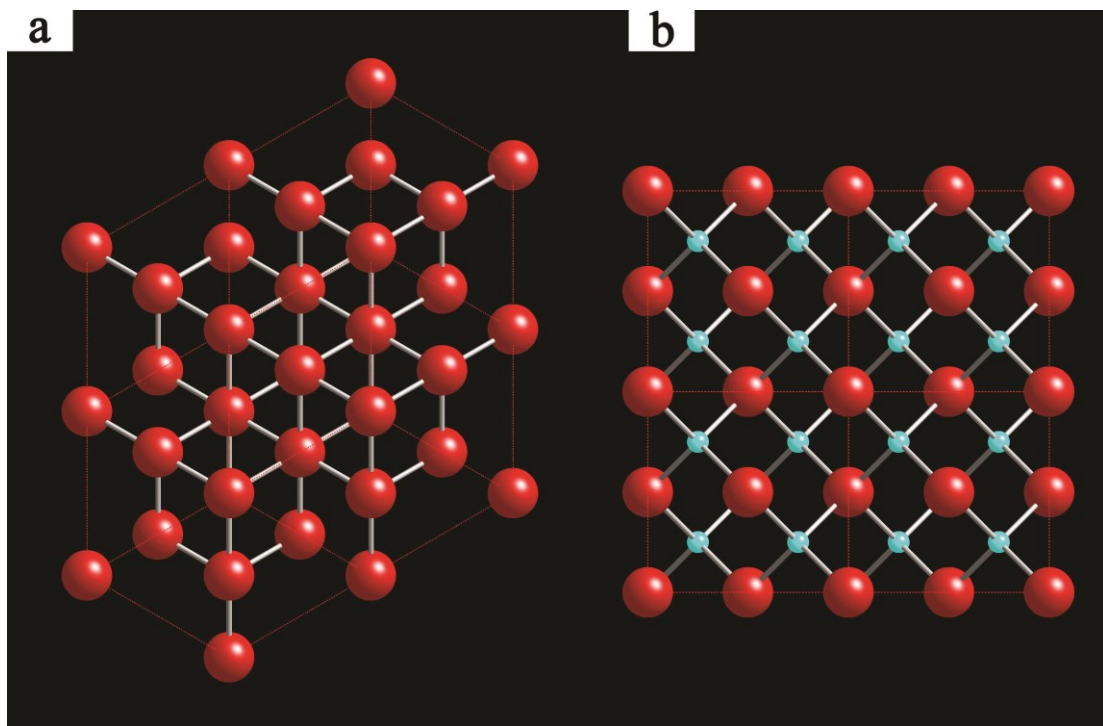


Figure 1.2: Schematic of zincblende structure in III-N crystal, cut parallel to a: (111) and b: (100) crystallographic planes.

In the rock salt structure, the stacking order of the anions is the same, while the cubic close-packed lattice of cations is positioned half a lattice constant downward, parallel to a cube edge. In the first two structures each ion is coordinated by four

adjacent ions of the opposite charge. This number changes to six, in the case of rock salt structure.

The thermodynamically stable structure for bulk AlN, GaN, and InN at ambient conditions is wurtzite. The zincblende structure for GaN and InN has been stabilized by epitaxial growth of thin films on substrates such as Si, MgO, and GaAs¹. The rock salt structure is only stable at elevated pressures. In the case of GaN, a transition from zincblende to rock salt is expected at elevated pressures as high as 50 GPa¹.

1.1.2 Properties and applications

Table 1.1 shows the major physical and optical properties of the wurtzitic III-nitride materials. A wide band gap, along with high thermal stability are the key features of this material. More importantly, as schematically illustrated in Fig. 1.3, by making binary or ternary alloys of GaN, InN and AlN, one can tailor the band gap over a wide range of wavelengths from IR to UV. This facilitates the application of III-nitride materials for general lighting, i.e. replacing conventional light bulbs. This will have tremendous technological and commercial ramifications. However, the realization of this potential largely depends upon the possibility of manufacturing affordable GaN thin films. This involves the growth process as well as the substrate.

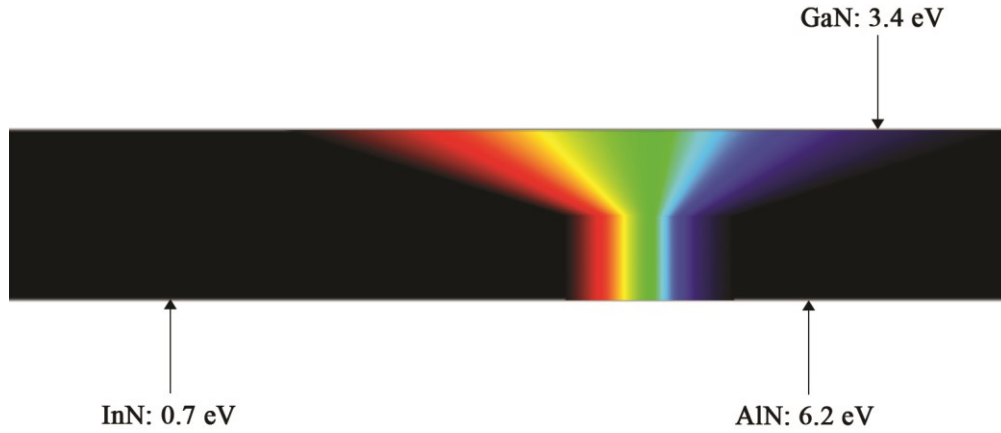


Figure 1.3: Illustration of the values of the optical band gap for different III-N semiconductors.

Table 1.1: Prominent physical and optical properties of wurtzite III-N materials²

Parameter	AlN	GaN	InN
Energy band gap (T = 300 K) (eV)	6.2	3.39	0.7 ³
Lattice constant (T = 300 K) a (Å)	3.112	3.189	3.545
Lattice constant (T = 300 K) c (Å)	4.982	5.186	5.703
Thermal conductivity (Wcm ⁻¹ K ⁻¹)	2.0	1.3	-
Thermal expansion coefficient α_a (10 ⁻⁶ K ⁻¹)	5.27	4.3	5.6
Refractive index n (632 nm)	2.15 ⁴	2.38 ⁴	3.15 ⁵
Dielectric constant ϵ	8.5	8.9	15.3

In addition to the mentioned parameters, AlN has the highest piezoelectricity among the III-nitrides⁶. This property, in combination with good mechanical properties, makes AlN thin films viable candidates for micromechanical resonators, such as film bulk acoustic resonators (FBARs)⁷. The fact that AlN has high chemical stability and corrosion resistance, as well as high thermal conductivity, means it is a suitable choice for use in chemical and biological sensors as well^{8,9}. In such sensors, adsorption of certain chemical compounds on the surface creates an electrostatic effect that leads to a change in polarization of a metallized AlN thin film¹⁰. In addition to thin films, a wide array of one-dimensional AlN structures have been fabricated, which include nanowires, nanotubes. These structures show highly improved field emission properties, compared to their bulk counterparts. This leads to a shorter device turn-on time¹¹,

A summary of the main parameters affecting the suitability of select wide band gap materials for high temperature/high frequency/high power applications is shown in Table 1.2. GaN shows great potential for such service conditions, due to its large band gap and high carrier mobility. Although theoretically diamond seems to be the most promising material for such applications, practical limitations e.g. difficulty in producing commercially viable wafers, cutting the wafers and doping counteract its competitive advantages^{12,13}. A combined figure-of-merit (CFOM) for high-frequency, high-power and high-temperature applications can be defined as

$$\text{CFOM} = \chi \epsilon \mu V_d E_b^2 \quad (1)$$

where χ is the thermal conductivity, ϵ the dielectric constant, μ the electron mobility, V_d the drift velocity, and E_b the breakdown field¹³. The values of the combined figure of merit for the four materials summarized in Table 1.2 have been calculated and compared in Fig. 1.4. GaN along with SiC show a great potential for these applications.

Table 1.2: Comparison of the essential electrical properties for four different candidate semiconductors for high-power electronics¹⁴

Property	Si	GaAs	4H-SiC	GaN
Band gap (eV)	1.12	1.42	3.25	3.40
Breakdown field (MV/cm)	0.25	0.4	3.0	4.0
Electron mobility (cm ² /Vs)	1350	6000	800	1300
Maximum velocity (10 ⁷ cm/s)	1.0	2.0	2.0	3.0
Thermal conductivity (W/cmK)	1.5	0.5	4.9	1.3
Relative dielectric constant	11.8	12.8	9.7	9.0

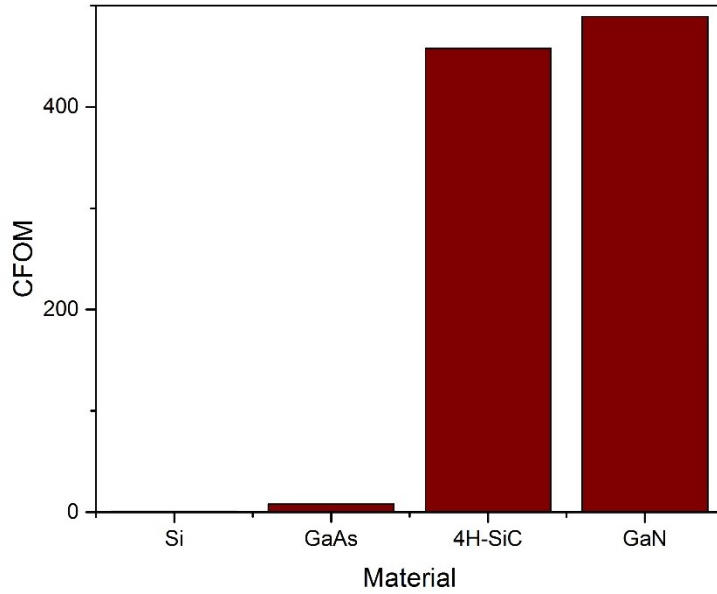


Figure 1.4: Comparison of the combined figure of merit (CFOM) for four different semiconductors, based on the values presented in Table 1.2.

Finally, Fig. 1.5 shows the forecasts for the global consumption of GaN semiconductors, according to Yole Development¹⁵. As seen, an exponential growth has been observed and predicted for the GaN semiconductor market in the current decade. Considering this importance, the potential substrates for deposition of GaN will be discussed in the next section.

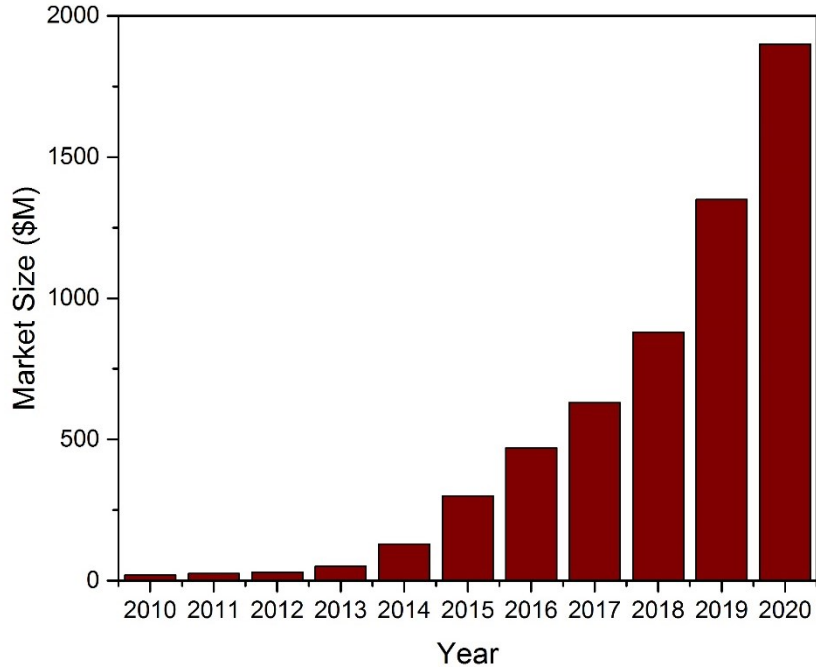


Figure 1.5: History and forecast for the GaN-based semiconductor device market size, according to data published by Yole Development¹⁵.

1.1.3 Potential substrates

The choice of substrate has an immense effect on the properties and performance of AlN and GaN thin films. Since bulk single crystals of these materials are not commercially viable yet, heteroepitaxy is the method of choice. In other words, AlN or GaN is deposited on a substrate of a different material. There are several factors, which collectively determine the suitability of a substrate for deposition. These factors include lattice constant, thermal and electrical properties and chemical reactivity. The major attributes of a thin film that are directly affected by the choice of substrate include crystal structure and orientation, polarity, strain and defect concentration, upon which the device performance of the material depends^{16,17}. The three most common substrates for III-nitride films are briefly discussed below.

Sapphire

Sapphire, single crystal aluminum oxide, was the first substrate to be used for GaN heteroepitaxy, and so far has remained the most popular candidate. The single crystal can be described by both rhombohedral and hexagonal unit cells. As shown in Fig. 1.6, the unit cell described in terms of hexagonal Miller-Bravais indices consists of six close packed (0001) planes of O^{2-} ions, sandwiching 12 planes of Al^{3+} ions that occupy two thirds of the available octahedral voids created by the O^{2-} ions.

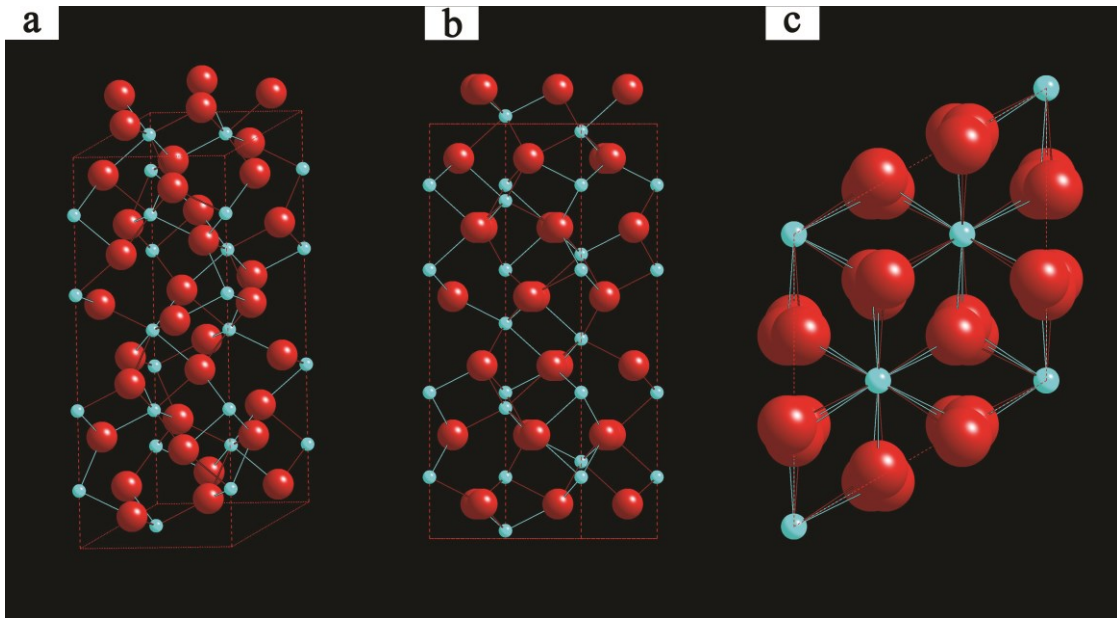


Figure 1.6: Schematic diagrams of a: three-dimensional lattice structure, b: (100) plane, and c: (111) planes of sapphire.

The crystal surface of sapphire most commonly employed for GaN deposition is the (0001) or c-plane. Ideally, it results in GaN film with (0001) orientation.

Tripathy et al.^{18,19} compared the quality of GaN layers with the same thickness (1.2 mm) grown on c-, a-, r-, and m-plane sapphire substrates by molecular beam epitaxy. GaN layers were smooth and flat on c- plane sapphire, slightly rougher on a-plane, and rough on r-plane and m-plane sapphire.

The large lattice constant mismatch of sapphire with AlN and GaN leads to high dislocation density (10^{10} cm^{-2}) in the epitaxial film. These high defect densities reduce the charge carrier mobility, reduce the minority carrier lifetime, and decrease the thermal conductivity, all of which degrade device performance^{20,21}. Sapphire's coefficient of thermal expansion is greater than GaN, thus, producing biaxial compressive stress in the layer as it cools from the deposition temperature. For thick films, the stress can cause both the film and the substrate to crack. The thermal conductivity of sapphire is low (about 0.25 W/cm K at 100° C), thus, it is relatively poor at dissipating heat compared to other substrate materials.

SiC

Silicon carbide has more than 250 different polymorphs. The basic sub-structure for all these are the tetrahedrons of SiC_4 or CSi_4 , whose various 1-D, 2-D or 3-D stacking can form various polymorphs. Three commercially available hexagonal polymorphs called 3C-SiC, 4H-SiC and 6H-SiC have the same space group as that of wurtzite III-nitrides. Silicon carbide features some benefits compared to sapphire. Probably the most notable of them are smaller lattice constant mismatch (3.1%) for (0001) oriented films, and a much higher thermal conductivity (3.8 W/cm K). Conductive substrates are available, making electrical contacts to the backside of the substrate possible, thereby simplifying the device structure

compared to sapphire substrates. The crystal planes in epitaxial AlN and GaN are parallel to those of the SiC substrate, making facet formation by cleaving easier.

Gallium nitride epitaxy directly on SiC is problematic, due to poor wetting between these materials^{1,22}. This can be remedied by using an AlN or $\text{Al}_x\text{Ga}_{(1-x)}\text{N}$ buffer layer. On the other hand, preparing smooth silicon carbide surfaces is difficult, thus, its surface roughness is an order of magnitude higher than that for sapphire. This roughness and any remnant subsurface polishing damage are sources of defects in the GaN epitaxial layer. The thermal expansion coefficient of SiC is less than that of AlN or GaN, thus, the films are typically under biaxial tension at room temperature. Lastly, the cost of silicon carbide substrates is high¹.

Silicon

From the commercial viewpoint, silicon is the most attractive substrate. The price of silicon wafers is extremely low in comparison to the other alternatives, and also the perfectness of the crystal is unparalleled. In addition, exceptionally smooth surface finishing methods are widely applicable for this substrate. Silicon has a diamond structure which could be envisioned as the combination of two interpenetrating FCC lattices, one positioned a quarter of a unit cell diameter away from the other, along the diameter. Fig. 1.7 shows the surface structure of silicon normal to various directions.

Table 1.3: Comparison of the main relevant properties for the potential candidate substrates for deposition of GaN; data after Ref²².

Material	Crystal Structure	Mismatch with AlN (%)	Mismatch with GaN (%)	Thermal expansion (10^6K^{-1})	
				a-axis	c-axis
GaN	Wurtzite	2.4	0	3.17	5.59
AlN	Wurtzite	0	2.4	5.27	4.15
InN	Wurtzite	11.9	9.9	3.8	2.9
Sapphire	Rhombohedral	13.0	15.6	5.0	9.03
SiC (6H)	Wurtzite	1	3.3	4.3	4.7
Si (111)	Diamond	23	21	2.6	
Ge (111)	Diamond	22.2	20.5	5.9	
ZnO	Wurtzite	4	1.8	6.5	3.0

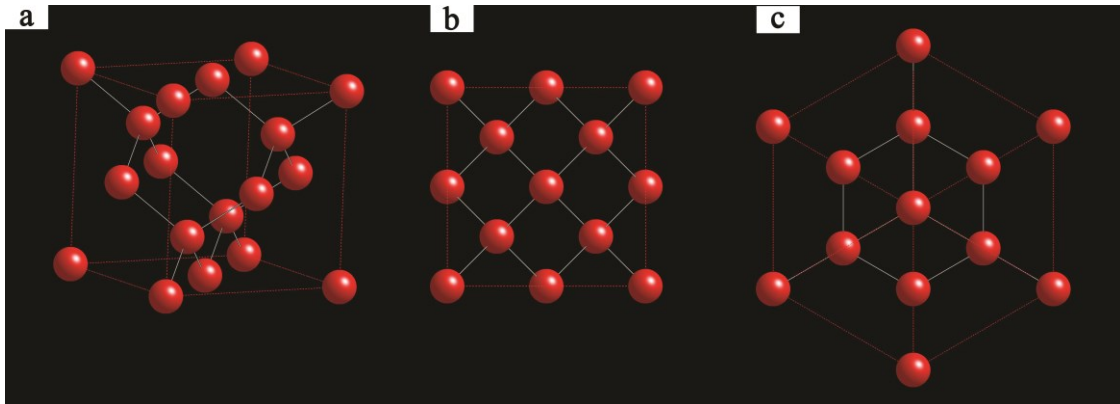


Figure 1.7: Schematic diagrams of a: three-dimensional lattice structure, b: (100) plane, and c: (111) planes of silicon.

Deposition of high quality III-nitride films on silicon substrate faces several problems. First of all, there is a large difference in lattice constant and coefficient

of thermal expansion between silicon on one hand and AlN and GaN, on the other hand. This causes formation of misfit dislocations and several other lattice defects. Moreover, the silicon surface tends to form an amorphous nitride layer, which disrupts the crystallographic continuity of the system^{17,23}. Table 1.3 compares some basic crystallographic and physical parameters of wurtzitic group III nitrides against those of the available substrates²².

1.1.4 Conventional deposition methods

Two of the major methods currently employed for deposition of GaN at industrial and research scales are briefly discussed below.

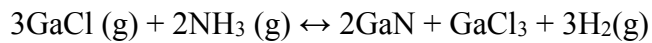
Chemical vapor deposition

Growth from the vapor phase is categorized on the basis of the sources used. If the sources are inorganic in nature, the term inorganic vapor phase epitaxy is used. This too is subdivided on the basis of the sources used. If a hydride source is used for the group V element, the term hydride vapor phase epitaxy (HVPE) is applied. If at least some of the sources are organic in nature, the terms organometallic vapor phase epitaxy (OMVPE), organometallic chemical vapor deposition (OMCVD), metalorganic chemical vapor deposition (MOCVD), or metalorganic vapor phase epitaxy (MOVPE) are employed^{19,22}.

In HVPE, the group III precursors are chlorides formed by flowing hydrogen chloride gas over the liquid metal in a quartz tube. The group V precursors are hydrides, which are fed into the reaction chamber separately, in order to avoid

premature reaction with the molten source metal. For GaN growth, the chloride and hydride precursors are GaCl which is formed by reacting Cl from HCl gas with molten Ga, and NH₃, respectively. The GaCl in the vapor phase is transported to the deposition zone by a carrier gas, which can be hydrogen, an inert gas, or a combination of the two.

In the original variant of HVPE, which was first employed in 1969 by Maruska and Tietjen [17] to deposit GaN on sapphire, HCl vapor flowing over a Ga melt leads to the formation of GaCl, which is transported downstream. On the substrate surface, the GaCl reacts with NH₃ and results in GaN through the following chemical reaction:



Organometallic vapor phase epitaxy has been employed to grow high-quality epitaxial III-N films and heterostructures for opto-electronic applications. Manasevit et al. ²⁵ applied this technique to the deposition of GaN and AlN in 1971. Using trimethylgallium (TMG) and ammonia (NH₃) as source gases for group III and V species, respectively, the authors obtained c-axis oriented films on sapphire (0001) and on 6H-SiC (0001) substrates. Replacing trimethylgallium with trimethylaluminum, they could achieve similar results for AlN.

Usually OMVPE reactors for group III nitride film growth incorporate laminar flow at high operating pressures and separate inlets for the nitride precursors and

ammonia to minimize predeposition reactions. In an OMVPE reactor, the main flow composed of reactant gases with a high velocity is directed through the nozzle parallel to a rotating substrate. The subflow gas composed of nitrogen and hydrogen is directed perpendicular to the substrate. The purpose of the flow normal to the substrate surface is to bring the reactant gases in contact with the substrate and to suppress thermal convection effects. Hydrogen is the carrier gas of choice. A rotating susceptor is used to enhance uniformity of the deposited film ²⁶.

Growth of nitride semiconductors by OMVPE relies on the transport of organometallic precursor gases, hydrides for the nitrogen source, and reacting them on or near the surface of a heated substrate. The deposition is through pyrolysis. The underlying chemical mechanisms are complex and involve a set of gas phase and surface reactions. The fundamental understanding of the processes involved is still evolving and is not considered to be fully understood yet.

Molecular beam epitaxy

In the molecular beam epitaxy (MBE) technique, thin films are formed in ultra-high vacuum on a heated substrate through various reactions between thermal molecular beams of the constituent elements and the surface species on the substrate. The composition of the epilayer and its doping level depend on the arrival rates of the constituent elements and dopants ²²

When growing III-nitrides via MBE, the metal component is often provided through a metal-organic source. The dopants are provided by Si for n-type and Mg for p-type, by sources whose temperatures are adjusted to yield the desired

evaporation rate, hence doping level. On the contrary, nitrogen, being one of the least reactive gases owing to its strong cohesive bonds may not be introduced to the system in its gaseous form. Dissociation of one molecule into two reactive nitrogen atoms requires a large amount of energy, which cannot be provided by thermal means²². In a plasma environment, however, and at reduced pressures, a significant dissociation of the nitrogen molecules takes place. Atomic nitrogen is reactive even at room temperature and bonds with many metals. Consequently, group III nitrides can be grown by plasma-assisted molecular beam epitaxy, where the plasma-induced dissociation of nitrogen molecules is combined with the evaporation of metal atoms. The other alternative is using ammonia as the source of nitrogen.

After introduction of two well-researched methods for deposition of GaN, the technique of atomic layer deposition will be discussed in the next section.

1.2 Atomic Layer Deposition

1.2.1 General principles of ALD

Atomic layer deposition is a particular variation of chemical vapor deposition that aims to improve the conformality of the growth and increase the level of the thickness control. ALD, as known today, essentially dates back to a 1977 US patent by Suntola and Anston²⁷. The initial interest in ALD gradually diminished in 1980's and early 1990's, before the new demands of semiconductor industry ignited a new wave of research in 2000's. As seen in Fig. 1.8, the number of scientific publications and patents on atomic layer deposition is currently going through an exponential growth.

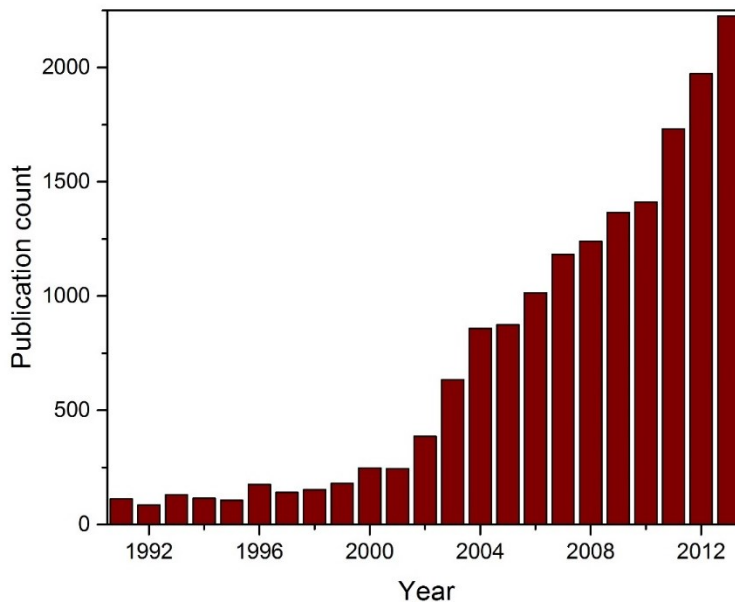


Figure 1.8: The total number of publications in Web of Science database, in which the terms “ALD” or “atomic layer deposition” have been mentioned as topics; the numbers include journal publications, as well as patents.

In contrast to CVD, where all the reactants enter the reaction chamber simultaneously, here the reactants are pumped into and purged from the chamber consecutively, in discrete phases of reaction. Therefore, instead of being continuous like CVD, an ALD reaction consists of a finite number of cycles; hence, the great degree of thickness control. The mechanism for a single cycle of ALD is schematically shown in Fig. 1.9. In phase I the first set of precursors enter the reactor and come in contact with the substrate. After the required amount of time for completion of the reaction, the remaining precursor molecules, along with the reaction by-products are purged away in phase II. The combination of phases I and II is called a half reaction. Phases III and IV are the repetition of I and II, except that the second precursor is used to complete the reaction. Although ALD is usually limited to two precursors, more can be used for deposition of ternary compounds²⁸ or for in-situ doping of semiconductors²⁹.

The most characteristic feature of the ALD reactions is that the partial reactions are “self-saturating”. This means that exposure of the surface to the flow of precursors for a longer time does not indefinitely increase the growth rate. One fortunate result of this phenomenon is the fact that in the case of three-dimensional substrates with complex shapes, various levels of exposure to reactants does not lead to locally different growth rates, as is the case for CVD. This is the root cause of the great conformality of the ALD process. One other inherent advantage of ALD over CVD is that the homogeneous reaction of the precursors, one of the most important problems in CVD, is ruled out, as the precursors enter the reactor separately. Therefore the most reactive precursors that may not be allowed for CVD can be

used in ALD, and this makes it possible to run the deposition at much lower substrate temperatures.

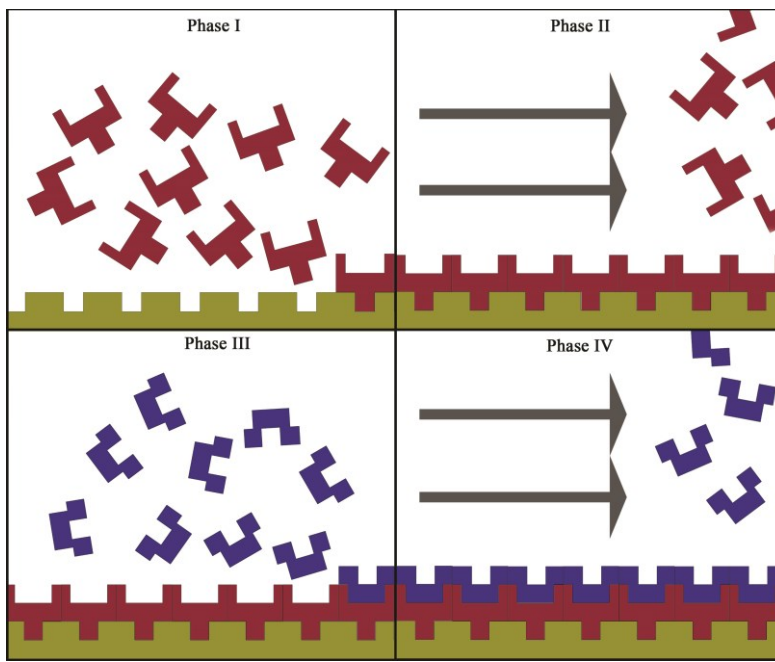


Figure 1.9: Schematic showing the four phases that constitute a single deposition cycle in ALD process; the red and blue species represent the two types of precursors.

In contrast, the growth rate is limited by the number of reaction sites on the surface, and a phenomenon called *steric hindrance*, which is the result of natural geometric constraints caused by the shape of the molecules. One implication of the self-saturated nature of the ALD reactions is that the growth rate is limited to one monolayer per cycle. In practice, the actual growth rate could be even lower. Therefore ALD is usually used for applications, where the need for conformality and thickness controllability outweighs the concerns about the deposition rate.

1.2.2 Plasma-Enhanced ALD (PEALD)

Traditional ALD is called thermal ALD, because the reaction energy is provided by heating the substrate. Alternatively, part of this energy can be supplied from a high-energy source like a plasma. This leads to plasma-enhanced ALD (PEALD), also known as plasma-assisted ALD (PAALD). In this variation, one precursor is replaced with a plasma source, e.g. oxygen plasma in the case of metal oxide films. This change offers a few general advantages. Using a high energy source increases the reaction rate, and makes it possible for the deposition to happen at a lower temperature. Moreover, using a plasma precursor removes the chance of creating unwanted precursors that might be adsorbed at the surface and embedded into the film. In addition, the plasma may have an activating effect, and increase the density of the surface reaction sites. In summary, PEALD films often have less contamination, and can be deposited faster at lower temperatures.

1.2.3 Potential Application of ALD

Micro/nano-electro mechanical systems (MMS/NEMS) constitute a vast and rapidly growing area of industry with immense service potential for atomic layer deposition. In general, any micro/nano scale system, in which an electrical signal interacts with a mechanical motion, can be considered a MEMS device. These devices often have complex three-dimensional parts, whose manufacture requires a conformal deposition method with a precise thickness control; hence, the great potential for ALD. Among the conventional deposition methods, CVD usually offers poor thickness control and conformality, and sputtering is fundamentally incapable of deposition on complex 3D surfaces. Accelerometers and gyroscopes

used in various devices such as car airbags, cellphones and the electronic gaming industry are two examples of high-demand MEMS devices. The head of the inkjet printers is another market, where Samsung has been considering ALD as a potential method for deposition of Ru-Ti-O alloys³⁰. In addition to applications, where ALD layers play a primary role in functioning of MEMS devices³¹, there are many situations that the moving parts in MEMS and NEMS devices can benefit from coatings that reduce wear, friction or adhesion³¹.

Magnetic heads for reading of hard drives are another commercial application for ALD. AlN and Al₂O₃ have been considered and used for this aim³². Coating of porous materials and particles is another field, in which ALD holds an intrinsic advantage over CVD. For instance, a recent study has investigated coating of LiMn₂O₄ particles with a one-nanometer thick layer of ZnO to improve the performance of lithium-ion batteries³³. ALD has recently been successfully applied for deposition of Al₂O₃ and HfO₂ as the antireflective and passivation layers on Si solar cells^{34,35}.

1.2.4 ALD of Various Types of Materials

Deposition of a variety of materials has been reported using atomic layer deposition. A large share of research has been concentrated on deposition of metal oxides, such as those of aluminum, zinc³⁶, titanium³⁷, zirconium³⁸ and hafnium³⁹. Thermal and plasma-enhanced deposition of Al₂O₃ using water vapor and oxygen plasma is perhaps the most researched and most well-known example of ALD⁴⁰. Ruthenium⁴¹, platinum⁴², tungsten⁴³, and nickel⁴⁴ are among the prominent examples of the metals thin films produced via ALD.

Among nitrides, ALD of TiN and TaN⁴⁵ attracted a lot of early attention, due to their application as diffusion barriers for copper interconnects. ALD of nitrides of group III materials, namely AlN, GaN, and InN has been studied less often. A potential reason could be the fact that the electrical and optical performance of these semiconductors heavily depends on their mass density, stoichiometry, crystal structure, crystal orientation, and the presence of impurities. Therefore the ALD process needs to be perfected, before the product can match the performance of the films deposited by CVD and sputtering. Although there are a number of successful depositions of AlN⁴⁶⁻⁴⁹ and GaN^{50,51} in the literature, the intricate interplay between the deposition parameters and the above-mentioned criteria is not well-researched.

1.3 The objective and structure of this thesis

The focal point of this research is at the intersection of two fields of research, each of which is attracting an increasing amount of interest in both academia and industry; namely the fields of III-nitride semiconductors and atomic layer deposition. As discussed earlier, ALD is being increasingly accepted as a deposition method with unique capabilities that make it irreplaceable by other methods. For this reason, this project addressed deposition of two compound semiconductors, AlN and GaN, by ALD. The aim of this research project was to implement and investigate the atomic layer deposition of AlN and GaN using a set of precursors not previously tried for this aim. To our knowledge, there is no report on using

N₂/H₂ plasma for deposition of AlN or GaN dating prior to the inception of this project² in 2010.

As explained in the preface, the findings of this project are presented in the form of four independent research papers. Chapter Two presents the AlN films deposited using our proposed recipe. The films have been characterized structurally and optically, and the effect of using different substrates has been discussed. The exact set of parameters used for the deposition of these films is the result of numerous optimization experiments, and this chapter is supposed to present a showcase of the results. In addition, in-situ spectroscopic ellipsometry was used to analyze the evolution of the optical properties during the growth process.

The most prominent roadblock on the way of AlN deposition was the high amount of oxygen content inside the films. Systematic experiments were carried out to spot and remove the source of this contamination. Despite the considerable reduction of the oxygen content, it never reached below ~9 at.% in AlN. Considering several other reports⁵²⁻⁶⁰ on the problem of oxygen contamination in AlN films, and the key effect it has on the film properties^{54,61}, we decided to devote the entire Chapter Three to a comprehensive XPS analysis of the AlN films, with special attention paid to the oxygen content, and its bonding to the lattice atoms at various depths.

Chapter Four is analogous to Chapter Two, structurally and content-wise, but is devoted to GaN. The fact that the optical band gap of GaN is within the range of most commercial optical apparatus made it possible for a more thorough optical

² There are recent reports in the literature on the use of nitrogen/hydrogen plasma for this purpose. However, the earliest was published three years after the start of this project.

characterization. Moreover, the higher conductivity, which is actually measurable by the available devices, facilitated the electrical characterization of the films. The fact that deposition of GaN crystals with the desired (002) preferential orientation was successfully implemented led to some interesting XRD studies, and curious observations via the transmission electron microscope, which are discussed in this chapter.

Among the several available deposition parameters in ALD, the substrate temperature was found to have a critical effect on the final properties of the films. Chapter Five summarizes and analyzes the results of our findings on the effect of this parameter on the growth, structure, and properties of the GaN films. As discussed in this chapter, changing the deposition temperature will have an immense effect on the structure and functionality of the films. In addition to their implications for deposition of GaN, the findings presented in this chapter are interesting for understanding ALD of crystalline films in general. The particular changes of surface roughness and the growth rate at the higher substrate temperatures have not been observed before for ALD. Similarly, the transition from the two-dimensional to the three-dimensional growth regime has not been reported for ALD, and it could be the key to the first epitaxial deposition of III-nitride materials via ALD.

In conclusion, the following four chapters present evidence for successful deposition of two types of III-nitride materials, analyze their process-structure-property relationships, and summarize some curious observations made in the process.

References

- (1) Mohammad, S. N.; Morkoc, H. Progress and Prospects of Group-III Semiconductors. *Prog. Quantum Electron.* 1996, 20, 361–525.
- (2) Razeghi, M.; Henini, M. *Optoelectronics Devices: III-Nitrides*; 2005.
- (3) Davydov, V. Y.; Klochikhin, A. A.; Seisyan, R. P.; Emtsev, V. V. Absorption and Emission of Hexagonal InN . Evidence of Narrow Fundamental Band Gap. *Phys. Status Solidi* 2002, 3, 1972–1974.
- (4) Polyanskiy, M. N. Refractive index database <http://refractiveindex.info>.
- (5) Djurišić, A. B.; Li, E. H. Modeling the Optical Constants of Hexagonal GaN, InN, and AlN. *J. Appl. Phys.* 1999, 85, 2848.
- (6) Tonisch, K.; Cimalla, V.; Foerster, C.; Romanus, H.; Ambacher, O.; Dontsov, D. Piezoelectric Properties of Polycrystalline AlN Thin Films for MEMS Application. *Sensors Actuators A Phys.* 2006, 132, 658–663.
- (7) Callaghan, L. A.; Lugh, V.; Requa, M. V.; Macdonald, N. C.; Clarke, D. R.; Turner, K. L. Fabrication and Testing of Beam Supported AlN FBARs. In *IEEE International Ultrasonics, Ferroelectrics, and Frequency Control Joint 50th Anniversary Conference*; 2004; Vol. 00, pp. 18–21.
- (8) Fu, J. L.; Tabrizian, R.; Ayazi, F. Dual-Mode AlN-on-Silicon Micromechanical Resonators for Temperature Sensing. *IEEE Trans. Electron Devices* 2014, 61, 591–597.
- (9) Qin, L.; Chen, Q.; Cheng, H.; Chen, Q.; Li, J.-F.; Wang, Q.-M. Viscosity Sensor Using ZnO and AlN Thin Film Bulk Acoustic Resonators with Tilted Polar c-Axis Orientations. *J. Appl. Phys.* 2011, 110, 094511.
- (10) Rothenberger, J. B.; Montenegro, D. E.; Prelas, M. a.; Ghosh, T. K.; Tompson, R. V.; Loyalka, S. K. An Aluminum Nitride-Based Chemical Sensor Using Q-DLTS. *Diam. Relat. Mater.* 2012, 23, 72–75.

- (11) Yong, K.-T.; Yu, S. F. AlN Nanowires: Synthesis, Physical Properties, and Nanoelectronics Applications. *J. Mater. Sci.* 2012, 47, 5341–5360.
- (12) Zolper, J. A Review of Junction Field Effect Transistors for High-Temperature and High-Power Electronics. *Solid. State. Electron.* 1998, 42, 2153–2156.
- (13) S. J. Pearton; C. R. Abernathy; M. E. Overberg; G. T. Thaler; A. H. Onstine; B. P. Gila; F. Ren; B. Lou; J. Kim. New Applications Advisable for Gallium Nitride. *Mater. Today* 2002, 5, 24–31.
- (14) Abernathy, C. R.; Overberg, M. E.; Thaler, G. T.; Onstine, A. H.; Gila, B. P.; Ren, F.; Lou, B.; Kim, J. New Applications for Gallium Nitride. *Rev. Lit. Arts Am.* 2002, 24–31.
- (15) Power GaN-2012 Edition; 2012.
- (16) Foxon, C. The Growth and Properties of Group III Nitrides. *J. Cryst. Growth* 1995, 150, 892–896.
- (17) Würfl, J. Reliability Considerations of III-Nitride Microelectronic Devices. *Microelectron. Reliab.* 1999, 39, 1737–1757.
- (18) Chiu, S.-Y.; Huang, H.-W.; Huang, T.-H.; Liang, K.-C.; Liu, K.-P.; Tsai, J.-H.; Lour, W.-S. Comprehensive Investigation on Planar Type of Pd–GaN Hydrogen Sensors. *Int. J. Hydrogen Energy* 2009, 34, 5604–5615.
- (19) Morkoç, H. Comprehensive Characterization of Hydride VPE Grown GaN Layers and Templates. *Mater. Sci. Eng. R Reports* 2001, 33, 135–207.
- (20) Red'kin, a. N.; Tatsii, V. I.; Makovei, Z. I.; Gruzintsev, a. N.; Yakimov, E. E. Chemical Vapor Deposition of GaN from Gallium and Ammonium Chloride. *Inorg. Mater.* 2004, 40, 1049–1053.
- (21) Kim, H.-J.; Byun, D.; Kim, G.; Kum, D.-W. Effects of Reactive Ion Beam Treatment of a Sapphire Surface to Optimize the Deposition of GaN Films. *J. Appl. Phys.* 2000, 87, 7940.

- (22) Wang, X.; Yoshikawa, a. Molecular Beam Epitaxy Growth of GaN, AlN and InN. *Prog. Cryst. Growth Charact. Mater.* 2004, 48-49, 42–103.
- (23) Strittmatter, A.; Krost, A.; Straßburg, M.; Türek, V.; Bimberg, D.; Bläsing, J.; Christen, J. Low-Pressure Metal Organic Chemical Vapor Deposition of GaN on silicon(111) Substrates Using an AlAs Nucleation Layer. *Appl. Phys. Lett.* 1999, 74, 1242.
- (24) Gogotsi, Y. *Nanomaterials Handbook*; CRC Press, 2006.
- (25) H.M. Manasevit, F.M. Erdman, A. W. I. S. The Use of Metalorganics in the Preparation of Semiconductor Materials. *J. Electrochem. Soc.* 1971, 118, 1864.
- (26) Morkoç, H. *Nitride Semiconductor Device: Principles and Simulation Properties of Group-IV , III-V and II-VI Semiconductors Nitride Semiconductors*; 2009.
- (27) Suntola, T.; Antson, J. Method for Producing Compound Thin Films, November 15, 1977.
- (28) Chong, Y. T.; Yau, E. M. Y.; Nielsch, K.; Bachmann, J. Direct Atomic Layer Deposition of Ternary Ferrites with Various Magnetic Properties. *Chem. Mater.* 2010, 22, 6506–6508.
- (29) Aarik, L.; Arroval, T.; Rammula, R.; Mändar, H.; Sammelseg, V.; Hudec, B.; Hušeková, K.; Fröhlich, K.; Aarik, J. Atomic Layer Deposition of High-Quality Al₂O₃ and Al-Doped TiO₂ Thin Films from Hydrogen-Free Precursors. *Thin Solid Films* 2014, 565, 19–24.
- (30) Min, J.; Kang, S.; Ha, Y. Heater of Inkjet Printhead, Inkjet Printhead Having the Heater and Method of Manufacturing the Inkjet Printhead, February 08, 2007.
- (31) Eigenfeld, N. T.; Gray, J. M.; Brown, J. J.; Skidmore, G. D.; George, S. M.; Bright, V. M. Ultra-Thin 3D Nano-Devices from Atomic Layer Deposition on Polyimide. *Adv. Mater.* 2014, 26, 3962–3967.

- (32) Hukanen, J.; Kanninen, T. United States Patent U-S- PATENT DOCUMENTS. US 6,759,081 B2, 2004.
- (33) Zhao, J.; Wang, Y. Ultrathin Surface Coatings for Improved Electrochemical Performance of Lithium Ion Battery Electrodes at Elevated Temperature. *J. Phys. Chem. C* 2012, 116, 11867–11876.
- (34) Geng, H.; Lin, T.; Letha, A. J.; Hwang, H.-L.; Kyznetsov, F. a.; Smirnova, T. P.; Saraev, A. a.; Kaichev, V. V. Advanced Passivation Techniques for Si Solar Cells with High-K Dielectric Materials. *Appl. Phys. Lett.* 2014, 105, 123905.
- (35) Dobrzański, L. A.; Szindler, M.; Drygała, A.; Szindler, M. M. Silicon Solar Cells with Al₂O₃ Antireflection Coating. *Cent. Eur. J. Phys.* 2014, 12, 666–670.
- (36) Guziewicz, E.; Kowalik, I. A.; Godlewski, M.; Kopalko, K.; Osinniy, V.; Wójcik, A.; Yatsunenko, S.; Łusakowska, E.; Paszkowicz, W.; Guziewicz, M. Extremely Low Temperature Growth of ZnO by Atomic Layer Deposition. *J. Appl. Phys.* 2008, 103, 033515.
- (37) Xie, Q.; Jiang, Y.-L.; Detavernier, C.; Deduytsche, D.; Van Meirhaeghe, R. L.; Ru, G.-P.; Li, B.-Z.; Qu, X.-P. Atomic Layer Deposition of TiO₂ from Tetrakis-Dimethyl-Amido Titanium or Ti Isopropoxide Precursors and H₂O. *J. Appl. Phys.* 2007, 102, 083521.
- (38) Dezelah, C. L.; Niinistö, J.; Kukli, K.; Munnik, F.; Lu, J.; Ritala, M.; Leskelä, M.; Niinistö, L. The Atomic Layer Deposition of HfO₂ and ZrO₂ Using Advanced Metallocene Precursors and H₂O as the Oxygen Source. *Chem. Vap. Depos.* 2008, 14, 358–365.
- (39) Kirsch, P. D.; Quevedo-Lopez, M. A.; Li, H.-J.; Senzaki, Y.; Peterson, J. J.; Song, S. C.; Krishnan, S. A.; Moumen, N.; Barnett, J.; Bersuker, G.; et al. Nucleation and Growth Study of Atomic Layer Deposited HfO₂ Gate Dielectrics Resulting in Improved Scaling and Electron Mobility. *J. Appl. Phys.* 2006, 99, 023508.

- (40) Puurunen, R. L. Surface Chemistry of Atomic Layer Deposition: A Case Study for the Trimethylaluminum/water Process. *J. Appl. Phys.* 2005, 97, 121301.
- (41) Aaltonen, T.; Alén, P.; Ritala, M.; Leskelä, M. Ruthenium Thin Films Grown by Atomic Layer Deposition. *Chem. Vap. Depos.* 2003, 9, 45–49.
- (42) Aaltonen, T.; Ritala, M.; Sajavaara, T.; Keinonen, J.; Leskelä, M. Atomic Layer Deposition of Platinum Thin Films. *Chem. Mater.* 2003, 15, 1924–1928.
- (43) Elam, J. W.; Nelson, C. E.; Grubbs, R. K.; George, S. M. Nucleation and Growth during Tungsten Atomic Layer Deposition on SiO₂ Surfaces. *Thin Solid Films* 2001, 386, 41–52.
- (44) Yuan, G.; Shimizu, H.; Momose, T.; Shimogaki, Y. Kinetic Study on Hot-Wire-Assisted Atomic Layer Deposition of Nickel Thin Films. *J. Vac. Sci. Technol. A Vacuum, Surfaces, Film.* 2014, 32, 01A104.
- (45) Knoop, H. C. M.; Baggetto, L.; Langereis, E.; van de Sanden, M. C. M.; Klootwijk, J. H.; Roozeboom, F.; Niessen, R. A. H.; Notten, P. H. L.; Kessels, W. M. M. Deposition of TiN and TaN by Remote Plasma ALD for Cu and Li Diffusion Barrier Applications. *J. Electrochem. Soc.* 2008, 155, G287.
- (46) Bosund, M.; Sajavaara, T.; Laitinen, M.; Huhtio, T.; Putkonen, M.; Airaksinen, V.-M.; Lipsanen, H. Properties of AlN Grown by Plasma Enhanced Atomic Layer Deposition. *Appl. Surf. Sci.* 2011, 257, 7827–7830.
- (47) Ozgit, C.; Donmez, I.; Alevli, M.; Biyikli, N. Self-Limiting Low-Temperature Growth of Crystalline AlN Thin Films by Plasma-Enhanced Atomic Layer Deposition. *Thin Solid Films* 2012, 520, 2750–2755.
- (48) Kim, K.-H.; Kwak, N.-W.; Lee, S. H. Fabrication and Properties of AlN Film on GaN Substrate by Using Remote Plasma Atomic Layer Deposition Method. *Electron. Mater. Lett.* 2009, 5, 83–86.
- (49) Lei, W.; Chen, Q. Crystal AlN Deposited at Low Temperature by Magnetic Field Enhanced Plasma Assisted Atomic Layer Deposition. *J. Vac. Sci. Technol. A Vacuum, Surfaces, Film.* 2013, 31, 01A114.

- (50) Ozgit, C.; Donmez, I.; Alevli, M.; Biyikli, N. Atomic Layer Deposition of GaN at Low Temperatures. *J. Vac. Sci. Technol. A Vacuum, Surfaces, Film.* 2012, 30, 01A124.
- (51) Kim, O. H.; Kim, D.; Anderson, T. Atomic Layer Deposition of GaN Using GaCl₃ and NH₃. *J. Vac. Sci. Technol. A Vacuum, Surfaces, Film.* 2009, 27, 923.
- (52) Harris, J. H.; Youngman, R. A.; Teller, R. G. On the Nature of the Oxygen-Related Defect in Aluminum Nitride. *J. Mater. Res.* 1990, 44128, 1763–1773.
- (53) Kazan, M.; Rufflé, B.; Zgheib, C.; Masri, P. Oxygen Behavior in Aluminum Nitride. *J. Appl. Phys.* 2005, 98, 103529.
- (54) Youngman, R. A.; Harris, J. H. Luminescence Studies of Oxygen-Related Defects in Aluminum Nitride. *J. Am. Ceram. Soc.* 1990, 46, 3238–3246.
- (55) Slack, G. A. Nonmetallic Crystals with High Thermal Conductivity. *J. Phys. Chem. Solids* 1973, 34, 321–335.
- (56) Tabary, P.; Servant, C. Crystalline and Microstructure Study of the AlN–Al₂O₃ Section in the Al–N–O System. I. Polytypes and Γ -AlON Spinel Phase. *J. Appl. Crystallogr.* 1999, 32, 241–252.
- (57) Adams, I.; AuCoin, T. R.; Wolff, G. A. Luminescence in the System Al₂O₃-AlN. *J. Electrochem. Soc.* 1962, 1050–1054.
- (58) Mccauley, J. W.; Krishnan, K. M.; Rai, R. S.; Thomas, G. Anion-Controlled Microstructures in the AlN-Al₂O₃ System. In *Ceramic Microstructures '86*; Pask; Evans, Eds.; Plenum Publishing Corporation, 1988; pp. 577–590.
- (59) Sakai, T. Hot-Pressing of the AlN-Al₂O₃ System. *J. Ceram. Assoc. Japan* 1978, 86, 125–130.
- (60) Tendeloo, G. Van; Faber, K. T.; Thomas, G. Characterization of AlN Ceramics Containing Long-Period Polytypes. *J. Mater. Sci.* 1983, 18, 525–532.

(61) Nepal, N.; Nam, K. B.; Nakarmi, M. L.; Lin, J. Y.; Jiang, H. X.; Zavada, J. M.; Wilson, R. G. Optical Properties of the Nitrogen Vacancy in AlN Epilayers. *Appl. Phys. Lett.* 2004, 84, 1090.

Chapter Two

Structural and Optical Characterization of Low-Temperature ALD Crystalline AlN

(Submitted for publication to Journal of Crystal Growth)

2.1. Introduction

AlN, along with other III-nitrides, constitute a family of semiconductors with an exceptional suite of engineering properties, and a promising technological future^{1,2}. AlN has engineering features that distinguish it from other III-nitrides. The high surface velocity of acoustic waves (SAW) makes it a suitable candidate for various SAW devices^{3,4}. Piezoelectric sensors and actuators are an attractive area of application for AlN, due to the intrinsic polarization, caused by lack of a center of symmetry in the wurtzite crystal structure^{5,6}. The material's resistance to harsh environments makes it useful for UV detectors in the aerospace industry^{7,8}. AlN features high thermal conductivity and large dielectric breakdown field; hence, its applications in high-power electronics^{9,10}. In addition, the fact that all III-nitrides have stable wurtzite structures with close lattice constants, provides the possibility of III-N alloys with tunable band gaps in the range of infrared all the way to ultraviolet^{1,2,11,12}.

Metallorganic chemical vapor deposition^{13,14}, pulsed laser deposition¹⁵, and molecular beam epitaxy¹⁶, have been used to grow AlN at high deposition temperatures. Reactive sputtering¹⁷ and ALD offer alternative methods that make it possible to deposit films at lower temperatures with good process control and high conformality^{18,19}. Compared to reactive sputtering, ALD offers better conformality, control, and scale-up potential²⁰.

The most common ALD recipes for deposition of AlN involve the use of halides or ammonia as precursors²¹⁻²⁶. The use of halides leads to film contamination²⁷, offers risks for the equipment, and poses environmental hazards. In the case of ammonia,

the inevitable incomplete reactions may cause considerable hydrogen contamination²⁸. Using a plasma process instead of thermal ALD has the advantage of lower process temperature, in addition to lower chance of precursor contamination caused by partially ionized ammonia molecules. There are recent reports on this approach with varying degrees of success²⁹⁻³¹.

Here we report on deposition of AlN, using nitrogen plasma and trimethylaluminum precursors, at 250°C. The reported deposition conditions are the results of extensive optimization experiments designed to minimize the defects, and obtain film characteristics as close as possible to those of the bulk material. Comprehensive structural, compositional, and optical characterization has been conducted to assess various aspects of film behavior and compare them to the films deposited via mainstream methods at higher temperatures.

2.2. Experimental Procedure

A thin film deposition research system (ALD-150L, Kurt J. Lesker), which features thermal as well as remote plasma capabilities was used for the depositions. Si (100), Si (111), and sapphire were used as substrates. Silicon substrates were cleaned with a standard buffered oxide etch procedure prior to deposition, while sapphire was used as received. During deposition the substrates were heated to 250°C. Extensive experiments were carried out to ensure the deposition parameters fell inside the limits of the ALD window, and that the characteristic self-limiting regime of ALD deposition was maintained. The deposition consisted of four stages: 0.02s trimethylaluminum dose, 7s Ar gas purge, 10s N₂/H₂ plasma, followed by another

7s Ar purge. The plasma power was set to 600W. An in-situ spectroscopic ellipsometry apparatus (J. A. Woollam M2000DI) allowed for precise control of the thickness, and assessment of the optical properties.

X-ray reflectometry measurements were performed using a Bruker-AXS D8-Discover machine with a Cu K α source. The data were recorded using a NaI scintillometer. Commander D8 and Leptos programs were used for data acquisition and analysis, respectively. A Rigaku rotating anode XRD system was used for grazing incidence X-ray diffraction³. The incidence angle was set at 1°, and the experiments were done using a Cu K α source. XRD data were analyzed by Jade software. A Bruker Dimension-Edge AFM system was used to map the sample surface, and measure surface roughness. Silicon tips were used in tapping mode, and the amplitude set point was 2.4 V. AFM results were analyzed using Bruker Nanoscope Analysis 1.5 software. A Kratos AXIS Ultra x-ray photoelectron spectroscopy (XPS) was used to study the chemical structure of the films, using Al (1486.69eV) X-ray source at 50° incidence angle⁴. An argon ion gun (4 KeV) was used to clean the surface of the samples. Fourier-transformed infrared spectroscopy (FTIR) experiments were carried out using a Vertex 70/70v FTIR spectrometer by Bruker. Data were analyzed using OPUS 6.0 software.

³ The XRD data presented in this chapter was collected by Shiraz Merali at Chemical and Materials Engineering Department of University of Alberta.

⁴ All the XPS data reported in this thesis has been collected by Dimitre Karpuzov or members of his team at Alberta Center for Surface Engineering and Science, at the request of the author.

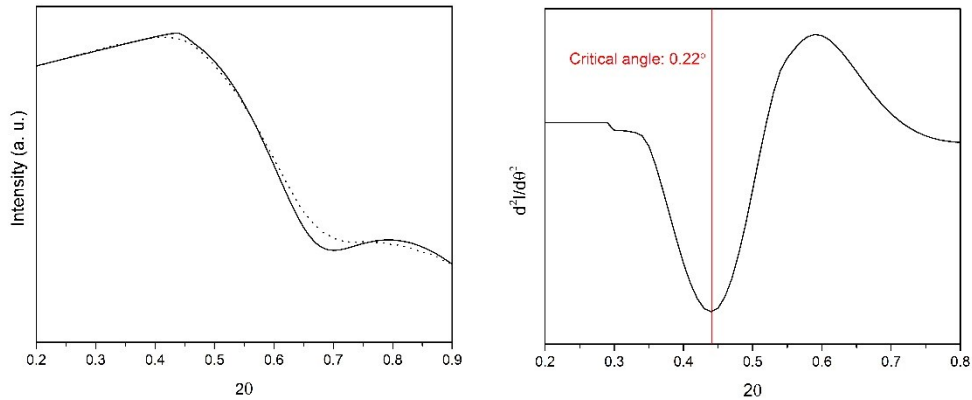


Figure 2.1: a) X-ray reflectometry spectra for AlN thin films b) determination of the critical angle.

2.3 Results and Discussion

2.3.1 Structure

X-ray reflectometry data from an AlN film after 300 cycles is shown in Figs. 2.1 and 2.2. Fig. 2.1 shows the data for the 2θ range of $0.2-0.8^\circ$. A sudden drop in intensity is observed. This is the angle at which total external refraction ends, and the x-rays start to penetrate the sample. In order to better determine this angle the second derivative of the curve, as shown in the inset of Fig. 2.1, was used and 0.22° was obtained for the critical angle. This is in line with previous observation reports on the critical angle of AlN thin films^{32,33}. As the value of the critical angle is directly related to the electronic density of the surface of the material, it is directly affected by porosity³⁴. In order to estimate the mass density of the films, computer simulation was performed using Bruker Leptos software. Simulation and experimental data are compared in Fig. 2.1. Fitting of the critical angle yields a value of 2.94 g cm^{-3} for the mass density, compared to the bulk density of 3.25 g cm^{-3} .

The pattern resulting from the interference of the x-rays reflected from the top surface and the film-substrate interface results in the emergence of Kiessig fringes at angles higher than the critical angle. While the distance between the two consecutive maxima gives thickness, density and roughness affect the signal amplitude and the overall attenuation rate. The fitted data are compared with the obtained experimental data, and illustrated in Fig. 2.2. Five parameters were fitted simultaneously using a genetic algorithm³⁵ resulting in values of film thickness, density and roughness of 19.7 nm, 3.07 g cm⁻³, and 0.5 nm, respectively. This roughness compares well with the measured average roughness of 0.7 nm, which was obtained from the arithmetic average of atomic force microscopy measurements.

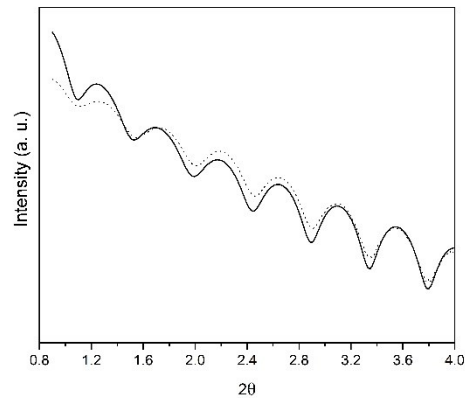


Figure 2.2: Kiessig fringes in AlN XRR spectrum; dotted and solid lines illustrate experimental and fitted data, respectively.

The grazing angle x-ray diffraction patterns for 2000-cycle AlN films deposited on three different substrates: Si (100), Si (111), and sapphire (001) are shown in Fig. 2.3. Four peaks at 33.5°, 37.8°, 59.6°, and 71.6° are in common among all three

films. These peaks correspond to (100), (101), (110), and (112) planes in wurtzite AlN lattice, respectively.

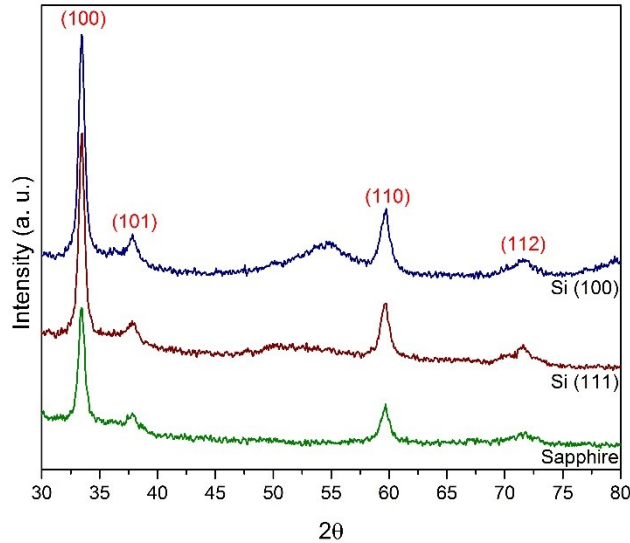


Figure 2.3: Grazing incidence X-ray diffraction spectra of AlN thin films deposited on different substrates; notations mark various AlN crystallographic planes.

The intensity ratio of the seven major peaks from the standard AlN powder diffraction file³⁶, compared to those of the films deposited in this work is summarized in Table 2.1. The distribution of the peak intensities of the three films is consistent, and noticeably different from that of the powder. Since the powder diffraction file represents the case of random grain orientation, any significant deviation from that indicates preferred orientation. In this case, the absence of (002), (102), and (103) peaks, combined with the low intensity of the (101) peak suggests preferential growth along the normal to the (100) plane. In other words, the unit cells lie on their side on the surface.

It has been previously reported that AlN films deposited by ALD have a tendency to crystallize in the (100) orientation, if they are crystalline^{23,30,31,37}. This is in contrast to sputtered AlN films, for which reports of c-plane orientation are more frequent³⁸⁻⁴³. In sputtered AlN films, higher power⁴⁴ and lower working pressure⁴⁵ have been reported to promote c-plane orientation. In the case of pulsed laser deposition, it has been reported that higher laser energy density strongly promotes c-plane rather than a-plane orientation⁴⁶.

Table 2.1: Relative XRD peak intensities for AlN thin films grown on various substrates, as compared to the standard powder diffraction pattern

	Powder	Si (100)	Si (111)	Sapphire
	AlN³⁶			
(100)	100	100	100	100
(002)	62	0	0	0
(101)	89	9	8	8
(102)	31	0	0	0
(110)	50	24	26	26
(103)	41	0	0	0
(200)	6	0	0	0
(112)	32	5	8	7

The atomic density of (002) planes are higher and have lower surface energy than (100) planes⁴⁴, therefore it is evident that achieving a (001) preferred orientation requires that surface atoms have a higher kinetic energy to permit rearrangement into the configuration with the lowest surface energy. While in low-temperature ALD the mobility of the atoms is lower, growth of the low-density (100) plane might be even more advantageous when steric hindrance is taken into account. The

fact that the relative intensity distribution of the XRD peaks closely match for the three substrates suggests that the kinetics of AlN growth, which in this case favors (100) orientation, overrules any effect induced by potential crystallographic orientation relationships between the films and the substrates.

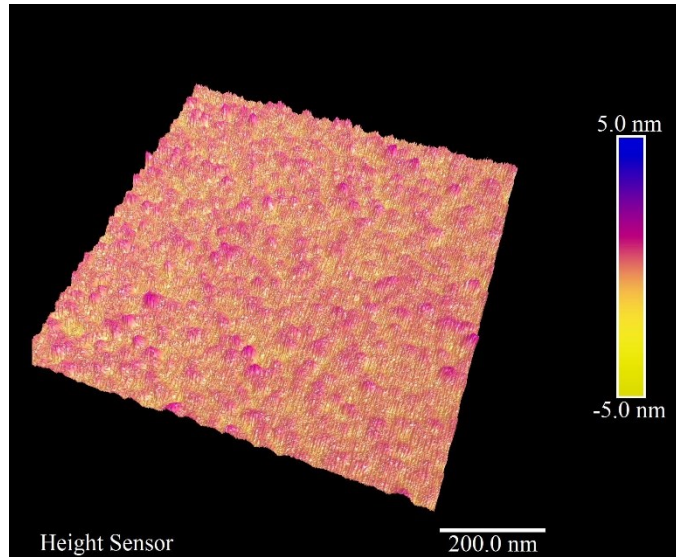


Figure 2.4: Atomic force microscopy image of a 40-nm AlN thin film.

AFM roughness analysis shows the arithmetic average of surface roughness to be 0.19 nm as shown in Fig.2.4. Since the AlN monolayer thickness is ~ 0.25 nm, the smoothness of the film indicates that the growth mechanism is layer-by-layer, rather than three-dimensional island growth.

2.3.2 Composition

An XPS study of the composition and bonding of the atoms in these films has been published previously⁴⁷. In this work we found that after sputter etching, the films still contained 3.4 at% carbon and 9.1 at.% oxygen. The low carbon content means that during ALD the nitrogen plasma has effectively removed most of the organic

ligands from the system, and no appreciable precursor condensation has occurred. The high oxygen composition is possibly due to residual native oxide on AlN since the affinity of AlN films for oxygen has been reported before^{38,39,48,49}. In addition, since our cleaning experiments use 4 keV Ar ions, some of this oxygen may be due to knock-on implantation of surface oxygen. The oxygen in our AlN films may affect the properties of the films^{50,51}. Due to the high reactivity of aluminum and oxygen, aluminum nitride films deposited through various methods are frequently reported to have significant amounts of oxygen^{30,39,45,52–54}.

In order to understand how the various constituents of the film are bonded together, high-resolution XPS spectra of Al 2p, O 1s, and N 1s peaks were analyzed, as illustrated in Fig. 2.5. The Al 2p peak can be deconvolved into two Gaussian-Lorentzian subpeaks centered at 74.7 and 75.6 eV. The energy difference between the two agrees with what has been reported in the literature for the energy of Al-O and Al-N peaks^{39,44,55}. In order to precisely assign these peaks, a comprehensive study was performed, whose detailed explanation is beyond the scope of this thesis, and has been reported elsewhere⁴⁷. It can be seen in Fig. 2.5 that both N 1s and O 1s peaks fit single Gaussian-Lorentzian distributions, and cannot be deconvolved into further subpeaks. This agrees with the hypothesis that only Al-O and Al-N bonds exist in the lattice.

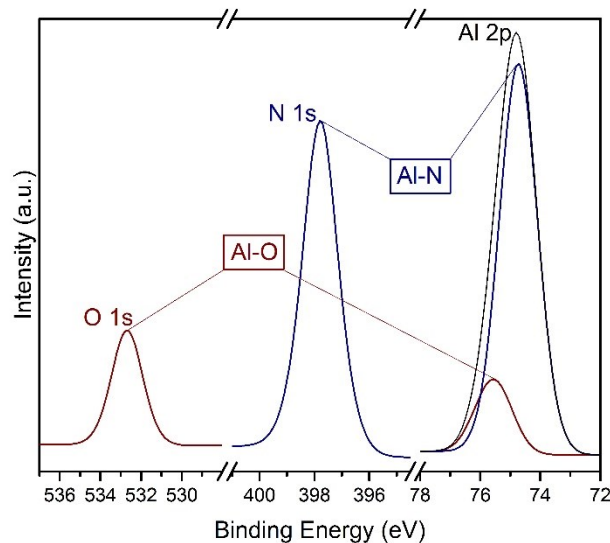


Figure 2.5: High-resolution XPS spectra of Al 2p, N 1s, and O 1s peaks; the corresponding peaks and subpeaks have been connected by lines. The intensities are adjusted for the purpose of illustration in a single diagram.

The N 1s peak was observed at 397.8 eV which is similar to previously reported values for nitrogen bonded to aluminum, when the difference in the position of C 1s reference peak is considered^{44,49,55}. The O 1s peak centered at 532.6 eV was consistent with what was observed from the oxygen peak of aluminum oxide, in the absence of nitrogen in our studies. This finding is in line with the models proposed on the nature of oxygen distribution in AlN lattice. It has been shown that, in the concentration range of 6-16.8 at.%, oxygen takes the form of planes made up of double Al-O tetrahedra. These planes are dispersed in the lattice, and their frequency of appearance depends upon oxygen concentration⁵⁶⁻⁶⁰. Therefore, when at thermodynamic equilibrium, oxygen atoms are expected to solely bond to aluminum atoms, with bond lengths relatively unaffected by the surrounding AlN lattice.

AlN is a diatomic compound and features heteronuclear bonds, whose lattice vibrations change the associated electric dipoles. Therefore AlN is expected to be an infrared-active material with characteristic absorption bands^{61,62}. In order to study the Al-N bond, infrared spectroscopy was employed and Fig. 2.6 shows the Fourier-transformed mid-infrared spectrum of a 50-nm AlN film deposited on Si (111). This spectrum is the result of subtraction of the Si (111) wafer spectrum exposed to air from a 50-nm AlN film deposited on a Si (111) wafer, within an hour after the native oxide was removed by buffer oxide etch cleaning.

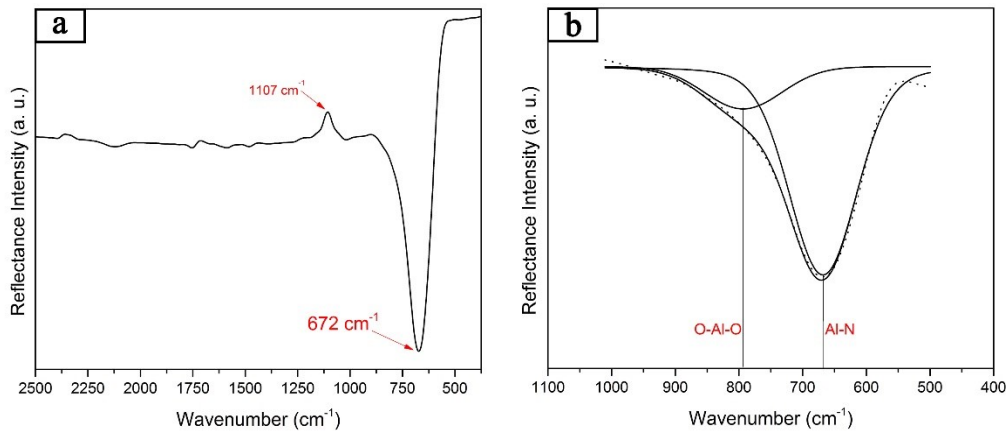


Figure 2.6: Fourier-transformed infrared spectrum of an AlN film deposited on Si (111) substrate taken in reflectance mode, b) Deconvolution of the peak centered at 672 cm^{-1} .

A major peak centered at 672 cm^{-1} can be observed. As seen, in addition to the baseline, the distribution of the peak itself shows asymmetry, with a tail on the high-energy side. A high-resolution scan of this peak is shown in Fig. 2.6b after baseline subtraction and deconvolution. Two Gaussian-Lorentzian subpeaks centered at 668 and 793 cm^{-1} can be observed. The subpeak at 668 cm^{-1} corresponds to the transverse optical phonon in the wurtzite AlN lattice^{63–67}. Several different

positions have been reported for this peak in the literature, as lattice strain and impurities shift the peak, due to their effect on the vibrational energy of the average Al-N bond. A narrow distribution of this subpeak indicates a well-defined network of Al-N bonds with a relatively uniform distribution of bond lengths. The obtained spectrum is comparable to what has been reported for AlN films deposited at higher temperatures⁶⁸ or annealed films⁶⁵.

It has been previously reported that inclusion of oxygen in AlN can lead to asymmetrical broadening of the Al-N transverse optical peak, owing to a contribution from the vibration in the Al-O bond^{69,70}. Al₂O₃ films have been reported to show broad features in the range of 500-850 cm⁻¹⁷¹. Colombari⁷² showed that the Al-O stretching vibration frequency depends on the coordination number of the aluminum ions. When aluminum ions are positioned in octahedral sites, the Al-O FTIR peak is in the range 500-600 cm⁻¹. On the other hand, tetrahedral coordination leads to peaks in the range of 750-850 cm⁻¹. Similar results have been reported by other researchers⁷³⁻⁷⁵. Therefore the observation of a subpeak at 793 cm⁻¹ indicates that oxygen ions are expected to be surrounded by aluminum ions in fourfold symmetry. This interpretation agrees with the literature on studies of how oxygen is expected to disperse inside the AlN wurtzite lattice at various concentrations^{56,76,77}. One observation supporting this interpretation is that no sign of the Al-O double-bond or the N-O bond was found in the spectrum.

The peak at 1107 cm⁻¹ is due to Si-O stretching vibrations⁷⁸. Considering the fact that silicon native oxide was removed prior to AlN deposition, this peak is not expected to appear in the AlN spectrum. However, when the silicon wafer was

measured to obtain a background spectrum, a 2-nm thick layer of native oxide had formed on the surface, giving rise to a Si-O peak. Subtraction of these two spectra left a peak with the opposite sign to those of Al-N and Al-O.

2.3.3. Optical Performance

Spectroscopic ellipsometry was used to evaluate the optical behavior of the films. The ellipsometry data were collected and analyzed both in-situ and post-deposition, in order to observe the post-deposition oxidation effects. The data were collected in the range of 193-1683 nm. The parametric semiconductor model, developed by Herzinger and Johs^{79,80} was used to describe the optical behavior of AlN. This model is known to be particularly effective in reproducing the optical properties of semiconductor systems that feature direct band gaps^{81,82}. In summary, the parametric semiconductor oscillator is the summation of several energy-bounded, Gaussian-broadened polynomial functions and a number of poles added to account for absorption outside the energy boundaries of the model. A total of two parametric semiconductor oscillators and one Gaussian oscillator were used for the AlN layer.

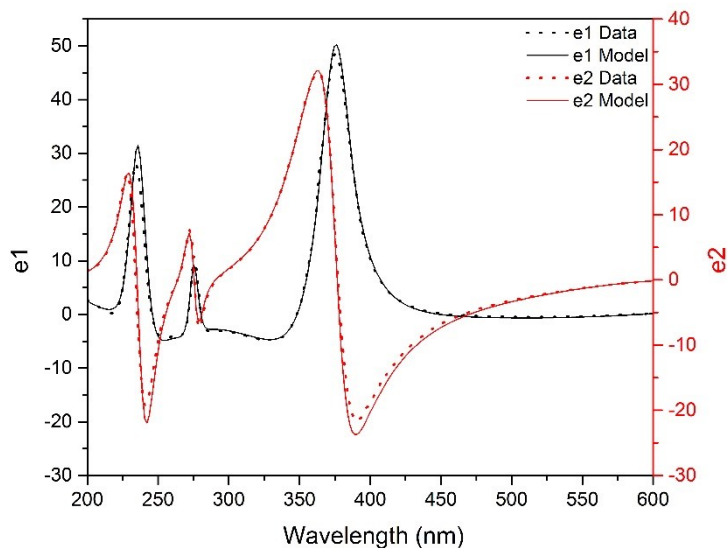


Figure 2.7: Variations of real and imaginary parts of the dielectric function in the wavelength range of 200-600 nm.

The post-deposition ellipsometry data are shown in Figs. 2.7-8. What is meant by post-deposition is that the films were exposed to air for at least twenty four hours prior to ellipsometry data collection. As confirmed by XPS and discussed earlier, the surface of these films are heavily oxidized. As a result, any treatment of these films as those with a homogeneous composition is physically inaccurate, regardless of how good the fit is. In order to account for this factor, and optically analyze the oxide overlayer, a multilayer structure was developed, in which aluminum nitride sits on top of the silicon substrate, followed by aluminum oxide. A transition layer was defined between the oxide and nitride layer, to simulate the gradual decrease in the oxygen content. A layer representing the surface roughness was placed on top. This layer was a mixture of the underlying layer and voids. The thickness of all the layers were considered to be fit parameters, along with a total of seventeen internal parameters for AlN.

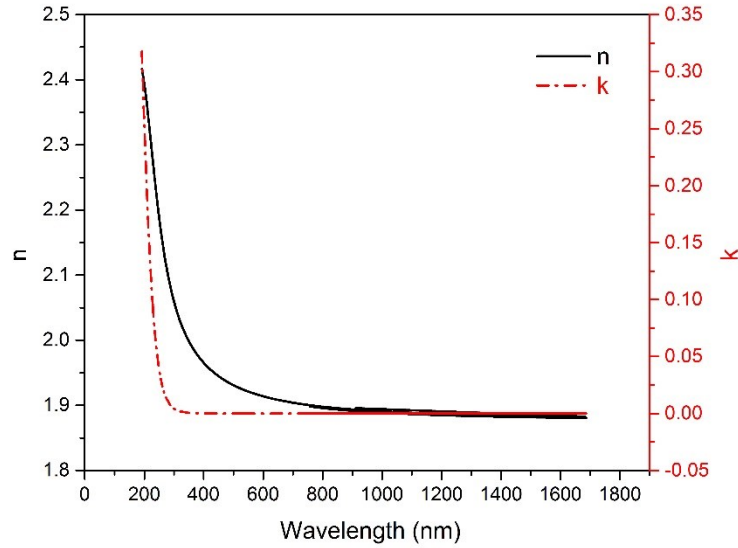


Figure 2.8: The derived values of refractive index and absorption coefficient.

The real and imaginary parts of the pseudo-dielectric function, ϵ_1 and ϵ_2 , of the final structure are shown in Fig. 2.7, and compared with the measured data. The graph shows a wavelength range, where the most noticeable variations in the dielectric function are observed. It is evident that the behavior of the constructed multilayer model closely matches that of the film. The final fit of the parameters suggests that the thickness of the pure aluminum oxide layer is zero, whereas the transition layer is ~ 5 nm. Fig. 2.8 shows the values of refractive index and absorption coefficient of the AlN layer. The value of refractive index at 632 nm is 1.96, compared to 2.15 for the bulk AlN⁸³. If one applies the Bruggeman effective medium approximation to these values, a density of 2.96 gcm^{-3} is achieved, which is close to what was obtained from XRR. The inherent porosity of the film, in conjunction with the contribution from the oxygen impurity are likely to be responsible for the refractive index being lower than the bulk value.

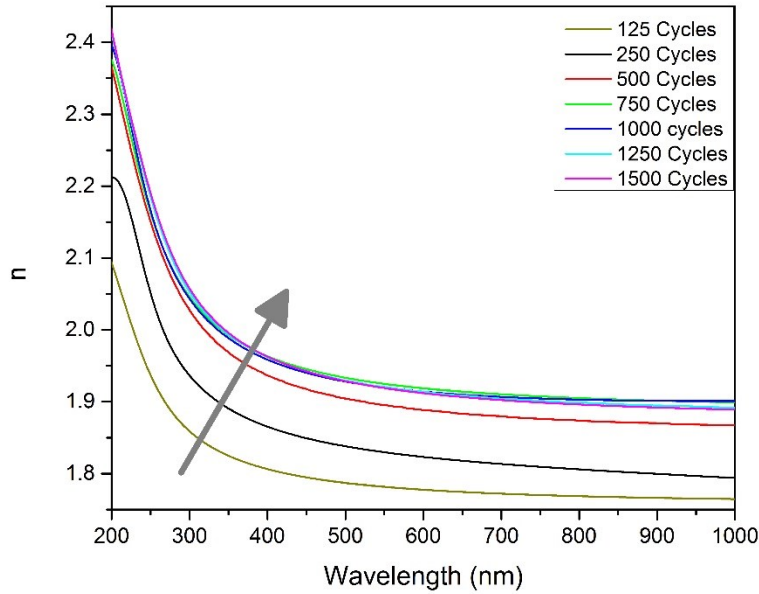


Figure 2.9: Variations of refractive index of AlN as a function of wavelength, for different numbers of deposition cycles.

In-situ ellipsometry is a versatile tool for the optical evaluation of ALD films during the growth where the measurements are performed at the deposition temperature. Since the refractive index of AlN changes little in this temperature range⁸⁴ in-situ measurements can be compared to room temperature data. Fig. 2.9 shows the variations of the refractive index as a function of wavelength for different number of deposition cycles. The refractive index depends upon the thickness of the AlN film and increasing the thickness leads to higher refractive index. In order to better illustrate these variations, the values of refractive index have been plotted as a function of thickness for three representative wavelengths, and shown in Fig. 2.10. As indicated by the exponential regression of the data, the refractive index change with thickness is large at the beginning, but levels off above 30 nm. The dependence of refractive index on the thickness of the films has been reported for

various semiconductors^{85–89} and this observation has been usually associated with increasing crystallite size.

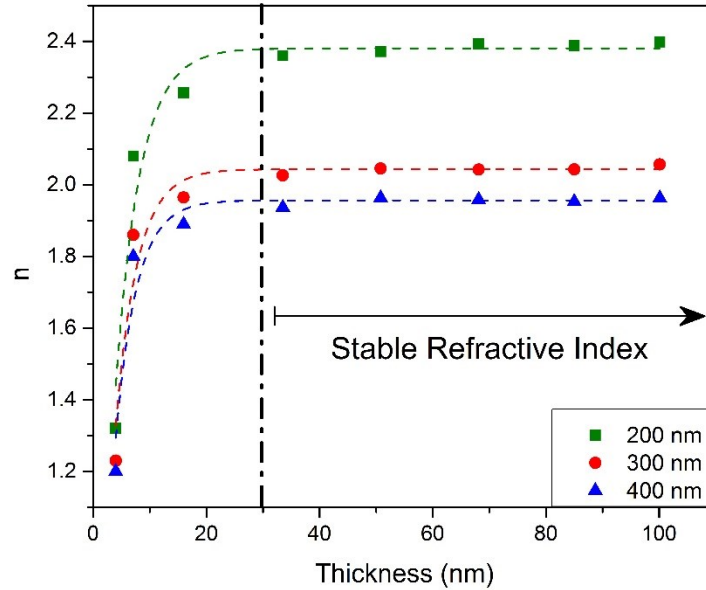


Figure 2.10: Values of the refractive index at three representative wavelengths, as a function of the film thickness; the region with a stable refractive index has been marked.

At photon energies close to the band gap, semiconductors with direct band gaps follow Eq. (2.1), known as Tauc plot^{90,91}. In this equation $\alpha = 4\pi k/\lambda$ is the absorption coefficient and k is the extinction coefficient. When the left hand side of this equation is plotted versus the photon energy, and a tangent is drawn to the linear section, the intercept of this tangent with the x-axis estimates the optical band gap. Fig. 2.11 demonstrates this procedure for three films with varying thicknesses. It is clear that, similar to refractive index, the optical band gap also depends on the film thickness. For the three films shown in Fig. 2.11, the band gap increases from 5.77 eV to 6.03 eV, as the thickness increases from 4 nm to 16 nm. Fig. 2.12 shows the trend of these changes for a wider range of thicknesses and it can be seen that

the value of the band gap levels off at ~ 6.04 eV for thickness >15 nm, which is close to the bulk value of 6.11 eV⁹².

$$(\alpha h\nu)^2 \propto (E - E_g) \quad (2.1)$$

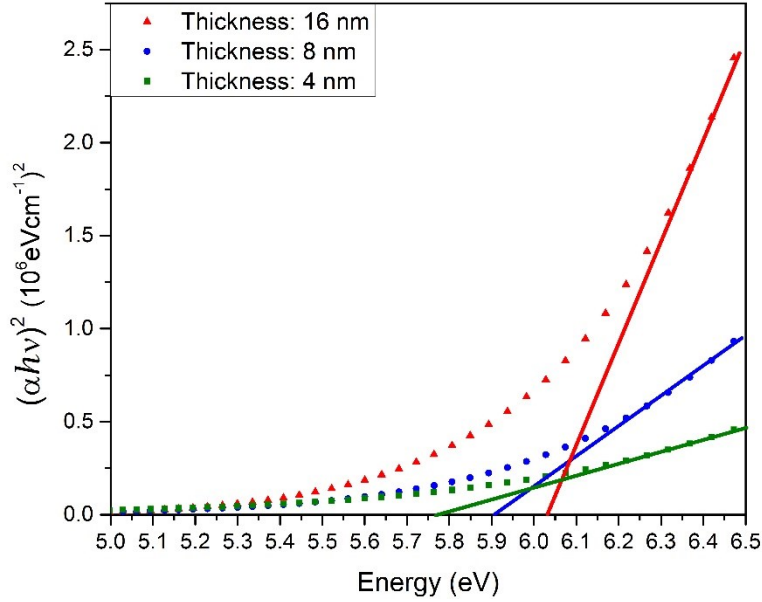


Figure 2.11: Demonstration of applying Tauc method for extraction of the optical band gap for films of different thicknesses.

The observations of thickness-dependent optical band gap has been reported for other semiconductors^{86–89,93–96}. In the case of CdSe, a decrease of 0.6 eV in optical band gap energy has been observed as the thickness increases from 250 nm to 400 nm⁸⁶. For CdS, reportedly, an increase in thickness from 40 to 113 nm results in band gap decreasing from 2.88 to 2.61 eV⁸⁹. Goh et al.⁸⁸ have reported that the optical parameters of Ge films reach stability only after 20-nm thickness is surpassed⁸⁸, whereas CuInS₂ films do not stabilize until a thickness of 200 nm is reached⁹⁴.

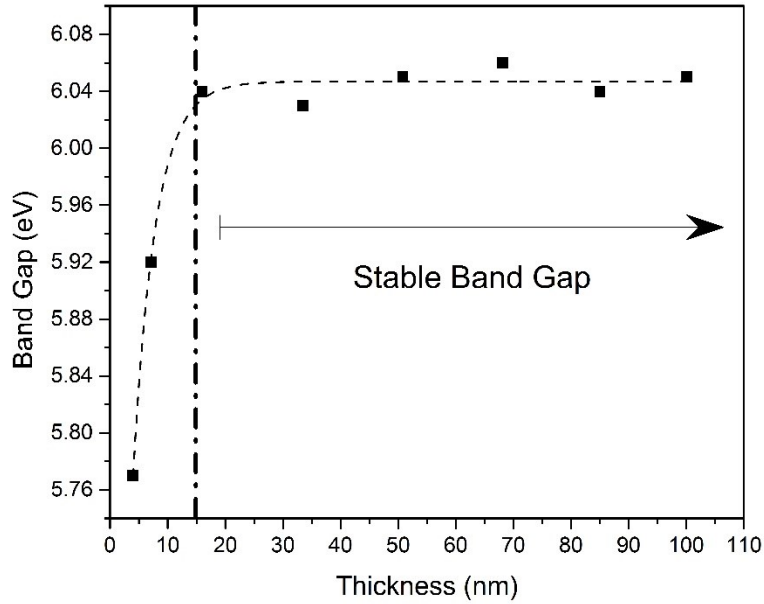


Figure 2.12: Plot of optical band gap vs. thickness for AlN; the region with a stable optical band gap has been marked.

Quantum confinement and the discrete nature of the energy spectrum of a two-dimensional system is the major reason that in extremely thin films (<15 nm) the band gap depends on thickness⁹⁷. Further variations beyond this thickness are the results of changes in crystal order and the average interatomic distance^{86,89,93,98,99}. The fact that no changes in band gap beyond 15 nm is observed in AlN thin films indicates that the essential metrics of crystal order are unchanged. This wide range of band gap stability is not common among PVD or CVD thin films, and has interesting engineering implications. On the other hand, the observation that the optical band gap is less than the bulk value, must be attributed to a variety of crystal defects, which may induce intermediate energy levels that merge with the conduction band, and lower the band gap¹⁰⁰.

2.4 Conclusions

Deposition of low-temperature crystalline aluminum nitride through atomic layer deposition has been reported. Extensive structural and optical characterization has been performed, to get an accurate assessment of the quality of the films. The thickness and density of the films were probed using X-ray reflectometry, and a value of 94% of the bulk density was obtained. Grazing incidence X-ray diffraction revealed that the films are crystalline with the wurtzite structure, and have a (100) preferred orientation. XPS studies showed that the films have oxygen impurities, but are low in carbon. XPS and FTIR, in combination, revealed that oxygen atoms are exclusively bonded to aluminum, and no sign of AlON compounds was detected.

In-situ and post-deposition spectroscopic ellipsometry was employed to study the optical performance of the films. A parametric semiconductor model precisely predicted the variations in the complex dielectric function. It was revealed that the refractive index varies with thickness, below 30 nm. Similarly, the optical band gap reaches a plateau after 15 nm. In summary, stable, thickness-independent optical performance was demonstrated, while the optical parameters were comparable to those of aluminum nitride films deposited at considerably higher temperatures.

References

- (1) Hardy, M. T.; Feezell, D. F.; DenBaars, S. P.; Nakamura, S. Group III-Nitride Lasers: A Materials Perspective. *Mater. Today* 2011, 14, 408–415.

- (2) Khan, A.; Balakrishnan, K.; Katona, T. Ultraviolet Light-Emitting Diodes Based on Group Three Nitrides. *Nat. Photonics* 2008, 2, 77–84.
- (3) Tsubouchi, K.; Mikoshiba, N. Zero-Temperature-Coefficient SAW Devices on AlN Epitaxial Films. *IEEE Trans. Sonics Ultrason.* 1985, SU-32, 634–644.
- (4) Clement, M.; Vergara, L.; Sangrador, J.; Iborra, E.; Sanz-Hervás, a. SAW Characteristics of AlN Films Sputtered on Silicon Substrates. *Ultrasonics* 2004, 42, 403–407.
- (5) Tonisch, K.; Cimalla, V.; Foerster, C.; Romanus, H.; Ambacher, O.; Dontsov, D. Piezoelectric Properties of Polycrystalline AlN Thin Films for MEMS Application. *Sensors Actuators A Phys.* 2006, 132, 658–663.
- (6) Bjurström, J.; Wingqvist, G.; Katardjiev, I. Synthesis of Textured Thin Piezoelectric AlN Films with a Nonzero c-Axis Mean Tilt for the Fabrication of Shear Mode Resonators. *IEEE Trans. Ultrason. Ferroelectr. Freq. Control* 2006, 53, 2095–2100.
- (7) Aubert, T.; Elmazria, O.; Assouar, B.; Blampain, E.; Hamdan, A.; Genève, D.; Weber, S. Investigations on AlN/sapphire Piezoelectric Bilayer Structure for High-Temperature SAW Applications. *IEEE Trans. Ultrason. Ferroelectr. Freq. Control* 2012, 59, 999–1005.
- (8) Aubert, T.; Elmazria, O.; Assouar, B.; Bouvot, L.; Oudich, M. Surface Acoustic Wave Devices Based on AlN/sapphire Structure for High Temperature Applications. *Appl. Phys. Lett.* 2010, 96, 203503.
- (9) Sahyoun, W.; Duchamp, J. Nonlinearities of AlN in Coupled Resonator Filters for High RF Power Levels. *IEEE Trans. Ultrason. Ferroelectr. Freq. Control* 2011, 58, 2162–2170.
- (10) Shen, L.; Heikman, S.; Moran, B.; Coffie, R.; Zhang, N.-Q.; Buttari, D.; Smorchkova, I. P.; Keller, S.; DenBaars, S. P.; Mishra, U. K. AlGaIn/AlN/GaN High-Power Microwave HEMT. *IEEE Electron Device Lett.* 2001, 22, 457–459.

- (11) Wu, J.; Walukiewicz, W. Band Gaps of InN and Group III Nitride Alloys. *Superlattices Microstruct.* 2003, 34, 63–75.
- (12) Yin, Z.; Tang, X. A Review of Energy Bandgap Engineering in III–V Semiconductor Alloys for Mid-Infrared Laser Applications. *Solid. State. Electron.* 2007, 51, 6–15.
- (13) Wang, L.; Pu, Y.; Chen, Y. F.; Mo, C. L.; Fang, W. Q.; Xiong, C. B.; Dai, J. N.; Jiang, F. Y. MOCVD Growth of ZnO Films on Si(111) Substrate Using a Thin AlN Buffer Layer. *J. Cryst. Growth* 2005, 284, 459–463.
- (14) Kung, P.; Zhang, X.; Bigan, E.; Razeghi, M. Low Pressure Metalorganic Chemical Vapor Deposition of High Quality AlN and GaN Thin Films on Sapphire and Silicon Substrates Patrick. In *Proc. SPIE 2397, Optoelectronic Integrated Circuit Materials, Physics, and Devices*; 1995; Vol. 2397, pp. 311–320.
- (15) Vispute, R. D.; Narayan, J.; Wu, H.; Jagannadham, K. Epitaxial Growth of AlN Thin Films on Silicon (111) Substrates by Pulsed Laser Deposition. *J. Appl. Phys.* 1995, 77, 4724.
- (16) Sanchez-Garcia, M. a.; Calleja, E.; Monroy, E.; Sanchez, F. J.; Calle, F.; Muñoz, E.; Beresford, R. The Effect of the III/V Ratio and Substrate Temperature on the Morphology and Properties of GaN- and AlN-Layers Grown by Molecular Beam Epitaxy on Si(1 1 1). *J. Cryst. Growth* 1998, 183, 23–30.
- (17) Ishihara, M.; Li, S. .; Yumoto, H.; Akashi, K.; Ide, Y. Control of Preferential Orientation of AlN Films Prepared by the Reactive Sputtering Method. *Thin Solid Films* 1998, 316, 152–157.
- (18) Profijt, H. B.; Potts, S. E.; van de Sanden, M. C. M.; Kessels, W. M. M. Plasma-Assisted Atomic Layer Deposition: Basics, Opportunities, and Challenges. *J. Vac. Sci. Technol. A Vacuum, Surfaces, Film.* 2011, 29, 050801.
- (19) George, S. M. Atomic Layer Deposition: An Overview. *Chem. Rev.* 2010, 110, 111–131.

- (20) Johnson, R. W.; Hultqvist, A.; Bent, S. F. A Brief Review of Atomic Layer Deposition: From Fundamentals to Applications. *Mater. Today* 2014, 17, 236–246.
- (21) Liu, G.; Deguns, E. W.; Lecordier, L.; Sundaram, G.; Becker, J. S. Atomic Layer Deposition of AlN with Tris(Dimethylamido)aluminum and NH₃. *ECS Trans.* 2011, 41, 219–225.
- (22) Longrie, D.; Deduytsche, D.; Haemers, J.; Driesen, K.; Detavernier, C. A Rotary Reactor for Thermal and Plasma-Enhanced Atomic Layer Deposition on Powders and Small Objects. *Surf. Coatings Technol.* 2012, 213, 183–191.
- (23) Alevli, M.; Ozgit, C.; Donmez, I.; Biyikli, N. Structural Properties of AlN Films Deposited by Plasma-Enhanced Atomic Layer Deposition at Different Growth Temperatures. *Phys. Status Solidi* 2012, 209, 266–271.
- (24) Lee, Y. J.; Kang, S. Growth of Aluminum Nitride Thin Films Prepared by Plasma-Enhanced Atomic Layer Deposition. *Thin Solid Films* 2004, 446, 227–231.
- (25) Liu, X.; Ramanathan, S.; Lee, E.; Seidel, T. E. Atomic Layer Deposition of Aluminum Nitride Thin Films from Trimethyl Aluminum (TMA) and Ammonia. In *Materials Research Society Symposium*; 2004; Vol. 811, pp. 1–6.
- (26) Dendooven, J.; Deduytsche, D.; Musschoot, J.; Vanmeirhaeghe, R. L.; Detavernier, C. Conformality of Al₂O₃ and AlN Deposited by Plasma-Enhanced Atomic Layer Deposition. *J. Electrochem. Soc.* 2010, 157, G111–G116.
- (27) Kim, O. H.; Kim, D.; Anderson, T. Atomic Layer Deposition of GaN Using GaCl₃ and NH₃. *J. Vac. Sci. Technol. A Vacuum, Surfaces, Film.* 2009, 27, 923.
- (28) Bosund, M.; Sajavaara, T.; Laitinen, M.; Huhtio, T.; Putkonen, M.; Airaksinen, V.-M.; Lipsanen, H. Properties of AlN Grown by Plasma Enhanced Atomic Layer Deposition. *Appl. Surf. Sci.* 2011, 257, 7827–7830.
- (29) Ozgit-Akgun, C.; Goldenberg, E.; Okyay, A. K.; Biyikli, N. Hollow Cathode Plasma-Assisted Atomic Layer Deposition of Crystalline AlN, GaN and Al_xGa_{1-x}N Thin Films at Low Temperatures. *J. Mater. Chem. C* 2014, 2, 2123.

- (30) Lei, W.; Chen, Q. Crystal AlN Deposited at Low Temperature by Magnetic Field Enhanced Plasma Assisted Atomic Layer Deposition. *J. Vac. Sci. Technol. A Vacuum, Surfaces, Film.* 2013, 31, 01A114.
- (31) Alevli, M.; Ozgit, C.; Donmez, I.; Biyikli, N. The Influence of N₂/H₂ and Ammonia N Source Materials on Optical and Structural Properties of AlN Films Grown by Plasma Enhanced Atomic Layer Deposition. *J. Cryst. Growth* 2011, 335, 51–57.
- (32) Venkataraj, S.; Severin, D.; Drese, R.; Koerfer, F.; Wuttig, M. Structural, Optical and Mechanical Properties of Aluminium Nitride Films Prepared by Reactive DC Magnetron Sputtering. *Thin Solid Films* 2006, 502, 235–239.
- (33) Kalisch, H.; Heuken, M.; Vescan, A.; Trampert, A. Formation of a Monocrystalline, M-Plane AlN Layer by the Nitridation of Γ -LiAlO₂(100). *Appl. Phys. Express* 2012, 105501.
- (34) Chason, E.; Mayer, T. M. Thin Film and Surface Characterization by Specular X-Ray Reflectivity. *Crit. Rev. Solid State Mater. Sci.* 1997, 22, 1–67.
- (35) Wormington, M.; Panaccione, C.; Matney, K. M.; Bowen, D. K. Characterization of Structures from X-Ray Scattering Data Using Genetic Algorithms. *Philos. Trans. R. Soc. A Math. Phys. Eng. Sci.* 1999, 2827–2848.
- (36) Powder Diffraction File 03-065-3409, International Center for Diffraction Data, PDF-2/Release 2007.
- (37) Ozgit, C.; Donmez, I.; Alevli, M.; Biyikli, N. Self-Limiting Low-Temperature Growth of Crystalline AlN Thin Films by Plasma-Enhanced Atomic Layer Deposition. *Thin Solid Films* 2012, 520, 2750–2755.
- (38) Jose, F.; Ramaseshan, R.; Dash, S.; Bera, S.; Tyagi, a K.; Raj, B. Response of Magnetron Sputtered AlN Films to Controlled Atmosphere Annealing. *J. Phys. D. Appl. Phys.* 2010, 43, 075304.
- (39) García-Méndez, M.; Morales-Rodríguez, S.; Shaji, S.; Krishnan, B.; Bartolo-Pérez, P. Structural Properties of Aln Films with Oxygen Content

Deposited by Reactive Magnetron Sputtering: XRD and XPS Characterization. *Surf. Rev. Lett.* 2011, 18, 23–31.

(40) Iriarte, G. F.; Reyes, D. F.; González, D.; Rodríguez, J. G.; García, R.; Calle, F. Influence of Substrate Crystallography on the Room Temperature Synthesis of AlN Thin Films by Reactive Sputtering. *Appl. Surf. Sci.* 2011, 257, 9306–9313.

(41) Wang, C. C.; Chiu, M. C.; Shiao, M. H.; Shieu, F. S. Characterization of AlN Thin Films Prepared by Unbalanced Magnetron Sputtering. *J. Electrochem. Soc.* 2004, 151, F252.

(42) Jin, H.; Zhou, J.; Dong, S. R.; Feng, B.; Luo, J. K.; Wang, D. M.; Milne, W. I.; Yang, C. Y. Deposition of c-Axis Orientation Aluminum Nitride Films on Flexible Polymer Substrates by Reactive Direct-Current Magnetron Sputtering. *Thin Solid Films* 2012, 520, 4863–4870.

(43) Takikawa, H.; Kimura, K.; Miyano, R.; Sakakibara, T.; Bendavid, A.; Martin, P. J.; Matsumuro, A.; Tsutsumi, K. Effect of Substrate Bias on AlN Thin Film Preparation in Shielded Reactive Vacuum Arc Deposition. *Thin Solid Films* 2001, 386, 276–280.

(44) Chen, D.; Xu, D.; Wang, J.; Zhang, Y. Investigation of Chemical Etching of AlN Film with Different Textures by X-Ray Photoelectron Spectroscopy. *J. Phys. D. Appl. Phys.* 2008, 41, 235303.

(45) Yao, Z. Q.; Li, Y. Q.; Tang, J. X.; Zhang, W. J.; Lee, S. T. Growth and Photoluminescence Studies of AlN Thin Films with Different Orientation Degrees. *Diam. Relat. Mater.* 2008, 17, 1785–1790.

(46) Wang, J.; Chen, D.; Xu, Y.; Liu, Q.; Zhang, L. Influence of the Crystal Texture on Raman Spectroscopy of the AlN Films Prepared by Pulse Laser Deposition. *J. Spectrosc.* 2013, 2013, 1–6.

(47) Motamedi, P.; Cadien, K. XPS Analysis of AlN Thin Films Deposited by Plasma Enhanced Atomic Layer Deposition. *Appl. Surf. Sci.* 2014, 315, 104–109.

- (48) Liao, H. M. Surface Composition of AlN Powders Studied by X-Ray Photoelectron Spectroscopy and Bremsstrahlung-Excited Auger Electron Spectroscopy. *J. Vac. Sci. Technol. A Vacuum, Surfaces, Film.* 1993, 11, 2681.
- (49) Zhang, Y. Characterization of as-Received Hydrophobic Treated AlN Powder Using XPS. *J. Mater. Sci. Lett.* 2002, 21, 1603–1605.
- (50) Youngman, R. A.; Harris, J. H. Luminescence Studies of Oxygen-Related Defects in Aluminum Nitride. *J. Am. Ceram. Soc.* 1990, 46, 3238–3246.
- (51) Kazan, M.; Rufflé, B.; Zgheib, C.; Masri, P. Oxygen Behavior in Aluminum Nitride. *J. Appl. Phys.* 2005, 98, 103529.
- (52) Rosenberger, L.; Baird, R.; McCullen, E.; GregoryAuner; Shreve, G. XPS Analysis of Aluminum Nitride Films Deposited by Plasma Source Molecular Beam Epitax. *Surf. Interface Anal.* 2008, 40, 1254–1261.
- (53) Naik, R. S.; Reif, R.; Lutsky, J. J.; Sodini, C. G. Low-Temperature Deposition of Highly Textured Aluminum Nitride by Direct Current Magnetron Sputtering for Applications in Thin-Film Resonators. *J. Electrochem. Soc.* 1999, 146, 691–696.
- (54) García Molleja, J.; Gómez, B. J.; Ferrón, J.; Gautron, E.; Bürgi, J.; Abdallah, B.; Djouadi, M. A.; Feugeas, J.; Jouan, P.-Y. AlN Thin Films Deposited by DC Reactive Magnetron Sputtering: Effect of Oxygen on Film Growth. *Eur. Phys. J. Appl. Phys.* 2013, 64, 20302.
- (55) Gredelj, S.; Gerson, A. R.; Kumar, S.; Cavallaro, G. P. Characterization of Aluminium Surfaces with and without Plasma Nitriding by X-Ray Photoelectron Spectroscopy. *Appl. Surf. Sci.* 2001, 174, 240–250.
- (56) Harris, J. H.; Youngman, R. A.; Teller, R. G. On the Nature of the Oxygen-Related Defect in Aluminum Nitride. *J. Mater. Res.* 1990, 44128, 1763–1773.
- (57) Slack, G. A. Nonmetallic Crystals with High Thermal Conductivity. *J. Phys. Chem. Solids* 1973, 34, 321–335.

- (58) Brien, V.; Pigeat, P. Correlation between the Oxygen Content and the Morphology of AlN Films Grown by R.f. Magnetron Sputtering. *J. Cryst. Growth* 2008, 310, 3890–3895.
- (59) Mccauley, J. W.; Krishnan, K. M.; Rai, R. S.; Thomas, G. Anion-Controlled Microstructures in the AlN-Al₂O₃ System. In *Ceramic Microstructures '86*; Pask; Evans, Eds.; Plenum Publishing Corporation, 1988; pp. 577–590.
- (60) Sakai, T. Hot-Pressing of the AlN-Al₂O₃ System. *J. Ceram. Assoc. Japan* 1978, 86, 125–130.
- (61) Stuart, B. *Infrared Spectroscopy: Fundamentals and Application*; Wiley, 2004.
- (62) Tolstoy, V. P.; Skryshevsky, I. V. C. V. A. *Handbook of Infrared Spectroscopy of Ultrathin Films*; Wiley-Interscience Publication, 2003.
- (63) Collins, A. T.; Lightowers, E. C.; Dean, P. J. Lattice Vibration Spectra of Aluminum Nitride. *Phys. Rev.* 1967, 158, 833–838.
- (64) Balasubramanian, C.; Bellucci, S.; Cinque, G.; Marcelli, a; Guidi, M. C.; Piccinini, M.; Popov, a; Soldatov, a; Onorato, P. Characterization of Aluminium Nitride Nanostructures by XANES and FTIR Spectroscopies with Synchrotron Radiation. *J. Phys. Condens. Matter* 2006, 18, S2095–S2104.
- (65) Kar, J. P.; Bose, G.; Tuli, S. Influence of Rapid Thermal Annealing on Morphological and Electrical Properties of RF Sputtered AlN Films. *Mater. Sci. Semicond. Process.* 2005, 8, 646–651.
- (66) Pobedinskas, P.; Ruttens, B.; D'Haen, J.; Haenen, K. Optical Phonon Lifetimes in Sputtered AlN Thin Films. *Appl. Phys. Lett.* 2012, 100, 191906.
- (67) Hobert, H.; Dunken, H. H.; Meinschien, J.; Stafast, H. Infrared and Raman Spectroscopic Investigation of Thin Films of AlN and SiC on Si Substrates. *Vib. Spectrosc.* 1999, 19, 205–211.

- (68) Kuchibhatla, S.; Rodak, L. E.; Korakakis, D. Fourier Transform Infrared Spectroscopy Characterization of AlN Thin Films Grown on Sacrificial Silicon Oxide Layers via Metal Organic Vapor Phase Epitaxy. *Thin Solid Films* 2010, 519, 117–121.
- (69) Kazan, M.; Rufflé, B.; Zgheib, C.; Masri, P. Oxygen Behavior in Aluminum Nitride. *J. Appl. Phys.* 2005, 98, 103529.
- (70) Hanada, T.; Kobayashi, M.; Tanabe, S.; Soga, N. Preparation and Physical Properties of Rf-Sputtered Amorphous Films in the Al₂O₃-AlN System. *J. Non. Cryst. Solids* 1991, 135, 227–235.
- (71) Katamreddy, R.; Inman, R.; Jursich, G.; Soulet, A.; Nicholls, A.; Takoudis, C. Post Deposition Annealing of Aluminum Oxide Deposited by Atomic Layer Deposition Using Tris(diethylamino)aluminum and Water Vapor on Si(100). *Thin Solid Films* 2007, 515, 6931–6937.
- (72) Colomban, P. Structure of Oxide Gels and Glasses by Infrared and Raman Scattering. *J. Mater. Sci.* 1989, 24, 3002–3010.
- (73) Mazza, D.; Vallino, M.; Busca, G.; Chimica, I.; Ingegneria, F. Mullite-Type Structures in the Systems Al₂O₃-Me₂O (Me = Na, K) and Al₂O₃-B₂O₃. *J. Am. Ceram. Soc.* 1992, 34, 1929–1934.
- (74) McMillan, P.; Piriou, B. The Structures and Vibrational Spectra of Crystals and Glasses in the Silica-Alumina System. *J. Non. Cryst. Solids* 1982, 53, 279–298.
- (75) Padmaja, P.; Anilkumar, G. .; Mukundan, P.; Aruldas, G.; Warriar, K. G. . Characterisation of Stoichiometric Sol-gel Mullite by Fourier Transform Infrared Spectroscopy. *Int. J. Inorg. Mater.* 2001, 3, 693–698.
- (76) Tendeloo, G. Van; Faber, K. T.; Thomas, G. Characterization of AlN Ceramics Containing Long-Period Polytypes. *J. Mater. Sci.* 1983, 18, 525–532.
- (77) Tabary, P.; Servant, C. Crystalline and Microstructure Study of the AlN–Al₂O₃ Section in the Al–N–O System. I. Polytypes and Γ -AlON Spinel Phase. *J. Appl. Crystallogr.* 1999, 32, 241–252.

- (78) Tian, R.; Seitz, O.; Li, M.; Hu, W. W.; Chabal, Y. J.; Gao, J. Infrared Characterization of Interfacial Si-O Bond Formation on Silanized Flat SiO₂/Si Surfaces. *Langmuir* 2010, 26, 4563–4566.
- (79) Herzinger, C. M.; Johs, B.; McGahan, W. a.; Woollam, J. a.; Paulson, W. Ellipsometric Determination of Optical Constants for Silicon and Thermally Grown Silicon Dioxide via a Multi-Sample, Multi-Wavelength, Multi-Angle Investigation. *J. Appl. Phys.* 1998, 83, 3323.
- (80) Herzinger, C. M.; Johs, B. D. Dielectric Function Parametric Model, And Method Of Use, 1998.
- (81) Ihn, Y. S.; Kim, T. J.; Ghong, T. H.; Kim, Y. D.; Aspnes, D. E.; Kossut, J. Parametric Modeling of the Dielectric Functions of Cd_{1-x}Mg_xTe Alloy Films. *Thin Solid Films* 2004, 455-456, 222–227.
- (82) Johs, B.; Herzinger, C. M.; Dinan, J. H.; Cornfeld, A.; Benson, J. D. Development of a Parametric Optical Constant Model for Hg_{1-x}Cd_xTe for Control of Composition by Spectroscopic Ellipsometry during MBE Growth. *Thin Solid Film.* 1998, 313-314, 137–142.
- (83) Bass, M.; DeCusatis, C.; Enoch, J.; Lakshminarayanan, V.; Li, G.; MacDonald, C.; Mahajan, V.; Stryland, E. Van. *Handbook of Optics, Third Edition Volume IV: Optical Properties of Materials, Nonlinear Optics, Quantum Optics;* McGraw Hill Professional, 2009; p. 1152.
- (84) Watanabe, N.; Kimoto, T.; Suda, J. The Temperature Dependence of the Refractive Indices of GaN and AlN from Room Temperature up to 515 °C. *J. Appl. Phys.* 2008, 104, 106101.
- (85) Chambouleyron, I.; Ventura, S. D.; Birgin, E. G.; Martínez, J. M. Optical Constants and Thickness Determination of Very Thin Amorphous Semiconductor Films. *J. Appl. Phys.* 2002, 92, 3093.
- (86) Akaltun, Y.; Yıldırım, M. A.; Ateş, A.; Yıldırım, M. The Relationship between Refractive Index-Energy Gap and the Film Thickness Effect on the

Characteristic Parameters of CdSe Thin Films. *Opt. Commun.* 2011, 284, 2307–2311.

(87) Das, N. S.; Ghosh, P. K.; Mitra, M. K.; Chattopadhyay, K. K. Effect of Film Thickness on the Energy Band Gap of Nanocrystalline CdS Thin Films Analyzed by Spectroscopic Ellipsometry. *Phys. E Low-dimensional Syst. Nanostructures* 2010, 42, 2097–2102.

(88) Goh, E. S. M.; Chen, T. P.; Sun, C. Q.; Liu, Y. C. Thickness Effect on the Band Gap and Optical Properties of Germanium Thin Films. *J. Appl. Phys.* 2010, 107, 024305.

(89) Kumar, S.; Kumar, S.; Sharma, P.; Sharma, V.; Katyal, S. C. CdS Nanofilms: Effect of Film Thickness on Morphology and Optical Band Gap. *J. Appl. Phys.* 2012, 112, 123512.

(90) Klingshirn, C. F. *Semiconductor Optics; Graduate Texts in Physics; Springer Berlin Heidelberg: Berlin, Heidelberg, 2012.*

(91) Tansley, T. L.; Foley, C. P. Optical Band Gap of Indium Nitride. *J. Appl. Phys.* 1986, 59, 3241.

(92) Li, J.; Nam, K. B.; Nakarmi, M. L.; Lin, J. Y.; Jiang, H. X.; Carrier, P.; Wei, S.-H. Band Structure and Fundamental Optical Transitions in Wurtzite AlN. *Appl. Phys. Lett.* 2003, 83, 5163.

(93) Reddy, R. S. Effect of Film Thickness on the Structural Morphological and Optical Properties of Nanocrystalline ZnO Films Formed by RF Magnetron Sputtering. *Adv. Mater. Lett.* 2012, 3, 239–245.

(94) Rabeh, M. Ben; Khedmi, N.; Fodha, M. a.; Kanzari, M. The Effect of Thickness on Optical Band Gap and N-Type Conductivity of CuInS₂ Thin Films Annealed in Air Atmosphere. *Energy Procedia* 2014, 44, 52–60.

(95) Rahal, A.; Benramache, S.; Benhaoua, B. The Effect of the Film Thickness and Doping Content of SnO₂:F Thin Films Prepared by the Ultrasonic Spray Method. *J. Semicond.* 2013, 34, 093003.

- (96) Ates, A.; Yıldırım, M. A.; Kundakcı, M.; Astam, A. Annealing and Light Effect on Optical and Electrical Properties of ZnS Thin Films Grown with the SILAR Method. *Mater. Sci. Semicond. Process.* 2007, 10, 281–286.
- (97) Gaponenko, S. V. *Optical Properties of Semiconductor Nanocrystals*; Cambridge University Press, 1998; p. 245.
- (98) Nair, M. T. .; Guerrero, L.; Arenas, O. L.; Nair, P. . Chemically Deposited Copper Oxide Thin Films: Structural, Optical and Electrical Characteristics. *Appl. Surf. Sci.* 1999, 150, 143–151.
- (99) Bao, D.; Yao, X.; Wakiya, N.; Shinozaki, K.; Mizutani, N. Band-Gap Energies of Sol-Gel-Derived SrTiO₃ Thin Films. *Appl. Phys. Lett.* 2001, 79, 3767.
- (100) Ealet, B.; Elyakhloufi, M. H.; Gillet, E.; Ricci, M. Electronic and Crystallographic Structure of Γ -Alumina Thin Films. *Thin Solid Films* 1994, 250, 92–100.

Chapter Three

XPS Analysis of AlN thin films deposited by plasma-enhanced atomic layer deposition

(Applied Surface Science, 2014 **315** 104-9)

3.1. Introduction

The wide band gap of AlN makes it a suitable candidate for several optoelectronic applications, including UV detectors and lasers. Moreover, excellent miscibility with similar III-N materials offers the potential of $\text{Al}_x\text{Ga}_y\text{In}_{(1-x-y)}\text{N}$ materials with adjustable band gap and lattice constant¹⁻⁵. Integration of AlN as a dielectric in GaN-based devices is an intriguing possibility facilitated by the low lattice mismatch (~2.4%) of the two wurtzite structures⁶. AlN can also be used in high power electronics due to its large dielectric breakdown field and high thermal conductivity⁷. The noncentrosymmetry of the AlN wurtzite unit cell causes intrinsic polarization, making it a good choice for piezoelectric sensors and actuators^{8,9}. The high velocity of surface acoustic waves (SAW) in AlN makes it a versatile material for various SAW devices, especially SAW receivers for harsh environments¹⁰⁻¹².

Atomic layer deposition (ALD) of AlN offers an attractive combination of advantages when compared to other deposition techniques such as metal-organic chemical vapor deposition and molecular beam epitaxy. Plasma-enhanced ALD (PEALD) of AlN can be accomplished at significantly lower temperatures, eliminating the problems associated with the difference in thermal expansion coefficient between the film and the substrate^{13,14}. In comparison to reactive sputtering, ALD offers excellent conformality and scale-up potential, combined with precise thickness control. All of these features make ALD a fitting choice for future device applications^{13,14}.

Current AlN ALD processes usually involve the use of halides or ammonia as precursors^{15–20}. The use of halides poses environmental risks, as well as possible equipment and product corrosion problems. In this study we used nitrogen plasma and trimethylaluminum as precursors, to address the present concerns. Using PEALD, compared to thermal processes, which use ammonia, has the intrinsic advantage of a lower deposition temperature window. On the other hand, using nitrogen plasma instead of ammonia allows for injecting the desired amount of hydrogen ions to the reactor as the reducing agent, and significantly lowers the concentration of unwanted partially ionized variants of ammonia. This increases the efficiency and decreases the minimum dose time of the plasma dose step.

Regardless of the choice of precursors, low temperature deposition of III-nitrides by ALD is known to have many difficulties. The films are often reported to be non-stoichiometric or contain a large amount of impurities, especially oxygen^{15,21–25}. In addition, a passive oxide layer is known to form on AlN, when it is exposed to air^{26,27}. The significant effect of oxygen impurity in AlN films has been demonstrated and investigated, especially for plasma processes^{17,20,28}. The structural variations of AlN containing different amounts of oxygen have also been extensively studied^{29–32}. It has also been demonstrated that small amounts of oxygen might significantly affect the electrical and optical properties of AlN^{31,33–35}. Although generally considered to be detrimental in nature, this phenomenon can also be exploited to effect desirable alterations in the AlN structure and properties, provided the exact chemical environment and lattice distribution of oxygen atoms are known.

In spite of the prevalence of the problem, few studies have tried to systematically investigate the nature of oxygen impurity in ALD III-nitride thin films. In this paper we focus on the evaluation of PEALD AlN films using X-ray photoelectron spectroscopy, XPS, with a particular emphasis on the bonding of oxygen impurities in AlN. The approaches presented here will be equally applicable to other nitride thin films.

3.2. Experimental Procedure

Depositions were carried out using a thin film deposition research system (ALD-150L, Kurt J. Lesker), which features thermal as well as remote plasma capabilities. Si (111) substrates were used for deposition. The substrates were cleaned with a standard buffered oxide etch cleaning procedure prior to deposition. During deposition the substrates were heated to 250°C. An in-situ spectroscopic ellipsometry apparatus by J. A. Woollam (M2000DI) allowed for precise control of the thickness.

Extensive experiments have been done to determine the optimal deposition parameters, and ensure they fall inside the limits of the ALD parameter window, and that the characteristic self-limiting regime of ALD deposition is achieved. The deposition consisted of four stages: 0.02s trimethylaluminum dose, 7s Ar gas purge, 10s N₂/H₂ (19:1) plasma, followed by another 7s Ar purge. The plasma power was set to 600W. The carrier gas flow rate for the precursor was 40 sccm. The flow rate of forming gas and its carrier gas (Ar) were 60 and 100 sccm, respectively. The growth rate was 0.068 nm/cycle, as determined by spectroscopic ellipsometry.

As explained later, for some samples metallic aluminum was coated on top of the PEALD AlN layer in order to protect the AlN and to permit the high resolution XPS spectrum of Al2p to be used as a reference. After ALD deposition these samples were transferred under high vacuum to an interconnected sputtering chamber where a 3-nm thick layer of aluminum was deposited via DC magnetron sputtering at 200W, 2mTorr and at room temperature.

A Kratos AXIS Ultra x-ray photoelectron spectroscopy (XPS) was used to study the chemical structure of the 50-nm thick films, using Al (1486.69eV) x-ray source at 50° incidence angle. Carbon 1s peak at 285 eV was used for calibration. An argon ion gun (4 keV) was used to probe the depth of the samples. The etch rate was experimentally determined to be ~2nm/min.

3.3. Results and Discussion

Fig. 3.1 shows the results of the XPS survey scans for an uncoated sample. As evident in Fig. 3.1a, aluminum and nitrogen are present at the surface. In addition, a considerable amount of carbon is observed, which is characteristic of uncleaned surfaces. The most noteworthy feature of this spectrum is the prominent oxygen peak, taller than those of aluminum and nitrogen. In order to calculate the atomic ratio of the four elements, high-resolution scans were performed on the areas around the peaks for O 1s, N 1s, C 1s, and Al 2p.

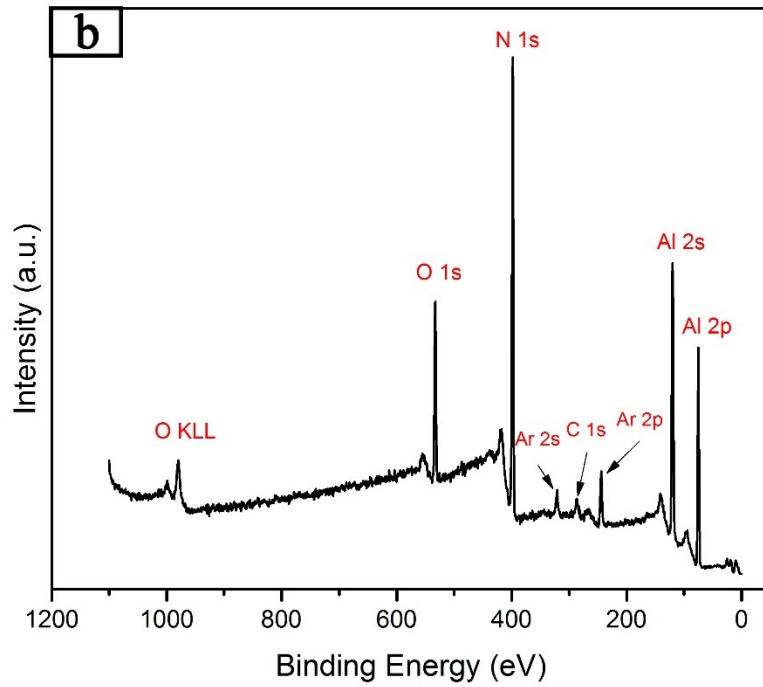
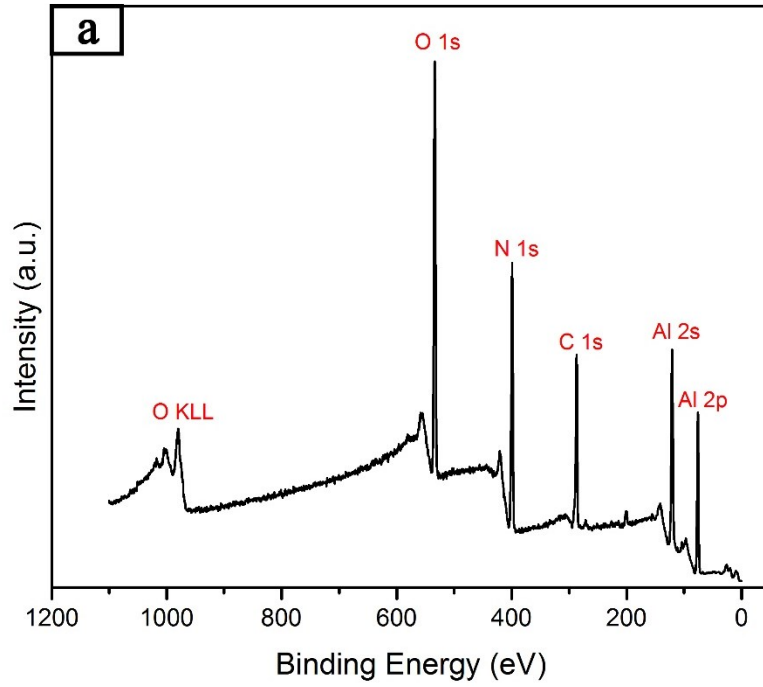


Figure 3.1: Survey scan of the uncoated sample a) before etching; b) after 20 minutes of etching.

Calculating the area under the four peaks, and applying the relative sensitivity factors of 2.930, 1.800, 1.000, and 0.537 for the above peaks in the mentioned order gives the atomic ratios reported in Table 3.1. As seen, equal amounts of oxygen and nitrogen exist at the surface. In Fig. 3.1b, the survey spectrum of the sample after 20 minutes of argon ion etching reveals three differences with Fig. 3.1a: 1) The carbon peak intensity has dropped to a very low value; 2) Oxygen peak shows a significant drop in intensity, yet still shows a noticeable presence; 3) Some argon atoms are embedded in the film, indicating argon is being implanted by the sputter cleaning process. Following the procedure described above, the atomic ratio of the four elements has been calculated and reported in Table 3.1.

Table 3.1: Chemical composition of the samples at various depths, as determined by high-resolution scans

Sample	Condition	Al (at.%)	C (at.%)	N (at.%)	O (at.%)	Si (at.%)
AlN	As deposited	35.3	21.4	21.6	21.4	0.0
	20-min etch	51.9	3.4	35.5	9.1	0.0
AlN-Al	As deposited	41.7	23.2	2.5	32.6	0.0
	1-min etch	69.6	0.9	8.4	21.1	0.0
	20-0min etch	51.7	3.0	35.5	9.7	0.0

An important question concerns the nature of the oxygen impurity inside the film, as well as its possible chemical interaction with aluminum and nitrogen. A high resolution XPS scan of the Al 2p peak reveals the nature of the aluminum bonding.

Fig. 3.2 shows the comparison of the Al 2p peaks for the uncoated sample before and after 20 minutes of etching. The center of the peak shifts from 75.4 eV to 74.9 eV. It should be noted that the center of the C 1s peak was observed at 286.3 eV throughout all the readings, whenever carbon was detected. Thorough analysis of the two peaks requires their proper deconvolution into their constituents, i.e. metallic, oxide, and nitride subpeaks.

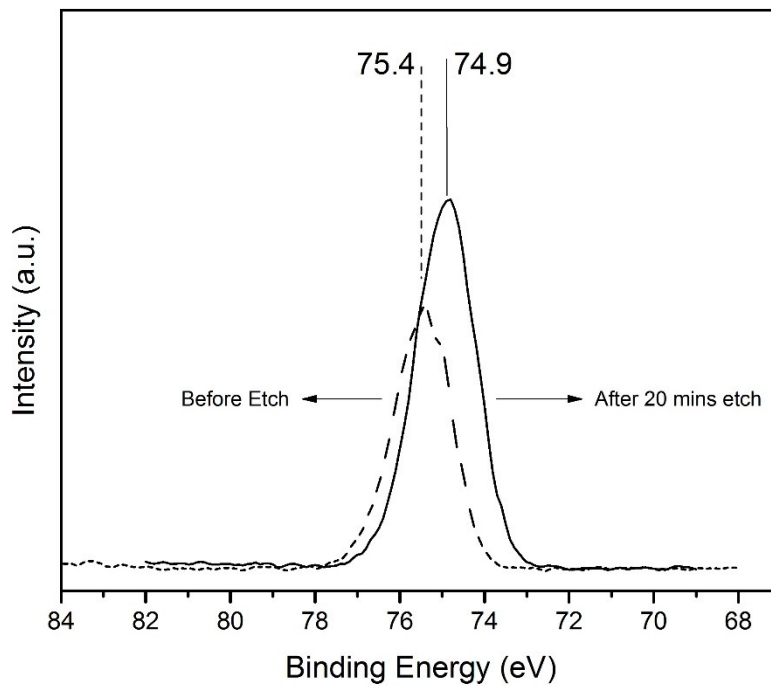


Figure 3.2: Comparison of the high resolution Al 2p peaks of the uncoated sample before and after 20 minutes of etching.

A survey of the literature reveals that although the difference between the values reported for the aforementioned peaks is relatively consistent, their exact positions vary, depending on experimental variables such as sample charging effects^{17,27,36-41}. Therefore, interpretation of the spectra is difficult and may lead to contradictory

conclusions. In order to reliably determine the precise position of the three subpeaks, a sample was deposited with the same PEALD recipe, and then coated with aluminum. The elemental analysis for the coated sample is reported in Table 3.1 which shows that the surface composition consists of aluminum, oxygen, and carbon, as expected. Metallic aluminum forms a stable oxide, 3-4 nm thick, when exposed to air ⁴². Since every nanometer of Al gives rise to 2.86 nm of Al₂O₃, approximately one third of the initial sputtered aluminum is expected to be left after formation of the native oxide. This method enables the use of the position of the metallic aluminum subpeak, as well as that of aluminum oxide, as references.

High-resolution XPS scans of the Al 2p peaks for the coated sample after 0, 1, and 20 minutes of etching are shown in Fig. 3.3. The surface spectrum (Fig. 3.3a) can be deconvolved into two Gaussian-Lorentzian subpeaks, centered at 73.0 eV and 75.6 eV. Considering the elemental analysis of the surface, these two subpeaks are assigned to metallic aluminum and aluminum oxide, respectively. Table 3.2 summarizes the values assigned to various peaks in this study, along with the corresponding reported values from the literature.

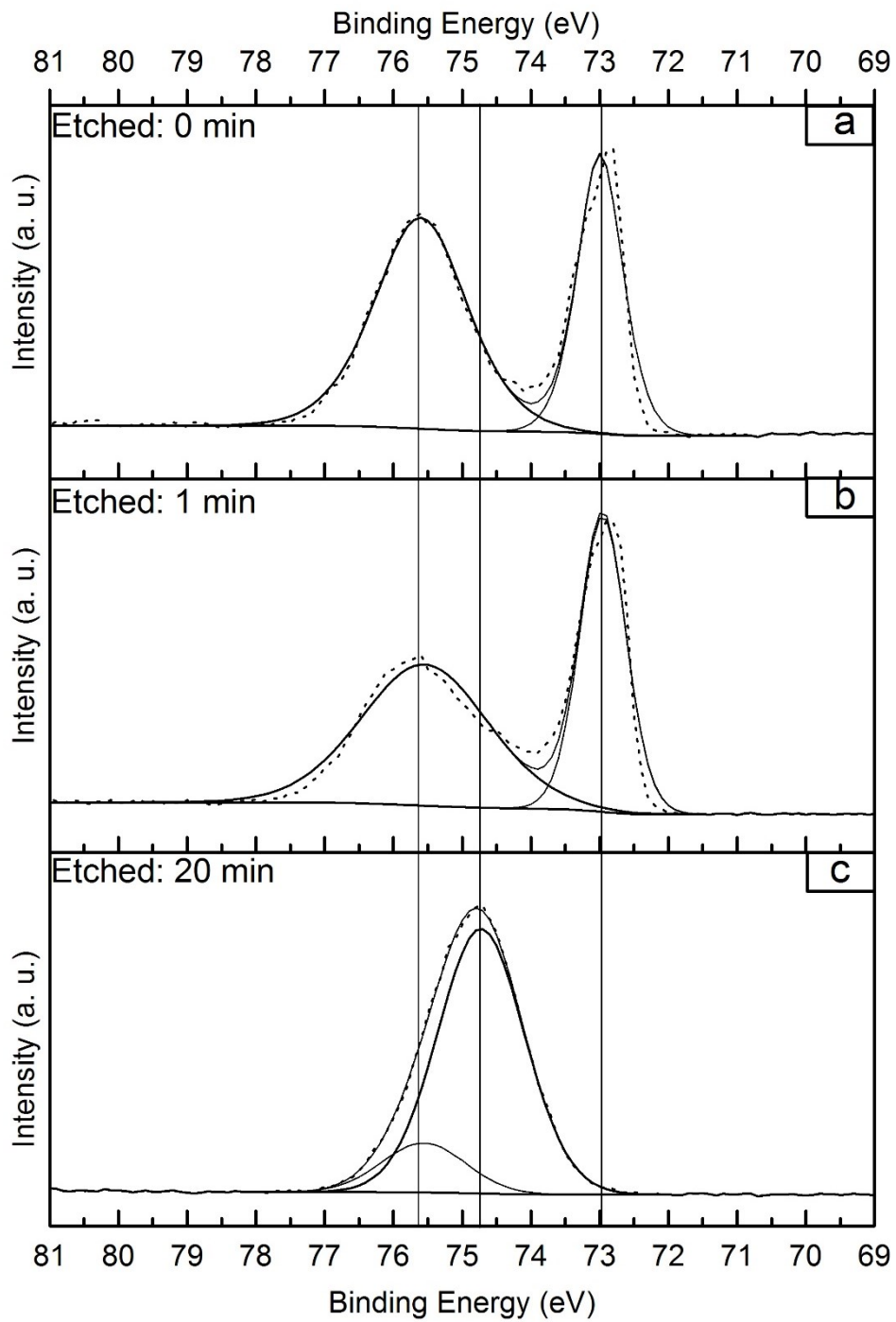


Figure 3.3: High resolution XPS AL 2p spectra of the Al-coated thin films a) before etching; b) after 1 minute of etching; c) after 20 minutes of etching.

Table 3.2: The observed atomic bonding at various sample depths and their corresponding electron subshell energies; the reported values in the literature have been offered for comparison

Chemical Bond	Observation depth	Subshell	Binding Energy (eV)	Previously Values*	Assigned
Al-Al	Sputtered layer	Al 2p	73.0	72.4 ¹⁷ 72.3 ²⁷ 72.4 ⁴³ 72.8 ³⁶ 72.8 ³⁷ 72.8 ³⁸	
		Al 2p	74.7	73.5 ¹⁷ 74.4 ²⁷ 74.7 ⁴³ 74.5 ³⁶ 74.1 ³⁷ 74.4 ³⁸ 74.3 ³⁹	
Al-N	ALD layer	N 1s	397.8	397.5 ²⁷ 396.8 ¹⁷ 397.9 ³⁶ 397.5 ⁴⁰ 397.3 ³⁹ 397.6 ⁴¹ 397.4 ³⁸	
		Al 2p	75.6	74.5 ¹⁷ 75.3 ²⁷ 75.6 ⁴³ 75.6 ³⁶ 74.7 ³⁷ 75.6 ³⁹	
		O 1s	532.6	531.7 ²⁷ 531.6 ³⁶ 531.6 ⁴⁴ 531.4 ⁴¹	
Al-O	Surface, ALD layer, sputtered layer	N 1s	398.4	398.5 ⁴⁰	
		O 1s	532.0	532.7 ²⁶	

* Note that the center of the C 1s peak was observed at 286.3 eV for all the measurements in this study. This statement does not stand for the reported literature values.

After one minute of etch the intensity ratio of the Al⁰ subpeak to that of the Al-O increases, giving support for the aforementioned assignment of the subpeaks, Fig. 3.3b. After 20 minutes of etch (Fig. 3.3c), the metallic component disappears, and the remaining peak is deconvolved into a minor oxide subpeak, and a major subpeak at 74.7 eV. As mentioned earlier, the literature reports on the exact

positions of metallic, oxide and nitride peaks are not consistent; however, the relative positions of the three subpeaks agree well with the three peaks observed here at 73.0 eV, 74.7 eV, and 75.6 eV^{17,27,36,37,43}. Considering the relative position of the three subpeaks and the assignment of two subpeaks to Al-Al and Al-O bonds, the remaining subpeak at 74.7 eV is assigned to the Al-N bond.

The deconvolution in Fig 3.3c has an important implication: Al forms separate bonds with oxygen and nitrogen; therefore no Al-O-N bonds have formed. Analysis of Fig 3.3c shows that the area under the Al-O subpeak makes up 15.2% of the total area. Given that comparison with the surface profile assures us that the peak at 75.6 eV corresponds to Al-O bond, the fact that 15.2% of the aluminum is exclusively bonded to oxygen requires at least 11.6% oxygen for formation of a stoichiometric aluminum oxide, which is more than what was found in the film (Table 3.2). Therefore no excess oxygen is left to create energetically less favorable Al-O-N bonds.

AlN exhibits a significant affinity towards oxygen, and the nature of oxygen accommodation in AlN structure has been extensively studied^{29,30,32-35,45-47}. According to the AlN-Al₂O₃ pseudo-binary phase diagram, as constructed by McCauley et al.²⁹, while crystallographically distinctive phases will form at high oxygen concentrations, below 16.8 at.% the general structure of 2H AlN (Ramsdell notation) is preserved, while aluminum oxide is introduced into the structure as various forms of defects. According to Slack⁴⁵, oxygen at very low concentrations substitutes for nitrogen, creating a cation vacancy in the process. However, Harris et al.³⁵ later explained that at concentrations higher than 0.75 at.%, it is

energetically favorable for aluminum vacancies and substitutional oxygen point defects to combine making an isolated AlO octahedron. When the concentration of oxygen reaches 6 at.% the octahedral defects organize in the form of interspaced planes regularly dispersed in the lattice, giving rise to various structures known as polytypoids (e.g. 6H, 12H, 27R, etc.), depending on the specific stacking sequence of the planes^{29,31,35,46,47}. Youngman and Harris³⁴ showed that in addition to regularly spaced stacking faults, randomly dispersed and usually curved anti-phase boundaries are favorable low-energy positions for accumulation of oxygen impurities. Therefore, contrary to prior claims, the exact stacking sequence of interspaced planes cannot be directly extracted from the atomic fraction of oxygen. Nevertheless, all the aforementioned researchers agree that in the atomic fraction range of 6-15 at.% oxygen atoms take the form of isolated double-planes, where they exclusively bond with aluminum atoms, and surround them in an octahedral spatial order, as observed in the corundum crystal structure. As a result, the implication deduced from Fig 3.3c agrees with existing models on the positioning and bonding of oxygen atoms in the AlN wurtzite structure. In addition, according to these models AlN retains the original 2H polytypoid (point group $P6_3mc$) and its bond length is unaffected by oxygen; hence, the assignment of the subpeak at 74.7 eV to the Al-N bond.

High resolution XPS spectra of the N 1s peaks are shown in Fig 3.4 for 0, 1, and 20 sputter etch times. The intensity of the N 1s peak is negligible near the surface, compared to the depth of the sample. After twenty minutes of etch, the N 1s peak is centered at 397.8 eV. Based on the analysis of Fig. 3.3-c, all of the nitrogen inside

the film is expected to be exclusively bonded to aluminum. The position of the peak in Fig 3.4-c agrees well with several reports on N-Al bonding, when the difference in the C 1s peak center position is taken into account^{17,27,36,38-41}. At the surface, the small amount of observed nitrogen shows a peak centered at 398.4 eV. Considering the high degree of organic contamination, this nitrogen peak may be attributed to one of the several nitrogen-based ligands prevalent in organic contaminants. According to Baltrusaitis et al.⁴⁸, adsorption of nitrate ligands on the surface of metallic oxides can lead to several nitrogen-containing compounds, and these compounds will cause a N 1s peak center shift of -3.9 to 3.2 eV, with respect to that of pure AlN.

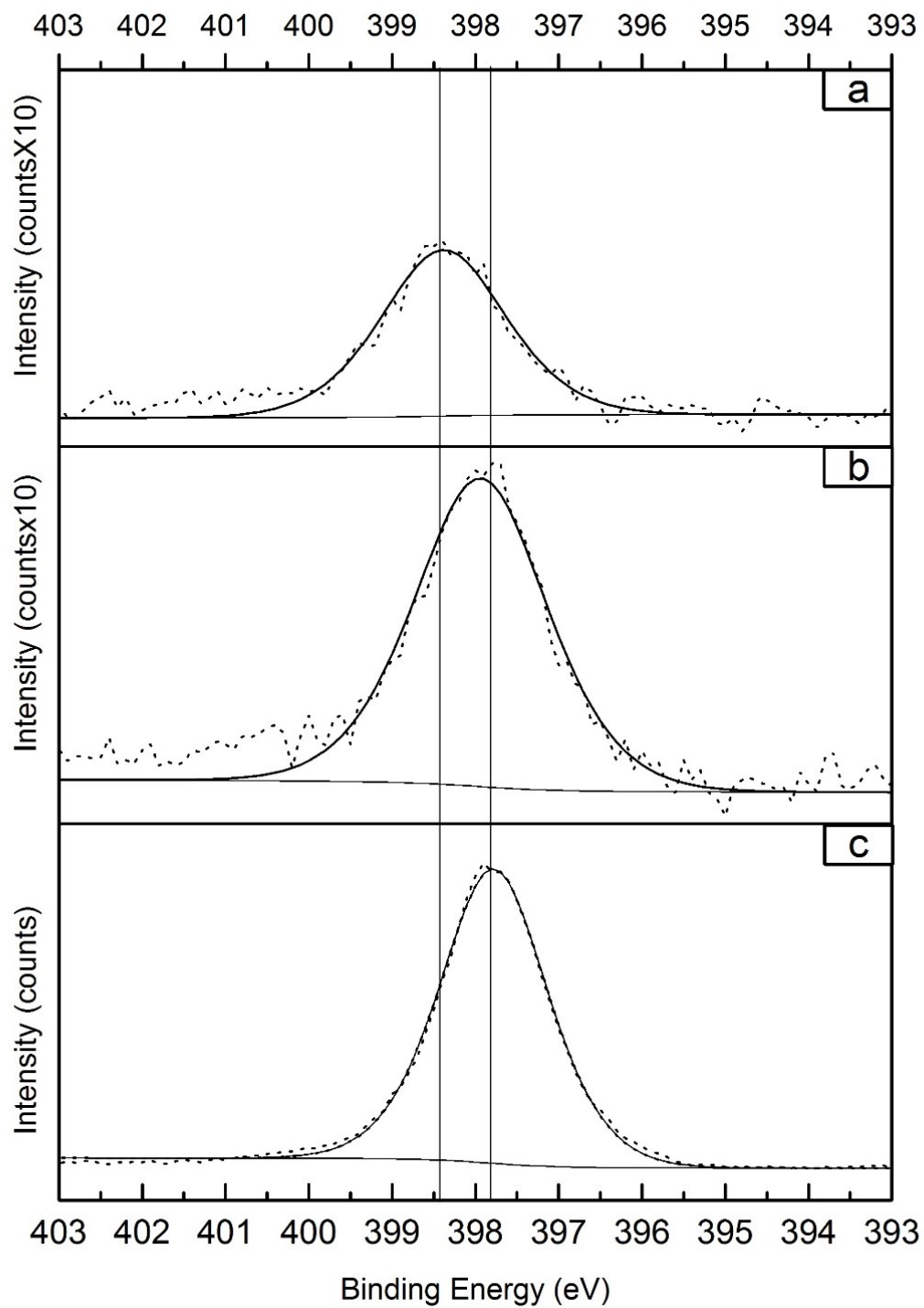


Figure 3.4: High resolution XPS N 1s spectra of the Al-coated thin films a) before etching; b) after 1 minute of etching; c) after 20 minutes of etching.

Fig. 3.5 shows the variations of the O 1s peaks versus depth. Etch times correspond to those of Figs. 3.3 and 4, for ease of comparison. After 20 minutes of etch, the oxygen 1s peak is comprised of a single Gaussian-Lorentzian subpeak (Fig 3.5-c). This is also true for the one minute spectrum as well (Fig 3.5-b). At the surface however, three constituent subpeaks are observed at 532.1, 532.8, and 534.0 eV. The major subpeak centered at 532.8 eV is precisely in line with that of the etched samples. This subpeak is assigned to the O-Al bond, because its area makes up 81% of the total area. Considering the high reactivity of pure aluminum with oxygen, O-Al is expected to be the predominant bond around the oxygen atoms at the surface. The presence of minor O 1s peaks is common, when organic contaminants are present. In this study, the subpeak at 532.1 shows an energy difference of 0.7 eV with the O-Al subpeak. This difference agrees with what is reported elsewhere for nitrate groups²⁶. The presence of 2.5 at.% nitrogen at the surface also facilitates the assignment of this subpeak to nitrate groups. The oxygen required for formation of nitrates consuming all of the available nitrogen would be 7.5 at.%. This would leave $32.6 - 7.5 = 25.1$ at.% oxygen bonded to aluminum, which in turn involves 16.73 at.% aluminum. Considering the total atomic percentage of aluminum is 41.7, a total of 24.97 at.% aluminum must be in metallic form. In other words, the ratio of the oxidized aluminum to metallic aluminum is $16.73/24.97 = 0.67$. Analysis of Fig. 3.3-a shows that the area under the metallic aluminum peak comprises 62.3% of the total area, which is close to the anticipated number. The subpeak at 534.0 eV may be assigned to hydroxyl functional groups on the surface. Chen et al.²⁷ studied the etching of AlN in KOH solutions and reported that the O-Al bond and

the hydroxyl group show a difference of 1.4 eV in the position of O 1s binding energy. In this study, the subpeak at 534.0 eV shows a 1.2 eV shift with respect to O-Al subpeak. Considering the difference in chemical environment of the two studies (KOH solution vs air), it is likely that this subpeak belongs to the hydroxyl group.

The fact that the centers of the peaks assigned to the O-Al bond are in line at different depths may be considered as a final confirmation that oxygen has not formed any oxynitride bonds, and verifies the previously discussed proposition on the distribution of the oxygen atoms in the lattice.

It is important to mention why it was decided that the areas under the curves for different elements should not be compared directly. This is due to different effective attenuation lengths (EAL) for N 1s, O 1s, and Al 2p electrons. As discussed earlier, it is expected that after one minute of etch, at least 2.5 nm of aluminum oxide is remaining, along with the accompanying excess aluminum. Since the kinetic energies of the Al, N, and O core electrons are different (1411.6 eV, 1088.9 eV, and 954.5 eV, respectively), they will arguably attenuate at different rates, while passing through the top layer. In order to determine the extent of this effect, open source software offered by the National Institute of Standards and Technology (NIST), NIST Electron Effective-Attenuation-Length Database (EEALD) V 1.3, was used⁴⁹. The thickness of the aluminum and aluminum oxide, as well as the core electron energies, was entered into the EEALD software which found that aluminum core electrons register a ~50% higher ratio of their original intensity, compared to oxygen core electrons. Therefore, although comparing the intensity of

the electrons within the same range of kinetic energy is possible, no direct comparison between various elements is advisable for the current sample geometry.

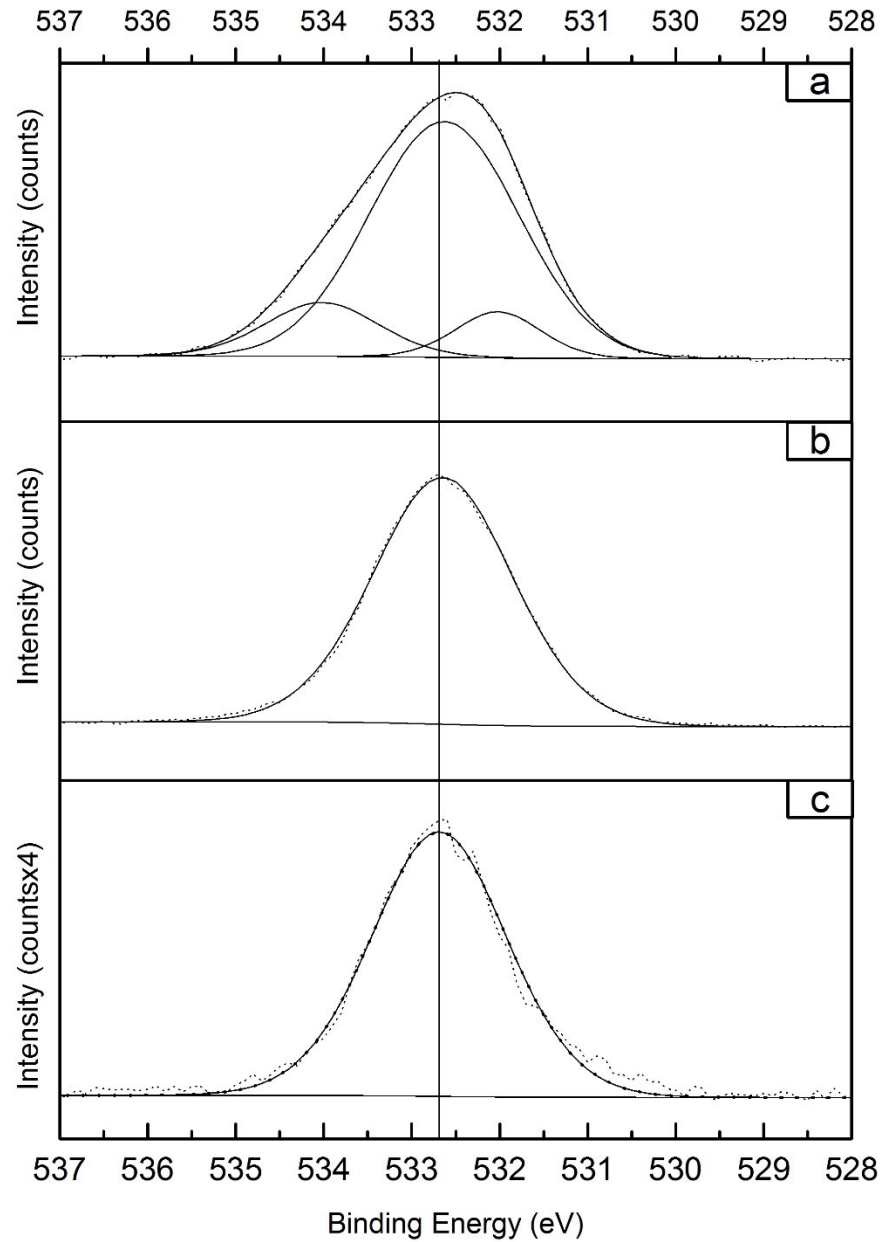


Figure 3.5: High resolution XPS O 1s spectra of the Al-coated thin films a) before etching; b) after 1 minute of etch; c) after 20 minutes of etch.

3.4. Conclusion

High resolution x-ray photoelectron spectroscopy was used to analyze AlN films deposited by low temperature plasma-enhanced atomic layer deposition. Deposition of a thin aluminum layer via sputtering allowed for the protection of the film from the oxidation effect of the atmosphere, providing a measure of chemical stability of the films. Also, the existence of metallic aluminum and aluminum oxide provided reference spectra to aid the analysis of XPS data. It was observed that, apart from the surface, the chemical nature of the films is unaffected by air oxidation. A consistent amount of oxygen impurity was observed in the bulk of the films (8-9 at. %). Extensive analysis of the XPS data indicates that oxygen is exclusively bonded to aluminum, and no Al-O-N bonds were observed.

References

- (1) Asif Khan, M.; Shatalov, M.; Maruska, H. P.; Wang, H. M.; Kuokstis, E. III-Nitride UV Devices. *Jpn. J. Appl. Phys.* 2005, 44, 7191–7206.
- (2) Mohammad, S. N.; Morkoc, H. Progress and Prospects of Group-III Semiconductors. *Prog. Quantum Electron.* 1996, 20, 361–525.
- (3) Search, H.; Journals, C.; Contact, A.; Iopscience, M.; Address, I. P. Group III Nitride Semiconductors for Short Wavelength Light-Emitting Devices. 1.
- (4) Khan, A.; Balakrishnan, K.; Katona, T. Ultraviolet Light-Emitting Diodes Based on Group Three Nitrides. *Nat. Photonics* 2008, 2, 77–84.
- (5) Orton, J. w; Foxon, C. T. Group III Nitride Semiconductors for Short Wavelength Light-Emitting Devices. *Reports Prog. Phys.* 1998, 61, 1–75.

- (6) Jain, S. C.; Willander, M.; Narayan, J.; Overstraeten, R. Van. III-Nitrides: Growth, Characterization and Properties. *Appl. Phys. Rev.* 2000, 87, 965–1006.
- (7) Steranka, F. M.; Bhat, J.; Collins, D.; Cook, L.; Craford, M. G.; Fletcher, R.; Gardner, N.; Grillot, P.; Goetz, W.; Keuper, M.; et al. High Power LEDs - Technology Status and Market Applications. *Phys. Status Solidi* 2002, 194, 380–388.
- (8) Muralt, P. Recent Progress in Materials Issues for Piezoelectric MEMS. *J. Am. Ceram. Soc.* 2008, 91, 1385–1396.
- (9) Grandjean, N.; Damilano, B.; Dalmaso, S.; Leroux, M.; Laügt, M.; Massies, J. Built-in Electric-Field Effects in Wurtzite AlGa_N/Ga_N Quantum Wells. *J. Appl. Phys.* 1999, 86, 3714.
- (10) Lin, C.-M.; Chen, Y.-Y.; Felmetzger, V. V.; Lien, W.-C.; Riekkinen, T.; Senesky, D. G.; Pisano, A. P. Surface Acoustic Wave Devices on AlN/3C–SiC/Si Multilayer Structures. *J. Micromechanics Microengineering* 2013, 23, 025019.
- (11) Aubert, T.; Assouar, M. B.; Legrani, O.; Elmazria, O.; Tiusan, C.; Robert, S. Highly Textured Growth of AlN Films on Sapphire by Magnetron Sputtering for High Temperature Surface Acoustic Wave Applications. *J. Vac. Sci. Technol. A Vacuum, Surfaces, Film.* 2011, 29, 021010.
- (12) Aubert, T.; Elmazria, O.; Assouar, B.; Blampain, E.; Hamdan, A.; Genève, D.; Weber, S. Investigations on AlN/sapphire Piezoelectric Bilayer Structure for High-Temperature SAW Applications. *IEEE Trans. Ultrason. Ferroelectr. Freq. Control* 2012, 59, 999–1005.
- (13) Profijt, H. B.; Potts, S. E.; van de Sanden, M. C. M.; Kessels, W. M. M. Plasma-Assisted Atomic Layer Deposition: Basics, Opportunities, and Challenges. *J. Vac. Sci. Technol. A Vacuum, Surfaces, Film.* 2011, 29, 050801.
- (14) George, S. M. Atomic Layer Deposition: An Overview. *Chem. Rev.* 2010, 110, 111–131.

- (15) Liu, G.; Deguns, E. W.; Lecordier, L.; Sundaram, G.; Becker, J. S. Atomic Layer Deposition of AlN with Tris(Dimethylamido)aluminum and NH₃. *ECS Trans.* 2011, 41, 219–225.
- (16) Longrie, D.; Deduytsche, D.; Haemers, J.; Driesen, K.; Detavernier, C. A Rotary Reactor for Thermal and Plasma-Enhanced Atomic Layer Deposition on Powders and Small Objects. *Surf. Coatings Technol.* 2012, 213, 183–191.
- (17) Alevli, M.; Ozgit, C.; Donmez, I.; Biyikli, N. Structural Properties of AlN Films Deposited by Plasma-Enhanced Atomic Layer Deposition at Different Growth Temperatures. *Phys. Status Solidi* 2012, 209, 266–271.
- (18) Lee, Y. J.; Kang, S. Growth of Aluminum Nitride Thin Films Prepared by Plasma-Enhanced Atomic Layer Deposition. *Thin Solid Films* 2004, 446, 227–231.
- (19) Liu, X.; Ramanathan, S.; Lee, E.; Seidel, T. E. Atomic Layer Deposition of Aluminum Nitride Thin Films from Trimethyl Aluminum (TMA) and Ammonia. In *Materials Research Society Symposium*; 2004; Vol. 811, pp. 1–6.
- (20) Dendooven, J.; Deduytsche, D.; Musschoot, J.; Vanmeirhaeghe, R. L.; Detavernier, C. Conformality of Al₂O₃ and AlN Deposited by Plasma-Enhanced Atomic Layer Deposition. *J. Electrochem. Soc.* 2010, 157, G111–G116.
- (21) Ozgit, C.; Donmez, I.; Alevli, M.; Biyikli, N. Atomic Layer Deposition of GaN at Low Temperatures. *J. Vac. Sci. Technol. A Vacuum, Surfaces, Film.* 2012, 30, 01A124.
- (22) Kim, O. H.; Kim, D.; Anderson, T. Atomic Layer Deposition of GaN Using GaCl₃ and NH₃. *J. Vac. Sci. Technol. A Vacuum, Surfaces, Film.* 2009, 27, 923.
- (23) Lei, W.; Chen, Q. Crystal AlN Deposited at Low Temperature by Magnetic Field Enhanced Plasma Assisted Atomic Layer Deposition. *J. Vac. Sci. Technol. A Vacuum, Surfaces, Film.* 2013, 31, 01A114.

- (24) Bosund, M.; Sajavaara, T.; Laitinen, M.; Huhtio, T.; Putkonen, M.; Airaksinen, V.-M.; Lipsanen, H. Properties of AlN Grown by Plasma Enhanced Atomic Layer Deposition. *Appl. Surf. Sci.* 2011, 257, 7827–7830.
- (25) Alevli, M.; Ozgit, C.; Donmez, I.; Biyikli, N. The Influence of N₂/H₂ and Ammonia N Source Materials on Optical and Structural Properties of AlN Films Grown by Plasma Enhanced Atomic Layer Deposition. *J. Cryst. Growth* 2011, 335, 51–57.
- (26) King, S. W.; Barnak, J. P.; Bremser, M. D.; Tracy, K. M.; Ronning, C.; Davis, R. F.; Nemanich, R. J. Cleaning of AlN and GaN Surfaces. *J. Appl. Phys.* 1998, 84, 5248.
- (27) Chen, D.; Xu, D.; Wang, J.; Zhang, Y. Investigation of Chemical Etching of AlN Film with Different Textures by X-Ray Photoelectron Spectroscopy. *J. Phys. D. Appl. Phys.* 2008, 41, 235303.
- (28) Rosenberger, L.; Baird, R.; McCullen, E.; GregoryAuner; Shreve, G. XPS Analysis of Aluminum Nitride Films Deposited by Plasma Source Molecular Beam Epitax. *Surf. Interface Anal.* 2008, 40, 1254–1261.
- (29) Mccauley, J. W.; Krishnan, K. M.; Rai, R. S.; Thomas, G. Anion-Controlled Microstructures in the AlN-Al₂O₃ System. In *Ceramic Microstructures '86*; Pask; Evans, Eds.; Plenum Publishing Corporation, 1988; pp. 577–590.
- (30) Tendeloo, G. Van; Faber, K. T.; Thomas, G. Characterization of AlN Ceramics Containing Long-Period Polytypes. *J. Mater. Sci.* 1983, 18, 525–532.
- (31) Brien, V.; Pigeat, P. Correlation between the Oxygen Content and the Morphology of AlN Films Grown by R.f. Magnetron Sputtering. *J. Cryst. Growth* 2008, 310, 3890–3895.
- (32) Tabary, P.; Servant, C. Crystalline and Microstructure Study of the AlN–Al₂O₃ Section in the Al–N–O System. I. Polytypes and Γ -AlON Spinel Phase. *J. Appl. Crystallogr.* 1999, 32, 241–252.

- (33) Kazan, M.; Rufflé, B.; Zgheib, C.; Masri, P. Oxygen Behavior in Aluminum Nitride. *J. Appl. Phys.* 2005, 98, 103529.
- (34) Youngman, R. A.; Harris, J. H. Luminescence Studies of Oxygen-Related Defects in Aluminum Nitride. *J. Am. Ceram. Soc.* 1990, 46, 3238–3246.
- (35) Harris, J. H.; Youngman, R. A.; Teller, R. G. On the Nature of the Oxygen-Related Defect in Aluminum Nitride. *J. Mater. Res.* 1990, 44128, 1763–1773.
- (36) Gredeļj, S.; Gerson, A. R.; Kumar, S.; Cavallaro, G. P. Characterization of Aluminium Surfaces with and without Plasma Nitriding by X-Ray Photoelectron Spectroscopy. *Appl. Surf. Sci.* 2001, 174, 240–250.
- (37) Jose, F.; Ramaseshan, R.; Dash, S.; Bera, S.; Tyagi, a K.; Raj, B. Response of Magnetron Sputtered AlN Films to Controlled Atmosphere Annealing. *J. Phys. D. Appl. Phys.* 2010, 43, 075304.
- (38) Schoser, S.; Bräuchle, G.; Forget, J.; Kohlhof, K.; Weber, T.; Voigt, J.; Rauschenbach, B. XPS Investigation of AlN Formation in Aluminum Alloys Using Plasma Source Ion Implantation. *Surf. Coatings Technol.* 1998, 103-104, 222–226.
- (39) Wang, C. C.; Chiu, M. C.; Shiao, M. H.; Shieu, F. S. Characterization of AlN Thin Films Prepared by Unbalanced Magnetron Sputtering. *J. Electrochem. Soc.* 2004, 151, F252.
- (40) Manova, D.; Dimitrova, V.; Fukarek, W.; Karpuzovc, D. Investigation of D . c . -Reactive Magnetron-Sputtered AlN Thin Films by Electron Microprobe Analysis , X-Ray Photoelectron Spectroscopy and Polarised Infra-Red Reflection. *Surf. Coatings Technol.* 1998, 106, 205–208.
- (41) Zhang, Y. Characterization of as-Received Hydrophobic Treated AlN Powder Using XPS. *J. Mater. Sci. Lett.* 2002, 21, 1603–1605.
- (42) Aumann, C. E.; Skofronick, G. L.; Martin, J. A. Oxidation Behavior of Aluminum Nanopowders. *J. Vac. Sci. Technol. B Microelectron. Nanom. Struct.* 1995, 13, 1178.

- (43) García-Méndez, M.; Morales-Rodríguez, S.; Shaji, S.; Krishnan, B.; Bartolo-Pérez, P. Structural Properties of AlN Films with Oxygen Content Deposited by Reactive Magnetron Sputtering: XRD and XPS Characterization. *Surf. Rev. Lett.* 2011, 18, 23–31.
- (44) Kuang, X.-P.; Zhang, H.-Y.; Wang, G.-G.; Cui, L.; Zhu, C.; Jin, L.; Sun, R.; Han, J.-C. AlN Films Prepared on 6H-SiC Substrates under Various Sputtering Pressures by RF Reactive Magnetron Sputtering. *Appl. Surf. Sci.* 2012, 263, 62–68.
- (45) Slack, G. A. Nonmetallic Crystals with High Thermal Conductivity. *J. Phys. Chem. Solids* 1973, 34, 321–335.
- (46) Adams, I.; AuCoin, T. R.; Wolff, G. A. Luminescence in the System Al₂O₃-AlN. *J. Electrochem. Soc.* 1962, 1050–1054.
- (47) Sakai, T. Hot-Pressing of the AlN-Al₂O₃ System. *J. Ceram. Assoc. Japan* 1978, 86, 125–130.
- (48) Baltrusaitis, J.; Jayaweera, P. M.; Grassian, V. H. XPS Study of Nitrogen Dioxide Adsorption on Metal Oxide Particle Surfaces under Different Environmental Conditions. *Phys. Chem. Chem. Phys.* 2009, 11, 8295–8305.
- (49) Powell, C. J.; Jablonski, A. NIST Electron Effective-Absorption-Length Database - Version 1.3; National Institute of Standards and Technology: Gaithersburg, MD, 2011.

Chapter Four

As deposited p-type (002) GaN on sapphire grown by atomic layer deposition

(Submitted to Nature Materials for publication)

4.1 Introduction

GaN is one of the most important semiconductors of the 21st century. GaN-based materials have tunable direct band gaps in the UV to IR wavelengths range, which makes them an attractive choice for cost-effective high-performance opto-electronic devices such as light emitting diodes (LEDs) and laser diodes (LDs) ^{1,2}. High quality GaN thin films have been grown by MOCVD and MBE ³⁻⁵. However, deposition of epitaxial GaN films with (001) orientation, which is preferred for device applications^{6,7}, requires substrate temperatures higher than 600°C ⁸⁻¹². For instance, Yadav et al. ¹² deposited GaN films via radio frequency sputtering, and investigated the dependence of GaN crystal structure on substrate temperature. They reported that below 300°C the films were mostly amorphous while between 300° and 550°C the films were polycrystalline with (100) preferential orientation. The desired preferential orientation of (002) was only achieved at 700°C. Knox-Davies et al.¹³ have reported on the deposition of GaN via reactive sputtering at temperatures ranging from room temperature to 450°C with predominantly wurtzite polycrystalline films. On cooling from such high deposition temperatures the large differences between the coefficient of thermal expansion of GaN and that of the common substrates leads to a high density of interfacial crystal defects. This interfacial effect is attenuated by growing thicker films in the 3-5 micron range.

Atomic layer deposition (ALD) may offer a potential alternative for low-temperature deposition of GaN. However, there are few reports on the ALD of this material. Kim et al.¹⁴ have reported ALD of GaN using GaCl₃ and NH₃, leading to polycrystalline films having (002) preferential orientation with a broad XRD peak

at 650°C. Using halide precursors, however, may lead to film contamination¹⁴ and pose the threat of corrosion of metal contacts¹⁵. On the other hand, it has been reported that low-temperature deposition of GaN using trimethylgallium and NH₃ plasma resulted in amorphous GaN films with large amounts of impurities¹⁶. Ozgit et al.^{16,17} have reported that deposition of GaN using a conventional inductive plasma source produces amorphous films. However, using a hollow cathode plasma, they managed to deposit GaN films with (002) preferential orientation, which is incongruously reported to have been observed on Si (100), but not on sapphire (002). The authors have not explained this seemingly counter-intuitive observation.

In this paper, we report on the deposition of highly oriented (002) GaN on sapphire using triethylgallium (TEG) and 95% nitrogen/5% hydrogen plasma at 275°C. The hydrogen composition of the forming gas was chosen based on an estimate of quantity of hydrogen atoms needed to react with the methyl groups during the second ALD half reaction. The structural, optical and electrical properties of these films have been investigated using X-ray diffraction (XRD), X-ray reflectometry (XRR), atomic force microscopy (AFM), transmission electron microscopy (TEM), X-ray photoelectron spectroscopy (XPS), spectroscopic ellipsometry, and Hall Effect measurements.

4.2. Experimental Procedure

Depositions were carried out using an atomic layer deposition research system (ALD-150LX, Kurt J. Lesker) equipped with an *in situ* J. A. Woollam M-2000DI

ellipsometer with a fixed angle of 70° . Depositions were carried out at 275°C using a cycle that consisted of four consecutive pulses: 0.02s TEG dose, 7s Ar purge, 15s N_2/H_2 , and 5s Ar purge, repeated for 1000 cycles to deposit a film ~ 55 nm thick. A Kratos AXIS Ultra XPS system was used to study the chemical structure of the films, using Al (1486.69eV) x-ray source at 50° incidence angle. An argon sputtering ion gun working at 4 keV was used to clean the surface prior to collection of the XPS data. XRR and XRD measurements were performed using a Bruker-AXS D8-Discover machine with a Cu $K\alpha$ source ($K\alpha_2$ was removed before analysis). XRD data were collected using a Vantec 500 2-D detector and GADDS software, and analyzed using EVA software. XRR data and azimuthal scans were recorded using a NaI scintillometer. Commander D8 and Leptos programs were used for data acquisition and analysis, respectively. A Bruker Dimension-Edge AFM system was used to map the sample surface. Silicon tips were used in tapping mode, and the amplitude set point was 2.4 V. AFM results were analyzed using Bruker Nanoscope Analysis 1.5 software.

The structure and morphology of the ALD GaN films were characterized by TEM observation⁵. High resolution TEM (HRTEM) was performed in a Hitachi HF 3300 instrument operated at 300kV. Cross-section TEM samples were prepared using a Hitachi NB 5000 dual beam FIB/SEM. To minimize ion beam damage to the surface of the top layer (GaN), a 50 nm layer of C was deposited on GaN surface prior to FIB processing. Bulk milling of the sample was performed using a 40 keV Ga^+ beam. Final polishing was done using a 10 keV Ga^+ beam. The approximate

⁵ The TEM data was collected by Neda Dalili at National Institute for Nanotechnology.

thickness of the final lamellae, mounted on Cu grids, was 100 nm. Hall Effect measurements were done using a Nanometrics HL5500 system, which was operated at 0.01 μA constant current. Optical transmission data were collected using a Perkin-Elmer LAMBDA 1050 UV/Vis/NIR spectrophotometer.

4.3. Results and discussion

4.3.1. Composition

Fig. 4.1 shows the XPS spectrum of the GaN film after ~ 5 nm of the film surface was argon ion sputter etched to remove any organic or atmospheric post-deposition contamination. In addition to Ga XPS peaks, Ga Auger peaks, and the nitrogen XPS peak, those from O 1s and C 1s are present. The carbon is due to remnants of the ethyl groups in the TEG precursor, and its presence indicates some degree of incomplete reaction between the nitrogen plasma and the chemically adsorbed TEG. Oxygen, on the other hand, is an impurity that affects the electrical and optical properties of GaN^{18,19}. The presence of oxygen has been well documented and reported in III-N thin film growth, especially when the growth process involves a plasma^{14,16,20,21}, however the source of this impurity is not yet fully understood.

Table 4.1 lists the elemental composition of the film, obtained by XPS. Gallium and nitrogen atomic fractions are almost equal, while 2.5 at.% oxygen and 1.1 at.% carbon are detected. The AlN literature suggests that, at low concentrations of oxygen, the Al and O atoms inside the AlN lattice form Al_2O_3 ²². Recent XPS research²³ confirms that the oxidation state of Al bonded to oxygen is the same as that in Al_2O_3 . Extending this concept to GaN, and assuming that every three

oxygen atoms replace two nitrogen atoms in a stoichiometric compound, study of Table 4.1 reveals the existence of ~ 0.6 at.% gallium vacancy (2.5% oxygen is equivalent to 1.6%N, therefore in total there are 49.2% anions and 48.8% cations).

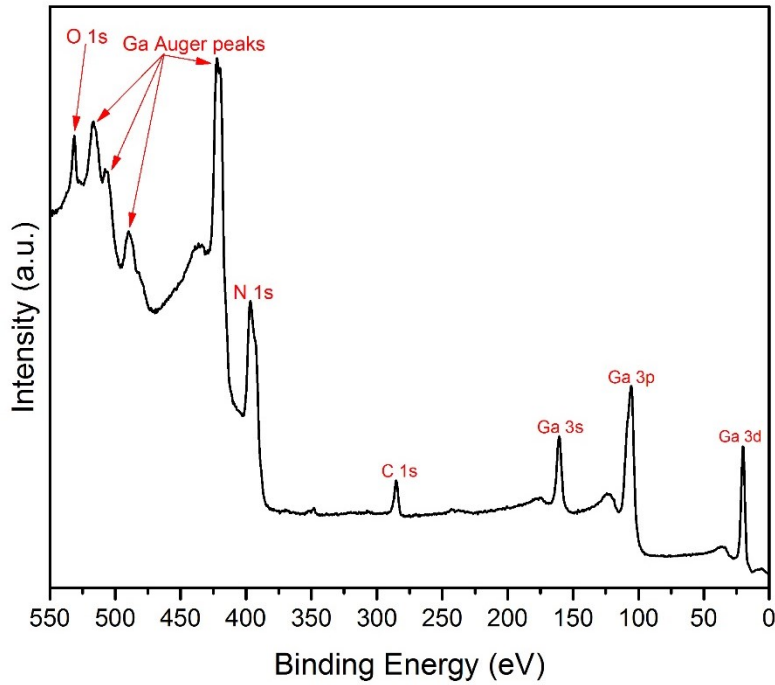


Figure 4.1: XPS survey spectrum of the GaN film after ion etch cleaning.

It is known that Ga vacancies have a strong tendency to react with oxygen, and deposit at the base of edge dislocations¹⁸. The combination of these defects will affect the optical properties of GaN^{19,24,25}, and is likely to be partially responsible for the deviation of the optical properties of the films from those of the bulk material, as explained later. This hypothesis agrees well with the results of Hall mobility measurements that show a strong possibility of oxygen overcompensation by Ga vacancies. This will be discussed later.

Table 4.1: Elemental composition of the GaN films, as determined by XPS

Element	Gallium	Nitrogen	Oxygen	Carbon
Representative subshell	Ga 3d	N 1s	O 1s	C 1s
Atomic fraction	48.8	47.6	2.5	1.1

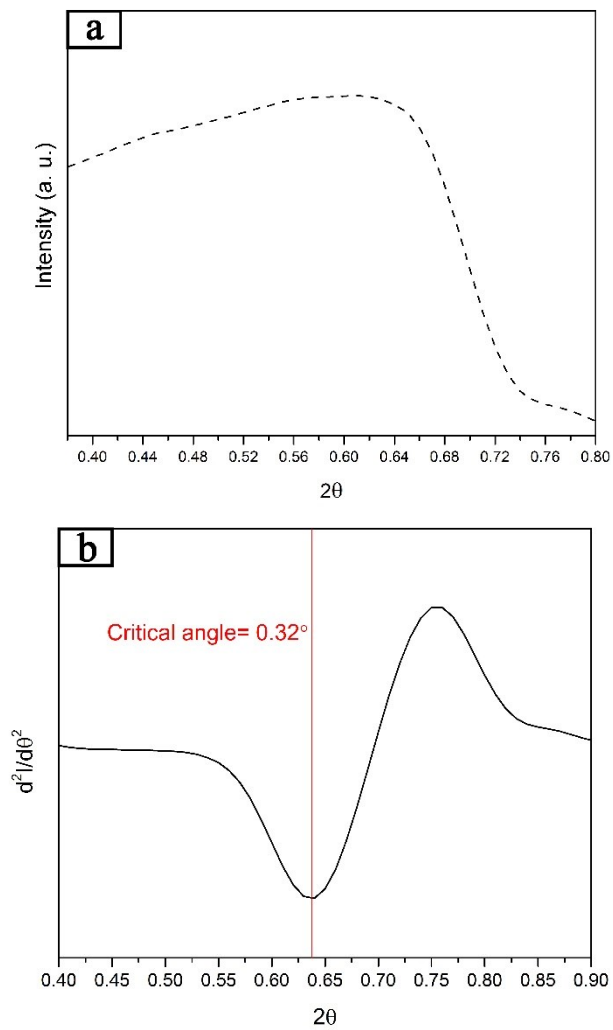


Figure 4.2: X-ray reflectometry spectra of a 1000-cycle ALD GaN film showing a) the critical angle and b) the method used to extract the critical angle.

4.3.2 Structure

XRR results for two different 2θ ranges are shown in Figs. 4.2 and 4.3. In Fig. 4.2a, the low-angle range, the reflected intensity shows a drop indicating the onset of x-ray penetration into the sample and the limit of total external reflection, also known as the critical angle. Since it is difficult to obtain a precise critical angle from the plot in Fig. 4.2a, the minimum of the second derivative of the intensity was chosen as the point of deflection, and the onset of X-ray penetration. This method, shown in Fig. 4.2b, gives a value of 0.32° for the critical angle. Bulk single crystal GaN is known to have a theoretical critical angle of 0.36° . Considering the relationship of $\theta_c \propto \sqrt{\rho}^{26}$, one can estimate the density of the film to be $\sim 95\%$ of the theoretical value.

The higher-angle XRR data in Fig. 4.3 show the characteristic reflectometry spectrum of single-layer thin films. A simulation using a genetic algorithm was run to model the film parameters. The RMS value of 3.1 nm for roughness, from atomic force microscopy, was input in the model. The data from simulation agree well with the experimental data. Simulation, run using Bruker Leptos software, gave the values of 55.6 nm and 6.08 g/cm^3 for thickness and mass density, respectively, the latter of which equals 98% of the theoretical value of bulk material. Evaluation of Kiessig fringes is a more accurate measure of density, compared to critical angle, as it takes into account the surface roughness. Nevertheless, the two methods independently give high values for the density of the film. As mentioned earlier, an in-situ ellipsometry system was used to monitor the deposition. A Cody-Lorentz model was found to offer a good description of the material's optical behavior. As

was the case in XRR, a roughness value of 3.1 nm measured by AFM was input to the model. The derived value for thickness is 53.2 nm, which is ~4% lower than what was obtained from XRR.

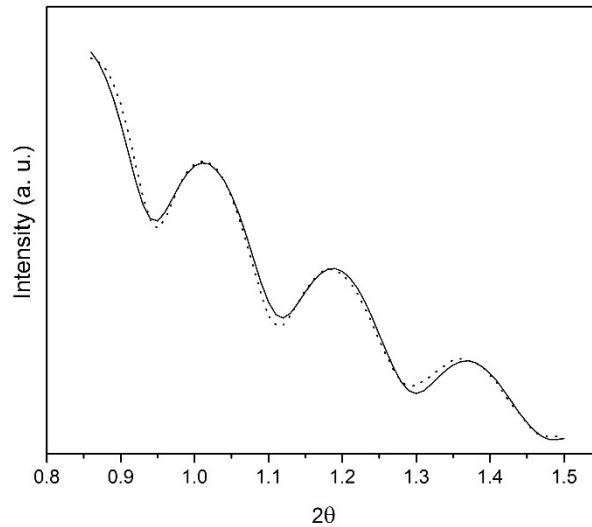


Figure 4.3: Characteristic Kiessig fringes in GaN XRR spectra.

A coupled scan XRD spectrum of the GaN PEALD film is shown in Fig. 4.4. Only two peaks at 34.5° and 41.7° (d-spacings 0.27 and 0.23 nm) are observed in the spectrum, which correspond to those of wurtzite GaN (002) and sapphire (006) reflections respectively. The absence of wurtzite GaN (100) and (101) reflections may be indicative of a single crystal or strongly oriented polycrystalline film with (002) preferred orientation. The FWHM of the GaN peak is 21.0 arc min, compared to 16.5 arc min for that of the single-crystal sapphire substrate.

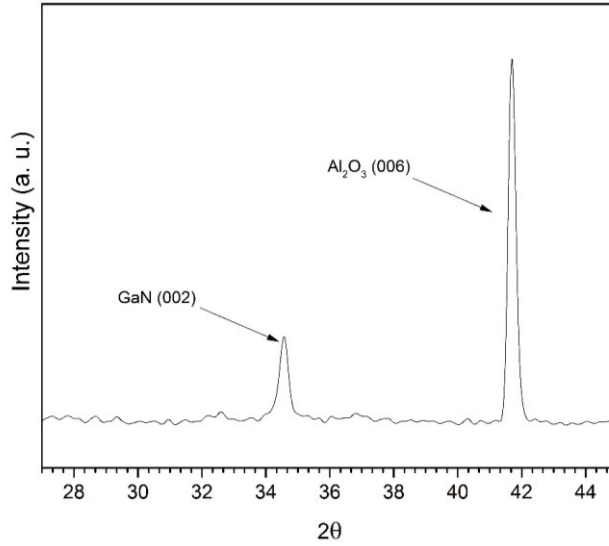


Figure 4.4: Coupled scan XRD spectrum of GaN on sapphire.

In order to probe the degree of out-of-plane tilting of crystals, a two-dimensional Hi-Star x-ray detector was employed. The rotation axes relative to the sample and the beam are schematically illustrated in Fig. 4.5. If the conventional out-of-plane rotation is denoted by ω (in a coupled scan, such as the one shown in Fig. 4.4, $\omega=2\theta$) and ϕ indicates the degree of in-plane rotation, then χ measures the out-of-plane rotation, whose axis is perpendicular to ω and ϕ rotations. The detector used in this study allows for simultaneous data collection for wide ranges of 2θ and χ ²⁷. Fig. 4.6 shows a GADDS frame centered at $2\theta=34.5^\circ$. Data collection time was ten times higher than it was for Fig. 4.4.

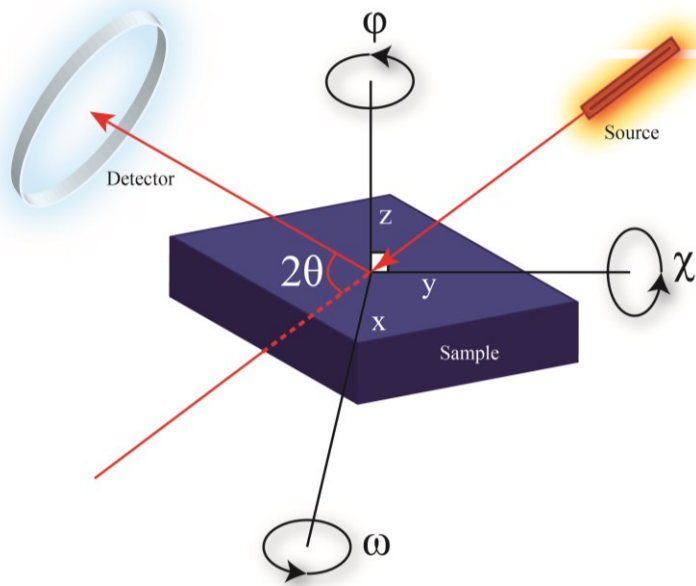


Figure 4.5: The schematic illustration of the geometrical parameters of the XRD tests.

It is expected that random out-of-plane orientation make cones of diffracted x-rays, which are detected as rings of uniform radial intensity distribution²⁸. Therefore the degree of radial nonuniformity is a measure of crystal order^{29,30}. It is clear from Fig. 4.6 that the film exhibits a high degree of order, while the 600-second-long collection time allows for detection of diffraction by the (101) plane, whose intensity is negligible compared to that of the dominant (002) diffraction. Fig. 4.6 shows an integration of the signals over 2θ , in the range of $33.5\text{-}35.5^\circ$, along χ , which confirms the narrow distribution of the diffracted beam. Figs. 4.4 and 4.6, in combination, provide clear evidence that the structure of the GaN films consists of highly ordered wurtzite crystals oriented along the (002) crystallographic axis.

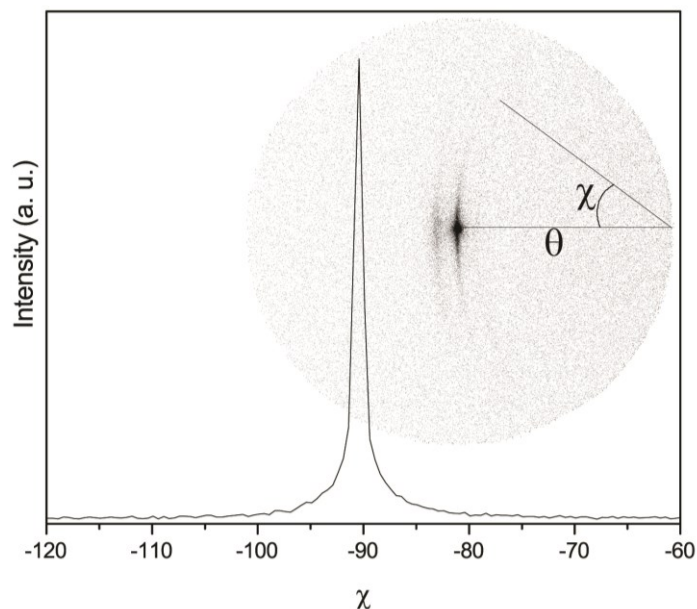


Figure 4.6: A two dimensional XRD frame of GaN on sapphire with the accompanying integration of the intensity along the χ axis.

In thin films with strong preferential orientation, the diffraction intensity of the planes parallel to the surface is extremely sensitive to sample orientation. The maximum intensity is achieved when the beam vector and surface normal are exactly coplanar, and that is rarely the case in practice. The effect of this misorientation was revealed in a ϕ -scan and shown in Fig. 4.7. The higher intensity spectrum is the (006) reflection of sapphire, while the other spectrum is the (002) reflection of GaN. For the two spectra, the ω angle was set to 20.8° and 17.2° respectively, and 2θ was kept constant at twice the mentioned values, while the sample was rotated 360° around the surface normal. The two independently recorded spectra were then superimposed for comparison. The most noteworthy feature of Fig. 4.7 is the large variation in the recorded intensity vs ϕ . As explained earlier, this effect is caused by noncoplanarity of the beam vector and the surface

normal. The exact coplanarity angle cannot be detected using a two-dimensional detector. Therefore a scintillometer was used to record the data in Fig. 4.7. Another noteworthy feature of Fig. 4.7 is the fact that the two spectra show maxima and minima at the same ϕ values. This is an indication that the normal to the sapphire (006) plane and GaN (002) plane are aligned. In other words, this is proof of crystallographic relationship between the two lattices, and a sign of epitaxy at the interface.

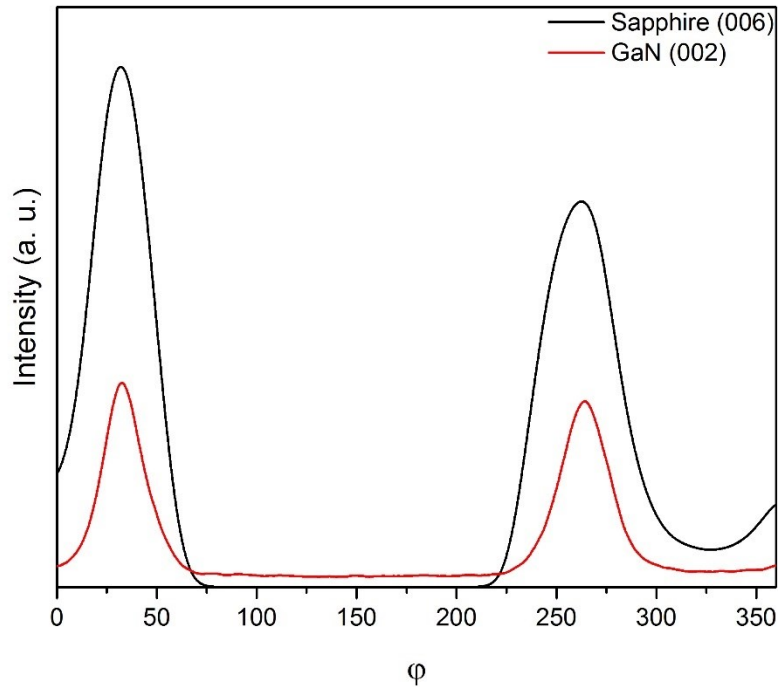


Figure 4.7: Superimposed azimuthal scans of sapphire (006) and GaN (002) XRD peaks.

4.3.3 Growth mechanism

Cross-sectional transmission electron microscopy images of the samples are shown in Fig. 4.8. Ion beam damage, due to the final polishing step of sample preparation by FIB, is evident in all TEM images. Fig. 4.8a shows that the films have a

polycrystalline structure with an epitaxial layer of ~5 nm at the sapphire interface. Fig. 4.8b shows this epitaxial layer in greater detail. To identify the structure of this epitaxial layer, convergent beam electron diffraction (CBED) analysis was performed. An example of a CBED pattern, shown in Fig. 4.9, reveals a single crystal array of spots which can be indexed to the [110] zone axis of wurtzite GaN. Furthermore, the lattice fringes in Fig. 4.8b correspond to the GaN c-plane interplanar distance, indicating the epitaxial layer is c-plane oriented. Eaglesham et al.³¹ showed that there is a maximum thickness for MBE homoepitaxial growth of Si (100), which is kinetically controlled, and temperature-dependent. They postulated that surface roughness is responsible for this break of epitaxy. Jorke et al.³² proposed a kinetic model, in which accumulation of crystal defects are considered for a transition from epitaxial structure to amorphous film. They argued that thermally activated mobility of the defects controls the thickness of the epitaxial layer. It has also been shown that MBE growth of GaN on AlN can change from Frank-Van der Merwe (layer by layer) regime to Stranski-Krastanov mode, depending on a delicate balance of temperature-to-precursor ratio³³. By studying the dislocation density of GaN layers grown on AlN, Daudin et al.^{33,34} hypothesized that edge misfit dislocations act as nucleation centers, which give rise to GaN dots on top of the original epitaxial layers, and eventually lead to breakdown of epitaxy. Liliental-Weber³⁵ demonstrated that a range of hollow crystal defects, mainly caused by impurities, are responsible for the transition of the GaN growth front from two-dimensional to three-dimensional. Oxygen was specifically mentioned as a likely candidate to cause these “nanotube” and “pinhole” defects. Oxygen atoms

or clusters can arguably create regions with different atomic bonding at the surface. This accelerates the growth in energetically favorable areas, and leads to lack of homogeneity in growth rate at the growth front and birth of 3-D islands. Further accumulation of the defects aggravates this situation and increases surface roughness. Thorough understanding of the growth mechanism needs further investigation.

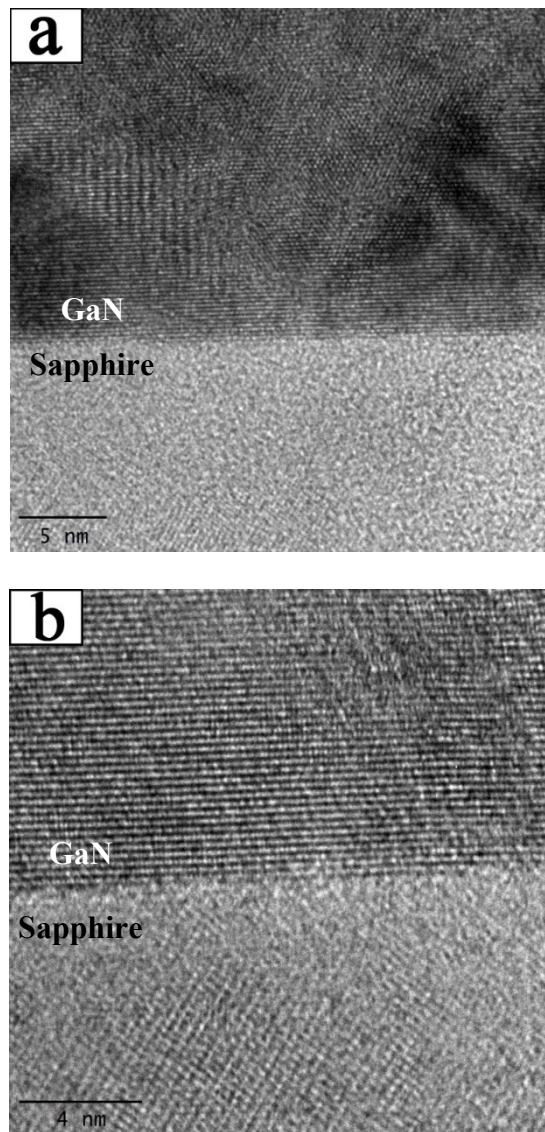


Figure 4.8: High resolution transmission electron micrographs of GaN-sapphire interface.

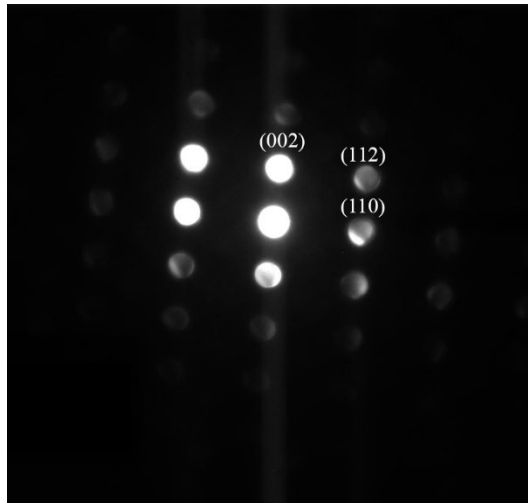


Figure 4.9: Convergent beam electron diffraction pattern of the epitaxial layer at the interface.

In order to study the phenomenology of the growth front, the top-view topography of the samples was studied via AFM. Fig. 4.10a shows the tapping phase image from the surface of the GaN films. This mode of imaging maps the surface based upon the phase lag in the oscillation of the cantilever, compared to that of the original signal. The phase image provides a better spatial resolution compared to a standard height image, and has been previously selected for the study of the grain structure of the thin films^{36,37}. Fig. 4.10a shows that the surface of the film consists of regularly-spaced features, whose outline is similar to the grain structure of a typical polycrystalline film. Finally, Fig. 4.10b shows a 3D reconstruction of the sample surface, using the height data, as prepared by Bruker NanoScope Analysis software. This is a visual representation of the growth front. The arithmetic average and root mean square values for roughness are 3.1 nm and 3.9 nm respectively. Considering the fact that the film is ~56 nm thick, these values are decidedly higher than the roughness resulting from a two-dimensional growth regime^{38,39}. This

supports the previous proposition that the two-dimensional growth regime that creates the initial epitaxial layer was not sustainable, and later transforms into a three-dimensional island growth. Defect-induced surface inhomogeneity, in conjunction with surface mobility values lower than what is needed for a step-flow growth regime are believed to be the major reasons behind this transition.



Figure 4.10: a) Phase image atomic force micrograph of the surface of the GaN films b) a three-dimensional reconstruction of the surface contour, extracted from the AFM height sensor data.

4.3.4. Electrical and Optical Properties

Hall mobility measurements were done using a Nanometrics HL5500 system at 0.32 Tesla. The results show a relatively low resistivity of 0.033 Ω -cm. In addition, the films are p-type with a carrier concentration of $1.68 \times 10^{18} \text{ cm}^{-3}$ and carrier mobility of 110 cm^2/Vs . Oxygen is a well-known donor in GaN, and is considered as one of the main sources of high donor concentration in nominally undoped GaN films^{40,41}. XPS results indicate an oxygen atomic concentration of $5 \times 10^{20} \text{ cm}^{-3}$. The fact that the films are p-type semiconductors, in absence of any other impurity, suggests an overcompensation of O by Ga vacancies. Positron annihilation spectroscopy, as well as theoretical calculations, have demonstrated that the two defects have a strong tendency to react and form stable complex defects with mobility considerable lower than the values observed for pure oxygen^{41,42}.

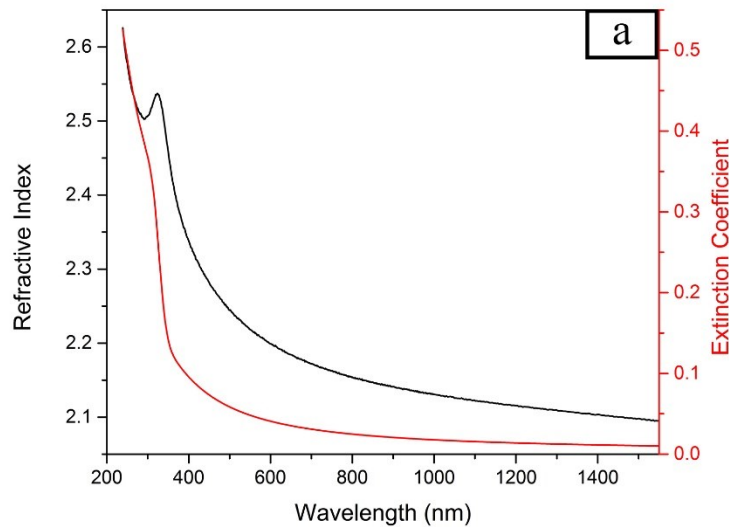


Figure 4.11: Variations of the refractive index and extinction coefficient, extracted from spectroscopic ellipsometry data.

The refractive index and absorption coefficient were measured using spectroscopic ellipsometry, and the dispersion curves are shown in Fig. 4.11. The value of refractive index at 632 nm is 2.21, compared to 2.38 for the bulk value. Considering the porosity of 2%, as obtained by XRR, one can apply the Bruggeman effective medium approximation to calculate the expected refractive index from the bulk value. This yields a value of 2.31, which is still higher than the thin film value.

In order to study the effect of structural variations on the refractive index, the results of in-situ spectroscopic ellipsometry were analyzed, and refractive index was derived at various depths. The results are displayed in Fig. 4.12. As observed, at ~10 nm, the decreasing trend of refractive index reverses to a rising trend. These results can be analyzed in view of the discussions presented in Section 4.3.3. As the films have an epitaxial structure during the first few nanometers of growth, the refractive index is high and closer to that of the bulk value. A transition from two-dimensional growth regime to three-dimensional growth results in higher porosity and lower crystalline quality, hence lower refractive index. Further increase in thickness yields larger crystals and lower concentration of defects, therefore higher index. While the rising trend has been reported for various semiconductors^{43,44}, the initial decrease is a rare observation caused by the specific structural evolution of this film.

It is known that in proximity of the band gap, semiconductors with direct optical band gaps, E_g , follow Eq. (1),

$$(\alpha h\nu)^2 \propto (E - E_g) \quad (4.1)$$

where $\alpha = 4\pi k/\lambda$ is the absorption coefficient, λ is wavelength, ν is frequency, h is Planck's constant, and k is the extinction coefficient⁴⁵. Therefore, when the left hand side of the Eq. (4.1) is plotted as a function of photon energy, one can expect the intercept of the tangent to the linear portion of the graph with the x-axis to give the approximate value of the optical band gap. In addition to ellipsometry, the absorption coefficient was also derived from spectrophotometry in transmission mode (Fig 4.13), in order to compare the results. Fig 4.14 shows the aforementioned procedure applied to the two sets of data and the resulting band gaps. As seen, the values resulting from ellipsometry and spectrophotometry are 3.62 and 3.55 eV respectively. The two numbers are both higher than the bulk value of 3.4 eV.

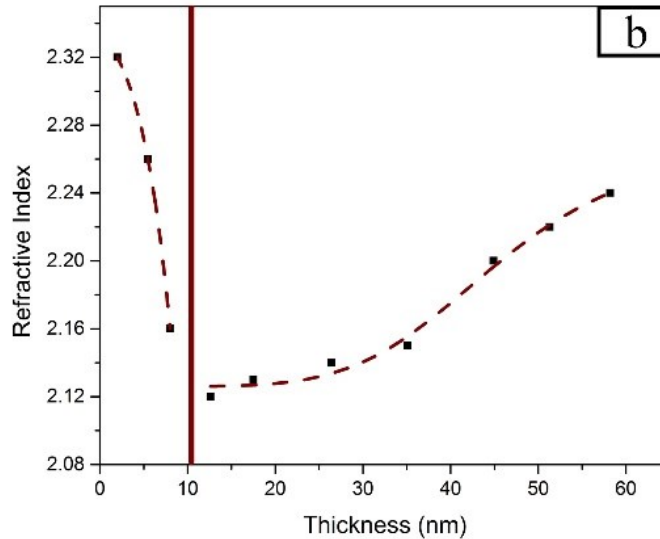


Figure 4.12: The evolution of the refractive index of GaN at 632 nm during the growth process.

It has been documented that the thickness of thin films affects their refractive index and optical band gap^{44,46-49}. In the case of CdS, it has been reported that an increase

in thickness from 40 to 113 nm results in narrowing of band gap from 2.88 to 2.61 eV, while the refractive index at 632 nm increases by 0.35⁴⁷. In the case of CdSe, a decrease of 0.6 eV in optical band gap energy has been reported as the thickness is increased from 250 nm to 400 nm⁴⁴. Goh et al.⁵⁰ have reported that the optical parameters of Ge films deposited by electron beam evaporation stabilize at thicknesses >20 nm⁵⁰, whereas CuInS₂ films deposited by thermal evaporation have been reported to reach stabilization for thicknesses >200 nm⁴⁸.

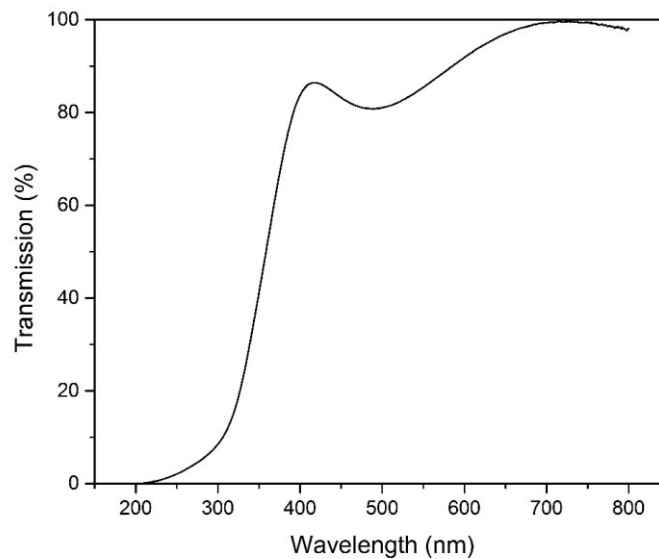


Figure 4.13: Transmission spectrophotometry data for GaN films on sapphire.

In addition, for very thin films (<15 nm), quantum confinement becomes relevant, and the energy spectrum of the two-dimensional system becomes discrete, which results in the size-dependency of the band gap⁵¹. However, in the case of thicker films, such as those studied in this work, the potential effect of thickness on optical parameters may be attributed to crystal disorder, caused by dislocations, stacking

faults and grain boundary misorientation. The presence of acceptor-like defect bands above the valance band could also lead to effective widening of the band gap⁵². Defect states between the conduction band and valance band will generally make the fundamental transition less probable, effectively resulting in a higher observed band gap energy⁴⁷.

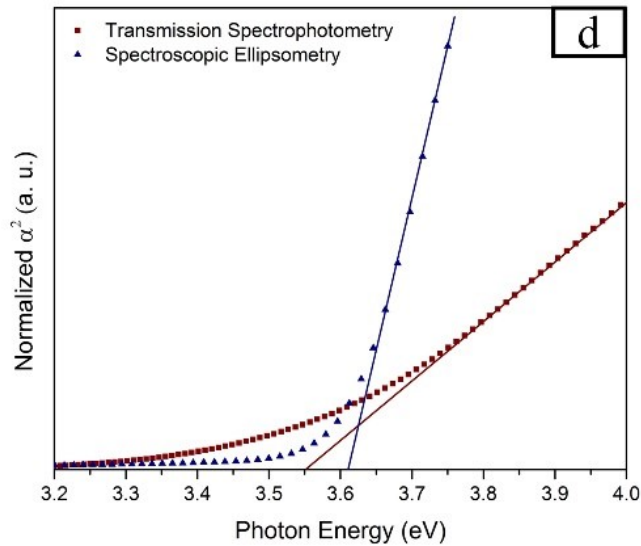


Figure 4.14: comparison of the optical band gap extracted from spectrophotometry and ellipsometry data.

4.4. Conclusions

We have presented compositional and structural evidence of the growth of gallium nitride thin films using atomic layer deposition at 275°C. XPS shows that the films are nearly stoichiometric with low amounts of oxygen and carbon impurities, compared to the values reported in the literature. X-ray reflectometry shows that the deposited GaN has a density equal to 98% of that of the bulk. X-ray diffraction

confirmed that the films are (002)-oriented and highly ordered with low out-of-plane misorientation. Superimposed azimuthal scans of GaN (002) peak and Sapphire (006) peak show evidence of the crystallographic relationship between the film and the substrate. Cross-sectional high resolution TEM micrographs shows that the films are epitaxial for the first ~ 5 nm, before turning polycrystalline. The combination of TEM and AFM observations reveal that the initial epitaxial growth is not sustainable, and transforms into a three-dimensional island growth regime after the first few nanometers of growth. Preliminary electrical measurements indicate that the films are p-type semiconductors with a resistivity of $0.033 \Omega\text{-cm}$, $1.68 \times 10^{18} \text{ cm}^{-3}$ carrier concentration and a carrier mobility of $110 \text{ cm}^2/\text{vs}$. These results have been interpreted in light of XPS stoichiometry analyses. Optical performance of the films has been evaluated using an in-situ spectroscopic ellipsometry. It is shown that the refractive index is slightly lower than the bulk value, and the amount of deviation is within the expected range for films of comparable thicknesses. A similar trend was observed for the optical band gap.

References

- (1) Khan, A.; Balakrishnan, K.; Katona, T. Ultraviolet Light-Emitting Diodes Based on Group Three Nitrides. *Nat. Photonics* 2008, 2, 77–84.
- (2) Asif Khan, M.; Shatalov, M.; Maruska, H. P.; Wang, H. M.; Kuokstis, E. III–Nitride UV Devices. *Jpn. J. Appl. Phys.* 2005, 44, 7191–7206.
- (3) Karam, N. H.; Parodos, T.; Colter, P.; McNulty, D.; Rowland, W.; Schetzina, J.; El-Masry, N.; Bedair, S. M. Growth of Device Quality GaN at $550 \text{ }^\circ\text{C}$ by Atomic Layer Epitaxy. *Appl. Phys. Lett.* 1995, 67, 94.

- (4) Liu, B. .; Lachab, M.; Jia, a; Yoshikawaa, a; Takahashi, K. MOCVD Growth of Device-Quality GaN on Sapphire Using a Three-Step Approach. *J. Cryst. Growth* 2002, 234, 637–645.
- (5) Kushi, K.; Sasamoto, H.; Sugihara, D.; Nakamura, S.; Kikuchi, A.; Kishino, K. High Speed Growth of Device Quality GaN and InGaN by RF-MBE. *Mater. Sci. Eng. B* 1999, 59, 65–68.
- (6) Ponce, F. a.; Bour, D. P.; Young, W. T.; Saunders, M.; Steeds, J. W. Determination of Lattice Polarity for Growth of GaN Bulk Single Crystals and Epitaxial Layers. *Appl. Phys. Lett.* 1996, 69, 337.
- (7) Park, S.-H.; Chuang, S.-L. Comparison of Zinc-Blende and Wurtzite GaN Semiconductors with Spontaneous Polarization and Piezoelectric Field Effects. *J. Appl. Phys.* 2000, 87, 353.
- (8) Park, M.; Maria, J.-P.; Cuomo, J. J.; Chang, Y. C.; Muth, J. F.; Kolbas, R. M.; Nemanich, R. J.; Carlson, E.; Bumgarner, J. X-Ray and Raman Analyses of GaN Produced by Ultrahigh-Rate Magnetron Sputter Epitaxy. *Appl. Phys. Lett.* 2002, 81, 1797.
- (9) Schiaber, Z. S.; Leite, D. M. G.; Bortoleto, J. R. R.; Lisboa-Filho, P. N.; da Silva, J. H. D. Effects of Substrate Temperature, Substrate Orientation, and Energetic Atomic Collisions on the Structure of GaN Films Grown by Reactive Sputtering. *J. Appl. Phys.* 2013, 114, 183515.
- (10) Yadav, B. S.; Singh, S.; Ganguli, T.; Kumar, R.; Major, S. S.; Srinivasa, R. S. Highly Oriented GaN Films Grown on ZnO Buffer Layer over Quartz Substrates by Reactive Sputtering of GaAs Target. *Thin Solid Films* 2008, 517, 488–493.
- (11) Hao, M.; Ishikawa, H.; Egawa, T. Formation Chemistry of High-Density Nanocraters on the Surface of Sapphire Substrates with an in Situ Etching and Growth Mechanism of Device-Quality GaN Films on the Etched Substrates. *Appl. Phys. Lett.* 2004, 84, 4041.

- (12) Yadav, B. S.; Major, S. S.; Srinivasa, R. S. Growth and Structure of Sputtered Gallium Nitride Films. *J. Appl. Phys.* 2007, 102, 073516.
- (13) Knox-Davies, E. C.; Shannon, J. M.; Silva, S. R. P. The Properties and Deposition Process of GaN Films Grown by Reactive Sputtering at Low Temperatures. *J. Appl. Phys.* 2006, 99, 073503.
- (14) Kim, O. H.; Kim, D.; Anderson, T. Atomic Layer Deposition of GaN Using GaCl₃ and NH₃. *J. Vac. Sci. Technol. A Vacuum, Surfaces, Film.* 2009, 27, 923.
- (15) King, D. M.; Du, X.; Cavanagh, A. S.; Weimer, A. W. Quantum Confinement in Amorphous TiO₂ Films Studied via Atomic Layer Deposition. *Nanotechnology* 2008, 19, 445401.
- (16) Ozgit, C.; Donmez, I.; Alevli, M.; Biyikli, N. Atomic Layer Deposition of GaN at Low Temperatures. *J. Vac. Sci. Technol. A Vacuum, Surfaces, Film.* 2012, 30, 01A124.
- (17) Ozgit-Akgun, C.; Goldenberg, E.; Okyay, A. K.; Biyikli, N. Hollow Cathode Plasma-Assisted Atomic Layer Deposition of Crystalline AlN, GaN and Al_xGa_{1-x}N Thin Films at Low Temperatures. *J. Mater. Chem. C* 2014, 2, 2123.
- (18) Elsner, J.; Jones, R.; Heggie, M.; Sitch, P.; Haugk, M.; Frauenheim, T.; Öberg, S.; Briddon, P. Deep Acceptors Trapped at Threading-Edge Dislocations in GaN. *Phys. Rev. B* 1998, 58, 12571–12574.
- (19) Toth, M.; Fleischer, K.; Phillips, M. R. Direct Experimental Evidence for the Role of Oxygen in the Luminescent Properties of GaN. *Phys. Rev. B* 2007, 59, 1575–1578.
- (20) Alevli, M.; Ozgit, C.; Donmez, I.; Biyikli, N. Structural Properties of AlN Films Deposited by Plasma-Enhanced Atomic Layer Deposition at Different Growth Temperatures. *Phys. Status Solidi* 2012, 209, 266–271.

- (21) Rosenberger, L.; Baird, R.; McCullen, E.; GregoryAuner; Shreve, G. XPS Analysis of Aluminum Nitride Films Deposited by Plasma Source Molecular Beam Epitax. *Surf. Interface Anal.* 2008, 40, 1254–1261.
- (22) Harris, J. H.; Youngman, R. A.; Teller, R. G. On the Nature of the Oxygen-Related Defect in Aluminum Nitride. *J. Mater. Res.* 1990, 44128, 1763–1773.
- (23) Motamedi, P.; Cadien, K. XPS Analysis of AlN Thin Films Deposited by Plasma Enhanced Atomic Layer Deposition. *Appl. Surf. Sci.* 2014, 315, 104–109.
- (24) Bermudez, V. .; Koleske, D. .; Wickenden, a. . The Dependence of the Structure and Electronic Properties of Wurtzite GaN Surfaces on the Method of Preparation. *Appl. Surf. Sci.* 1998, 126, 69–82.
- (25) Oila, J.; Kivioja, J.; Ranki, V.; Saarinen, K.; Look, D. C.; Molnar, R. J.; Park, S. S.; Lee, S. K.; Han, J. Y. Ga Vacancies as Dominant Intrinsic Acceptors in GaN Grown by Hydride Vapor Phase Epitaxy. *Appl. Phys. Lett.* 2003, 82, 3433.
- (26) Chason, E.; Mayer, T. M. Thin Film and Surface Characterization by Specular X-Ray Reflectivity. *Crit. Rev. Solid State Mater. Sci.* 1997, 22, 1–67.
- (27) Bruker AXS. General Area Detector Diffraction System (GADDS) User Manual; 4.1 ed.; Madison, WI.
- (28) Birkholz, M. *Thin Film Analysis by X-Ray Scattering*; Wiley, 2006; p. 378.
- (29) Sayed, S. Y.; Buriak, J. M. Epitaxial Growth of Nanostructured Gold Films on Germanium via Galvanic Displacement. *ACS Appl. Mater. Interfaces* 2010, 2, 3515–3524.
- (30) Nagata, T.; Volk, J.; Haemori, M.; Yamashita, Y.; Yoshikawa, H.; Hayakawa, R.; Yoshitake, M.; Ueda, S.; Kobayashi, K.; Chikyow, T. Schottky Barrier Height Behavior of Pt–Ru Alloy Contacts on Single-Crystal N-ZnO. *J. Appl. Phys.* 2010, 107, 103714.

- (31) Eaglesham, D. J.; Gossmann, H.; Cerullo, M. Limiting Thickness H Epi for Epitaxial Growth and Room-Temperature Si Growth on Si(100). *Phys. Rev. Lett.* 1990, 65, 1227–1230.
- (32) Jorke, H.; Kibbel, H.; Sch, F. LOW TEMPERATURE KINETICS OF Si(100) MBE GROWTH. *Thin Solid Films* 1989, 183, 307–313.
- (33) Daudin, B.; Feuillet, G.; Mula, G.; Mariette, H.; Rouviere, J. L.; Pelekanos, N.; Fishman, G.; Adelman, C.; Simon, J. Epitaxial Growth of GaN, AlN and InN : 2D / 3D Transition and Surfactant Effects. *Phys. Status Solidi* 1999, 621, 621–628.
- (34) Daudin, B.; Widmann, F.; Feuillet, G.; Samson, Y.; Arlery, M.; Rouvie, J. L. Stranski-Krastanov Growth Mode during the Molecular Beam Epitaxy of Highly Strained GaN. *Phys. Rev. B* 1997, 56, 7069–7072.
- (35) Liliental-Weber, Z. Derivation of Growth Mechanism of Nano-Defects in GaN from TEM Data. *J. Electron Microsc. (Tokyo)*. 2000, 49, 339–348.
- (36) Coq Germanicus, R.; Picard, E.; Domenges, B.; Danilo, K.; Rogel, R. Microstructure and Electrical Characterization Based on AFM of Very High-Doped Polysilicon Grains. *Appl. Surf. Sci.* 2007, 253, 6006–6012.
- (37) Pang, C. H.; Hing, P.; See, a. Application of Phase-Imaging Tapping-Mode Atomic-Force Microscopy to Investigate the Grain Growth and Surface Morphology of TiSi₂. *J. Vac. Sci. Technol. B Microelectron. Nanom. Struct.* 2002, 20, 1866.
- (38) Kapolnek, D.; Wu, X. H.; Heying, B.; Keller, S.; Keller, B. P.; Mishra, U. K.; DenBaars, S. P.; Speck, J. S. Structural Evolution in Epitaxial Metalorganic Chemical Vapor Deposition Grown GaN Films on Sapphire. *Appl. Phys. Lett.* 1995, 67, 1541.
- (39) Wu, X. H.; Kapolnek, D.; Tarsa, E. J.; Heying, B.; Keller, S.; Keller, B. P.; Mishra, U. K.; DenBaars, S. P.; Speck, J. S. Nucleation Layer Evolution in Metal-Organic Chemical Vapor Deposition Grown GaN. *Appl. Phys. Lett.* 1996, 68, 1371.

- (40) Wetzell, C.; Suski, T.; Ager III, J.; Weber, E.; Haller, E.; Fischer, S.; Meyer, B.; Molnar, R.; Perlin, P. Pressure Induced Deep Gap State of Oxygen in GaN. *Phys. Rev. Lett.* 1997, 78, 3923–3926.
- (41) Saarinen, K.; Ranki, V.; Suski, T.; Bockowski, M.; Grzegory, I. Vacancies as Compensating Centers in Bulk GaN: Doping Effects. *J. Cryst. Growth* 2002, 246, 281–286.
- (42) Rummukainen, M.; Oila, J.; Laakso, a.; Saarinen, K.; Ptak, a. J.; Myers, T. H. Vacancy Defects in O-Doped GaN Grown by Molecular-Beam Epitaxy: The Role of Growth Polarity and Stoichiometry. *Appl. Phys. Lett.* 2004, 84, 4887.
- (43) Chambouleyron, I.; Ventura, S. D.; Birgin, E. G.; Martínez, J. M. Optical Constants and Thickness Determination of Very Thin Amorphous Semiconductor Films. *J. Appl. Phys.* 2002, 92, 3093.
- (44) Akaltun, Y.; Yıldırım, M. A.; Ateş, A.; Yıldırım, M. The Relationship between Refractive Index-Energy Gap and the Film Thickness Effect on the Characteristic Parameters of CdSe Thin Films. *Opt. Commun.* 2011, 284, 2307–2311.
- (45) Klingshirn, C. F. *Semiconductor Optics; Graduate Texts in Physics; Springer Berlin Heidelberg: Berlin, Heidelberg, 2012.*
- (46) Reddy, R. S. Effect of Film Thickness on the Structural Morphological and Optical Properties of Nanocrystalline ZnO Films Formed by RF Magnetron Sputtering. *Adv. Mater. Lett.* 2012, 3, 239–245.
- (47) Kumar, S.; Kumar, S.; Sharma, P.; Sharma, V.; Katyal, S. C. CdS Nanofilms: Effect of Film Thickness on Morphology and Optical Band Gap. *J. Appl. Phys.* 2012, 112, 123512.
- (48) Rabeh, M. Ben; Khedmi, N.; Fodha, M. a.; Kanzari, M. The Effect of Thickness on Optical Band Gap and N-Type Conductivity of CuInS₂ Thin Films Annealed in Air Atmosphere. *Energy Procedia* 2014, 44, 52–60.

- (49) Rahal, A.; Benramache, S.; Benhaoua, B. The Effect of the Film Thickness and Doping Content of SnO₂:F Thin Films Prepared by the Ultrasonic Spray Method. *J. Semicond.* 2013, 34, 093003.
- (50) Goh, E. S. M.; Chen, T. P.; Sun, C. Q.; Liu, Y. C. Thickness Effect on the Band Gap and Optical Properties of Germanium Thin Films. *J. Appl. Phys.* 2010, 107, 024305.
- (51) Gaponenko, S. V. *Optical Properties of Semiconductor Nanocrystals*; Cambridge University Press, 1998; p. 245.
- (52) Meeder, A.; Marrón, D. F.; Rumberg, A.; Lux-Steiner, M. C.; Chu, V.; Conde, J. P. Direct Measurement of Urbach Tail and Gap State Absorption in CuGaSe₂ Thin Films by Photothermal Deflection Spectroscopy and the Constant Photocurrent Method. *J. Appl. Phys.* 2002, 92, 3016.

Chapter Five

The critical effect of growth temperature on the structure and properties of GaN deposited by ALD

(To be submitted to Crystal Growth and Design for publication)

5.1 Introduction

Gallium nitride is a semiconductor with several unique characteristics that make it a versatile choice for many engineering applications¹. The fact that AlN and InN are two semiconductors with similar structure and chemistry to those of GaN means GaN-based alloys can have a tunable optical band gap from infrared to ultraviolet range. This makes GaN an ideal candidate for laser diodes and light-emitting diodes¹⁻⁴. GaN-based materials are chemically and thermally stable, which makes them more versatile for sealed devices and environmental sensors^{5,6}. A high Young's modulus makes them more appropriate than silicon for resonant devices^{5,7}. The pyroelectric properties of these materials offer possibilities for MEMS and NEMS devices with novel functionalities^{8,9}.

Metal-organic chemical vapor deposition is the industry's established method of choice for large scale deposition of GaN¹⁰⁻¹². There has also been a noticeable amount of research done on reactive sputtering^{13,14}, molecular beam epitaxy^{15,16}, and pulsed laser deposition^{17,18} of GaN. While each method features its own advantages and shortcomings, there does not seem to be an established and well-researched method capable for producing crystalline GaN with preferential orientation at low temperatures. In addition, deposition of high-quality ultrathin films with a great degree of thickness control remains a challenge. Atomic layer deposition offers exceptional control over the film thickness, conformality, scale-up potential, and considerably lower deposition temperatures^{19,20}.

One key parameter that determines the final structure and performance of films grown by atomic layer deposition is substrate temperature. There are several studies dedicated to understanding how changing the growth temperature affects the behavior of ALD films²¹⁻²⁷. A survey of this literature shows that even when the chemical reactions of the deposition and the physical structure of the films are similar, changing the growth temperature can lead to diverse and even contrasting results.

Atomic layer deposition of GaN has not been extensively studied and there are only a few publications²⁸⁻³⁰. Furthermore, to our knowledge, there is no report on a comprehensive study on the effect of substrate temperature on the growth mechanism, structural evolution, and electrical properties of GaN. We have recently reported on the successful deposition of crystalline GaN thin films using atomic layer deposition. Further investigations revealed the crucial role of substrate temperature in the relationships among the growth mechanism, structure, and properties of GaN. This paper reports on these new findings, and paves the way for engineering GaN thin films with targeted structural parameters and electrical properties. A comprehensive analysis of the crystal structure, variations of the growth rate and possible relationship with the changes of the surface profile is presented. The effect of these structural changes on electrical resistivity, carrier mobility and refractive index of the films are discussed.

5.2 Experimental

GaN films were deposited in an atomic layer deposition research system (ALD-150LX, Kurt J. Lesker) equipped with an in situ J. A. Woollam M-2000DI ellipsometer with a fixed angle of 70° that has been described in detail elsewhere³¹. Trimethyl gallium (TEG) was used as the gallium precursor, and forming gas, with a nitrogen to hydrogen ratio of 19:1, was used as the other precursor. Pulse and purge times were optimized to achieve a saturated ALD process. All films were grown on sapphire substrates. Samples were deposited at actual substrate temperatures of 150° , 200° , 240° , 275° , 325° , 360° , and 425°C , rounded to the nearest 5°C . These temperature values represent the heater set point temperature corrected by calibrations that were done to determine the actual substrate surface temperature versus heater temperature. All deposition parameters except for the substrate temperature were kept constant for the samples. All substrates were exposed to the N_2/H_2 plasma for 60 seconds to clean and condition the substrate surface immediately prior to the initiation of deposition.

The growth rate and film thickness were collected from spectroscopic ellipsometry data. In order to isolate the effect of temperature on the complex dielectric function, total film thickness was derived from ex-situ measurements at room temperature, and in-situ measurements were exclusively used to study the effect of film thickness on optical properties. X-ray diffraction (XRD) and X-ray reflectometry (XRR) measurements were carried out using a Bruker-AXS D8-Discover machine with a Cu K_α source ($\text{K}_{\alpha 2}$ was removed before analysis). XRD data were collected using a Vantec 500 2-D detector and GADDS software, and analyzed using EVA software.

XRR data and azimuthal scans were recorded using a NaI scintillometer. Commander D8 and Leptos programs were used for data acquisition and analysis, respectively. A Bruker Dimension-Edge AFM system was used to map the sample surface. Silicon tips were used in tapping mode, and the amplitude set point was 2.4 V. AFM results were analyzed using Bruker Nanoscope Analysis 1.5 software. Hall effect measurements were done using a Nanometrics HL5500 system operated at 0.01 μA .

5.3 Results and Discussion

5.3.1 Deposition parameters

In order to establish the optimal deposition parameters for the ALD growth of GaN under saturated ALD conditions, the variation of growth rate, measured by X-ray reflectometry, was studied as a functional of the precursor pulse width. The plotted results are shown in Fig. 5.1. For both precursors, the growth reaches a saturation limit after a certain pulse width. This is indicative of a self-limited growth regime, which is typical of atomic layer deposition. Based on these studies, a single growth cycle consisted of four sections: 0.04s TEG exposure, 7s Ar purge, 15s N_2/H_2 plasma exposure, and 7s Ar purge.

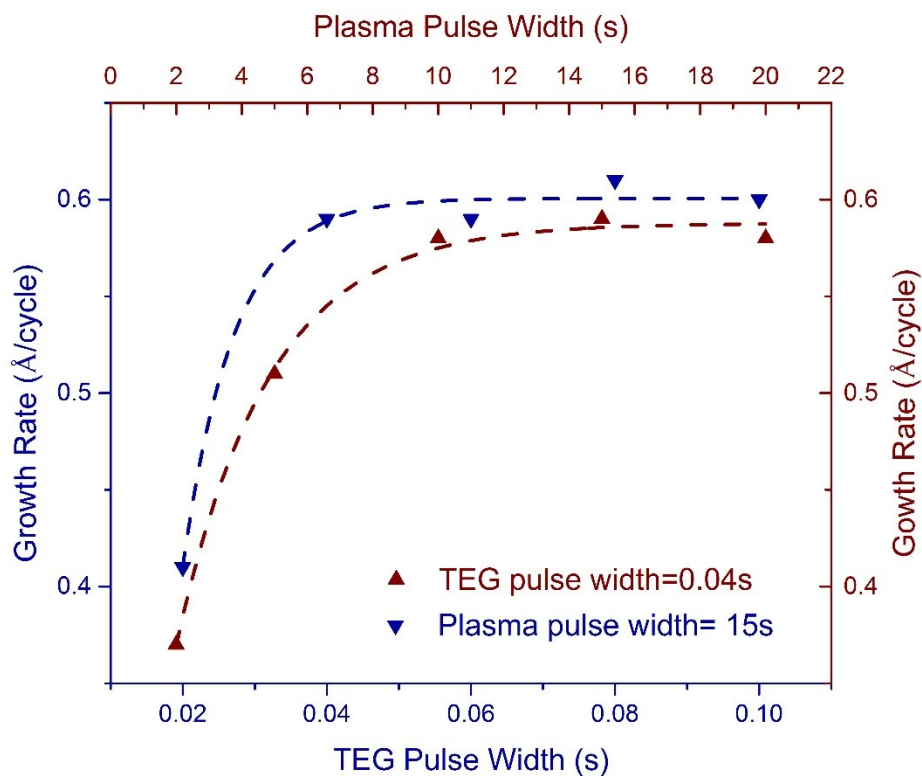


Figure 5.1: ALD saturation curves for the two precursors; the deposition temperature and plasma power were 275°C and 600W, respectively.

5.3.2 Crystal structure

Two-dimensional X-ray diffraction was used to analyze the crystal structure of the films. The schematic of the test setup is shown in Fig. 5.2. The detector collects data in a window of θ and χ angles. For the used settings, the output data is in the form of an image, in which θ increases leftwards from 32° to 43°, while χ changes

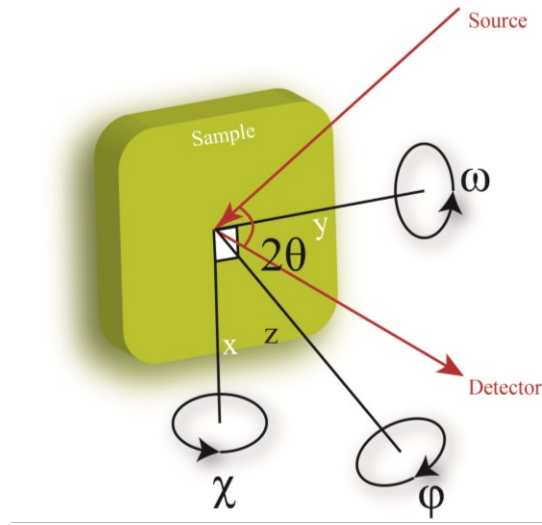


Figure 5.2: Schematic illustrating the geometric variables of XRD test.

along the arcs centered at $2\theta = 0^\circ$. At $2\theta = 36^\circ$, χ increases downwards from -90° to -81° . The imaginary horizontal line passing through the center of the image indicates $\chi = -90^\circ$. These images are the results of the data recorded while ω was scanned from 15° to 28° , and 2θ was kept constant at 34° . Under these conditions, random out-of-plane orientation creates cones of diffracted x-rays, which are intercepted by the detector, and revealed as rings with a uniform radial intensity distribution³². Therefore the degree of radial nonuniformity in the image is a measure of crystal order^{33,34}. Fig. 5.3 shows the two-dimensional XRD frames.

All the images feature a bright dot at $2\theta = 41.6^\circ$, which corresponds to the sapphire (006) reflection. The fact that this diffraction creates a dot with a very narrow distribution along χ indicates that the (006) reciprocal lattice vector becomes coplanar with the beam vector only at $\chi = -90$. This is expected from a single crystal wafer. Study of Fig. 5.3 shows that no significant trace of GaN crystals is detected

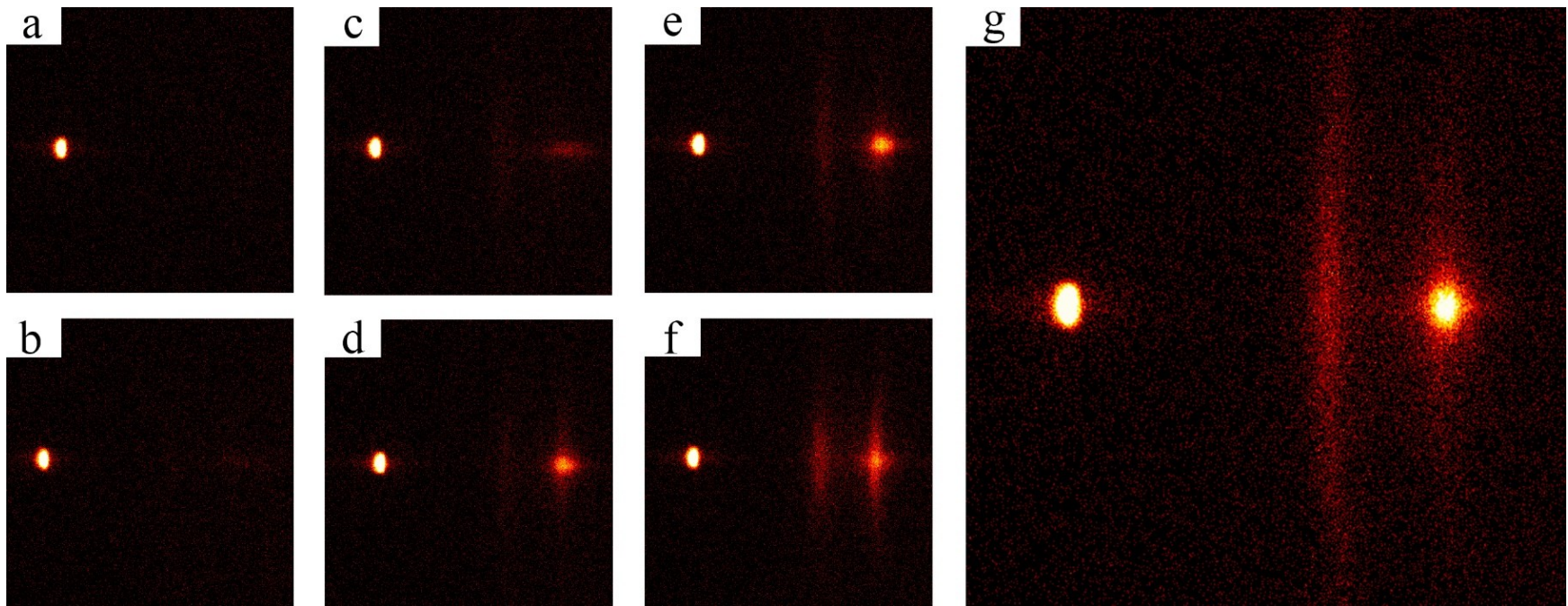


Figure 5.3: Two-dimensional XRD frames of 1000-cycle GaN films deposited at a) 150°C b) 200°C c) 240°C d) 275°C e) 325°C f) 360°C g) 425°C.

at 240°C and below. At 275°C (Fig. 5.3-d), a bright dot appears at 34.4°. This corresponds to the GaN (002) reflection. The absence of (100) and (101) reflections indicates a preferential growth orientation along the (002) plane normal. At this temperature the pattern looks similar to that of a single crystal. At higher deposition temperatures, the (002) dot keeps getting brighter, while an arc appears at $2\theta = 36.9^\circ$, and corresponds to GaN (101) reflection. At 425°C the (101) dot shows a significant increase in intensity and improvement in distribution, but the (101) arc is also more noticeable. The fact that the (101) intensity is distributed along an arc necessitates the integration of data over lines and arcs for comparison.

Figs. 5.4 and 5.5 show the results of integration over χ along 2θ and vice versa, respectively. As seen in Fig. 5.4, no measurable GaN crystallinity exists at 240°C and below. It seems that the strongest (002) preferential orientation is observed at 275°C. At higher temperatures the ratio of (101) to (002) peak keeps rising, hence the weaker preferential orientation. Fig. 5.5 compares the degree of preferential orientation along χ . All the samples deposited at and above 275°C show strong peaks at $\chi = -90^\circ$. In general, the preferential orientation is maintained or improved with increasing temperature, with the exception of the sample deposited at 360°, in which a slightly wider distribution is observed.

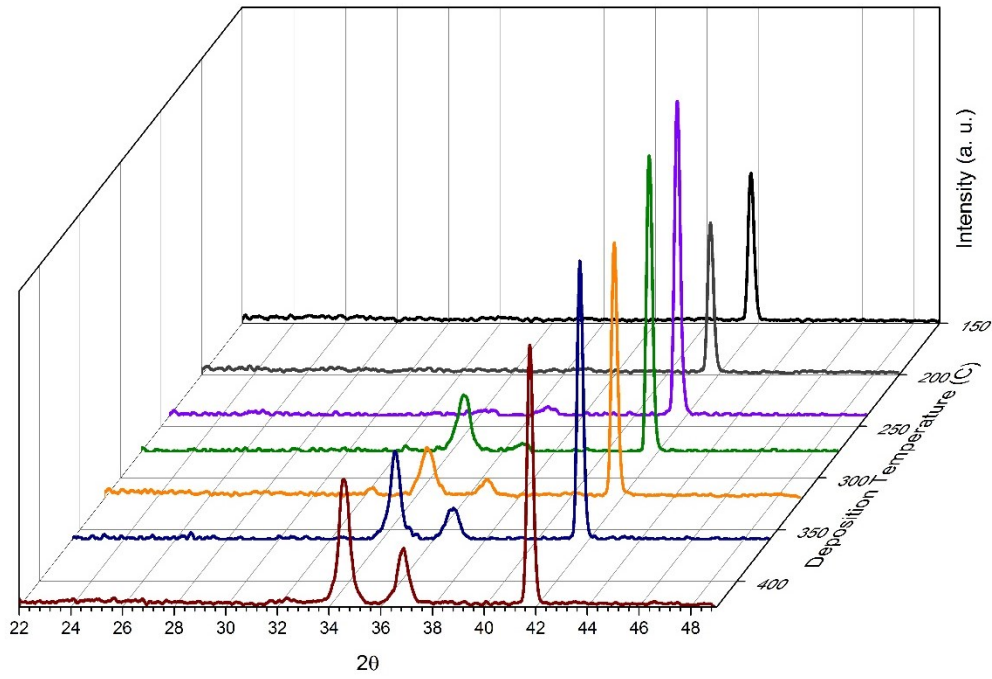


Figure 5.4: Integration of the diffraction intensity as a function of 2θ for GaN films deposited at various substrate temperatures.

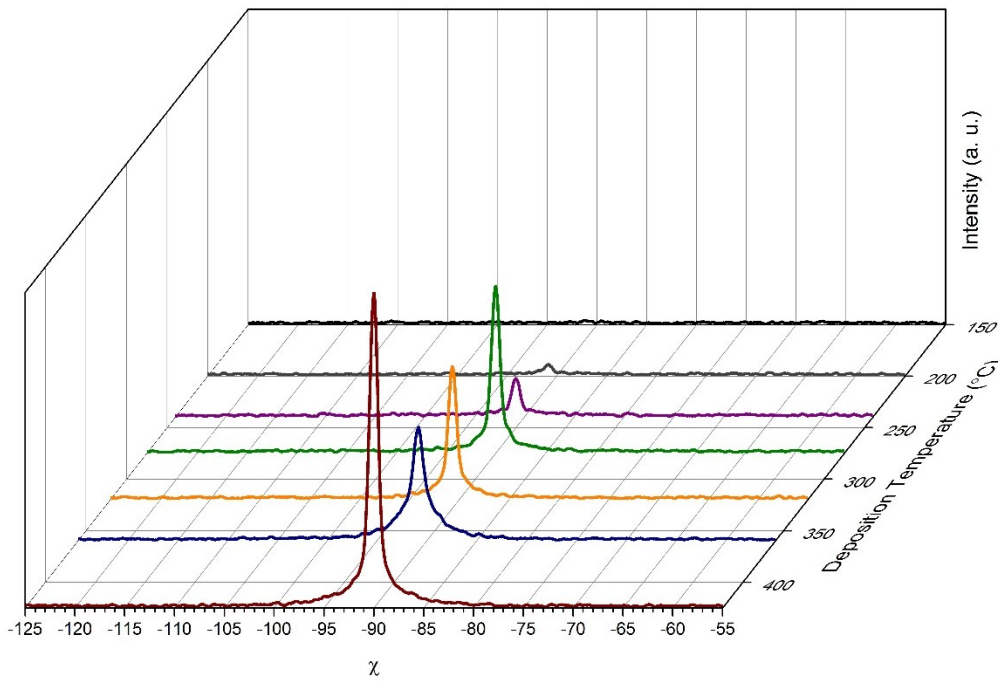


Figure 5.5: Integration of the diffraction intensity as a function of χ for GaN films deposited at various substrate temperatures.

While a general transition from amorphous to crystalline films has been reported before for ALD of semiconductors^{22,23,35,36}, the further changes of crystal structure observed after the onset of crystallinity at 275°C is not commonly reported. Yuan et al.²⁶ have reported the tendency of ALD ZnO grown on glass to lose preferential orientation at higher temperature, which is the more extreme case of what we observed for GaN between 275° and 425°C. Since both studies show an increased growth rate at higher temperatures, this could potentially explain the randomization of crystal orientation. In other words, the higher growth rate leaves less time for the atoms to relocate and minimize their surface energy, which is the root cause of the (002) preferential orientation.

Although a quantitative comparison of the peak intensities among different samples might be intriguing, great caution should be taken before proceeding. In thin films with strong preferential orientation, the diffraction intensity of the planes parallel to the surface is extremely sensitive to sample orientation. The maximum intensity is achieved when the beam vector and surface normal are exactly coplanar, and that is rarely the case in practice. The effect of this misorientation was revealed in a ϕ -scan and shown in Fig. 5.6. The top spectrum shows the (006) reflection of

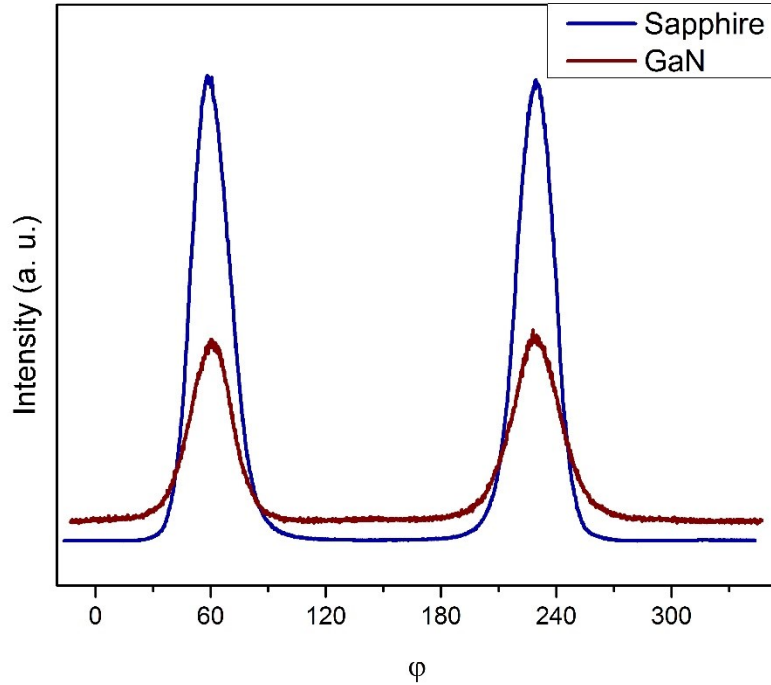


Figure 5.6: The azimuthal scans of sapphire (006) and GaN (002) deposited at 325°C.

sapphire, while the one on the bottom shows the (002) reflection of GaN. For the two spectra, the ω angle was set to 20.8° and 17.2° respectively, and 2θ was kept constant at twice the mentioned values, while the sample was rotated 360° around the surface normal. The two independently recorded spectra were then superimposed for comparison. The most noteworthy feature of Fig. 5.6 is the extensive variation of the recorded intensity vs. ϕ . As explained earlier, this effect was caused by noncoplanarity of the beam vector and the surface normal. Since the exact coplanarity angle can only be detected using a scintillometer, the XRD spectra featured in Fig. 5.4 recorded with a two-dimensional detector cannot be used for a quantitative comparison of (002) peak intensities. Another noteworthy feature of Fig. 5.6 is the fact that the two spectra show maxima at the same ϕ values. This is

an indication that the normal to the sapphire (006) plane and GaN (002) plane are aligned³⁷. In other words, this is proof of crystallographic relationship between the two lattices.

Considering the above discussion, any valid comparison between the samples should be performed when the peak intensity is at its maximum value. XRD rocking curves of GaN (002) peaks were used for this purpose. A ϕ -scan was performed individually for each sample, then ϕ was set at the value that provided the coplanarity condition. The rocking curves were then recorded under this condition, while 2θ was set at the peak position, and the variation of intensity vs. ω was recorded. The results are shown in Fig. 5.7. Analysis of the spectra reveals that the FWHM remains constant, while the peak intensity varies among the samples. This indicates that the distribution of interplanar distance remains unchanged for the samples, while the total diffraction intensity increases with increasing temperature. The intensity drop from 325° to 360°C could be an indication of either lower crystallinity or weaker preferential orientation of the sample deposited at 360°C.

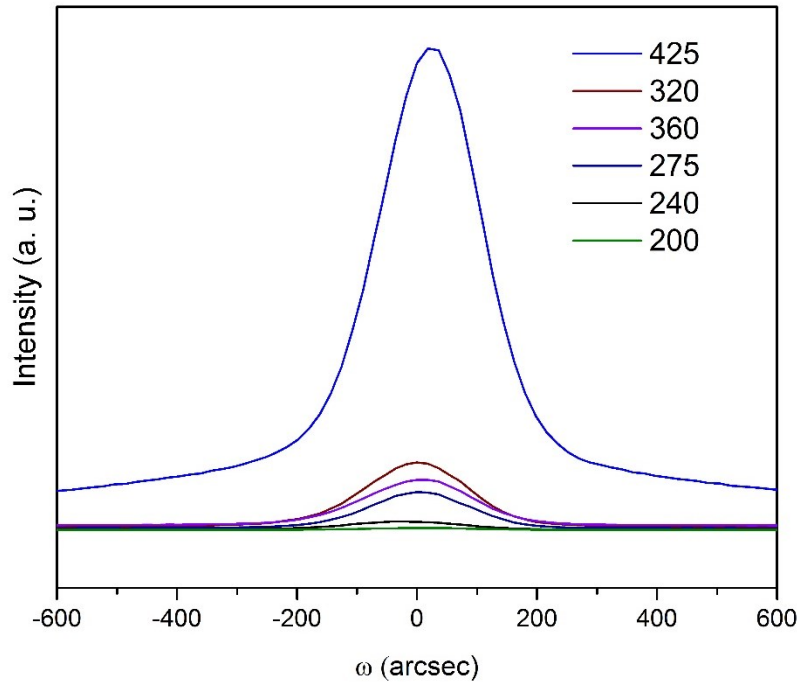


Figure 5.7: Evolution of XRD rocking curves of the GaN (002) peak with increasing substrate temperature.

As seen, the intensity at 425°C is markedly higher than all other samples. This is due to contributions from the degree of crystallinity, the preferential orientation, and the higher growth rate at this temperature, as discussed later.

5.3.3 Growth rate and mechanism

The variation of the growth rate, as the substrate temperature increases, is shown in an Arrhenius plot in Fig. 5.8. A steady rise in the growth rate is observed, for temperatures up to 360°C. An increase in the kinetic energy of the reactants is deemed responsible for this increase.

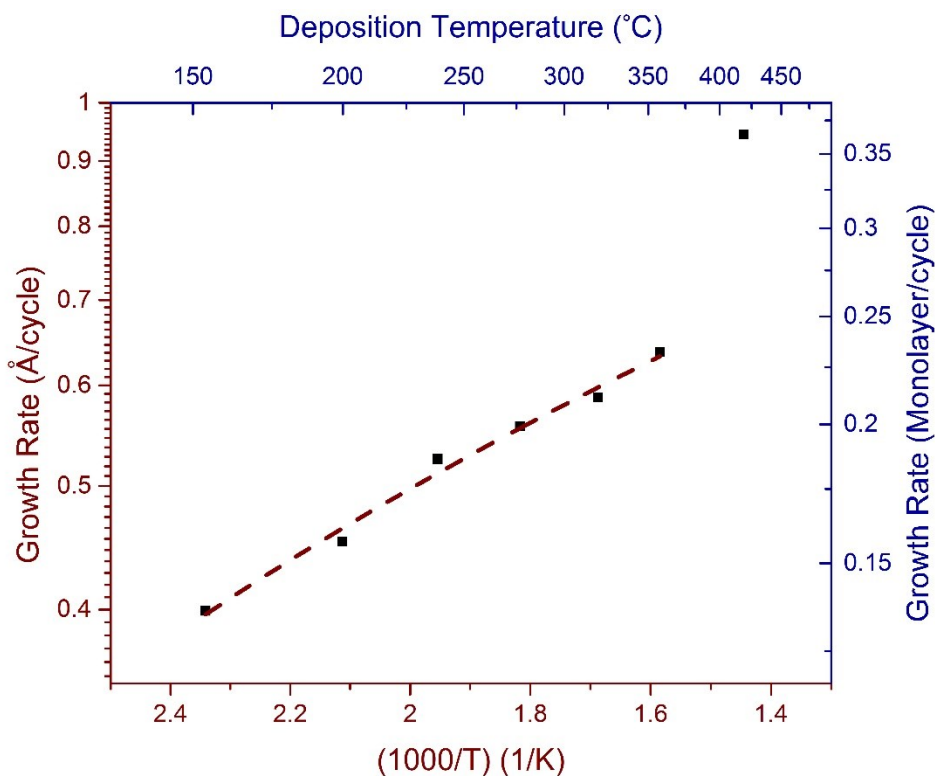


Figure 5.8: Growth rate of GaN as a function of growth temperature.

This result also indicates that the known mechanisms for potential decrease of the ALD growth rate vs. substrate temperature either are not activated or their effects are not strong enough to overcompensate that of the increased kinetic energy. In other words, no significant premature dissociation of the precursors or desorption of the deposited material occur within this temperature range. The general trend of increasing growth rate with temperature has been reported earlier for temperatures below 500°C^{28,29}. Considering the fact that the temperature of the precursor lines and the chamber walls are less than 150°C, which is well below the homogenous pyrolysis temperature of TEG^{38,39}, homogeneous decomposition is ruled out. Donnelly and coworkers^{40,41} have conducted mass spectrometric studies of thermal

decomposition of adsorbed TEG on GaAs. They reported that at higher temperatures ($>300^{\circ}\text{C}$) a greater portion of the decomposition products consists of hydrocarbons, and that Ga atom sticking probability increases. If a similar trend exists for GaN it could contribute to ALD growth, and lead to higher growth rates at elevated substrate temperatures. As seen in Fig. 5.8, an unusual jump in the growth rate is observed for deposition at 425°C . This peculiar result does not fit the aforementioned exponential trend. A survey of the literature shows that some authors have rushed to blame an increase in ALD growth rate at higher temperatures on a relatively vague phenomenon, called “CVD-like reactions”, hence ruling them out as ALD depositions, solely based upon the growth rate^{24,35}.

As discussed above, we are under the impression that the situation is not favorable for homogeneous pyrolysis of TEG. In addition, any CVD-like reaction among the products of pyrolysis would compromise the structural integrity of the films. This would manifest itself in the form of disturbed crystal order, lower mass density, and lower carrier mobility. None of these symptoms were observed for the films grown at 425°C . Furthermore, in case of pyrolysis and CVD-like reactions, there would be no constraint that limits the growth rate to the characteristic sub-monolayer-per-cycle growth rate of ALD. For the films under study in this thesis, even after the jump at 425°C , the growth rate is still below 0.5 ML/cycle, which is typical for ALD reactions. Given these three reasons, we are convinced that all the films have grown through valid ALD mechanisms. Therefore, explanation of the peculiarly high growth rate at 425°C requires a comprehensive and multifaceted approach that will be discussed later, in light of XRD and AFM studies.

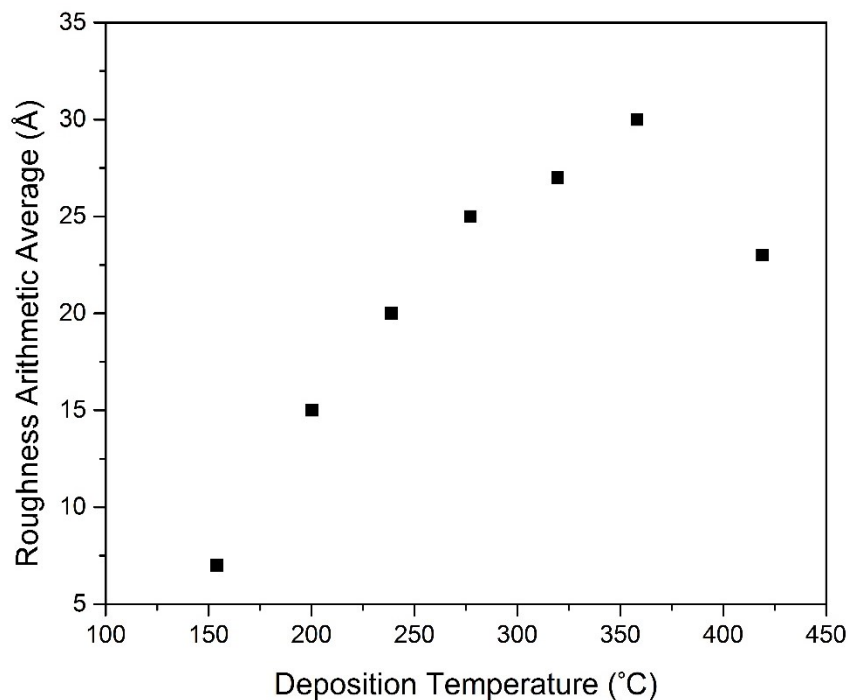


Figure 5.9: Variations of GaN surface roughness vs. deposition temperature.

Atomic force microscopy was employed to measure the average surface roughness of the films. The results are shown in Fig. 5.9. As seen, the roughness reaches a maximum at 360°C, before it starts to decrease. It is important to note that in our studies surface roughness was shown to increase with film thickness. Considering the fact that GPC at 425°C is 48% higher than that at 360°C and that the two films have the same number of ALD cycles, the sample deposited at higher temperature is thicker and expected to have a considerably higher surface roughness. Yet the opposite is observed. In order to understand this, the changes in the surface morphology must be closely studied.

Fig. 5.10 shows the AFM images from the surface of three films deposited for 1000 cycles at different temperatures. At 150°C the surface of the film is mostly two-

dimensional with occasional sporadic bumps. The 325°C landscape is markedly different, as the entire surface is covered with sharp hillocks of high aspect ratio. The average roughness is therefore expected to be substantially higher than Fig 5.10a. In contrast to this trend, in Fig. 5.10c the surface bumps have gotten thicker, and show a smaller aspect ratio. It seems that the bumps have a tendency to grow in diameter, as well as length. A good understanding of this behavior needs knowledge about the crystal structure and the nature of the directional growth in the films.

Comprehensive XRD studies (Figs. 5.3-7) have shown that the reciprocal lattice vector is parallel to the substrate (001) normal. As a result, the increase in the hillock aspect ratios, demonstrated by the increasing roughness, is due to accelerated growth in [001] crystallographic direction. Similarly, a decrease in aspect ratio indicates an accelerated growth along $\langle 100 \rangle$ and $\langle 101 \rangle$ directions. The fact that this acceleration happens at higher temperatures means it is temperature induced, and has a higher activation energy than that of the [001] direction. Gu et al.⁴² studied the lateral overgrowth of GaN and reported that the ratio of growth along the (002) and (100) surface normals varies significantly with deposition parameters such as the substrate temperature. Similar results have been reported by other researchers^{43,44} This concept has been schematically demonstrated in Fig. 5.11, where the surface hillocks are shown to be comprised of $\{10\bar{1}0\}$ and (0001) planes. As shown, increasing the growth temperatures affects the growth rate along $\{10\bar{1}0\}$ surface normals to a greater degree, compared to the (0001) normal.

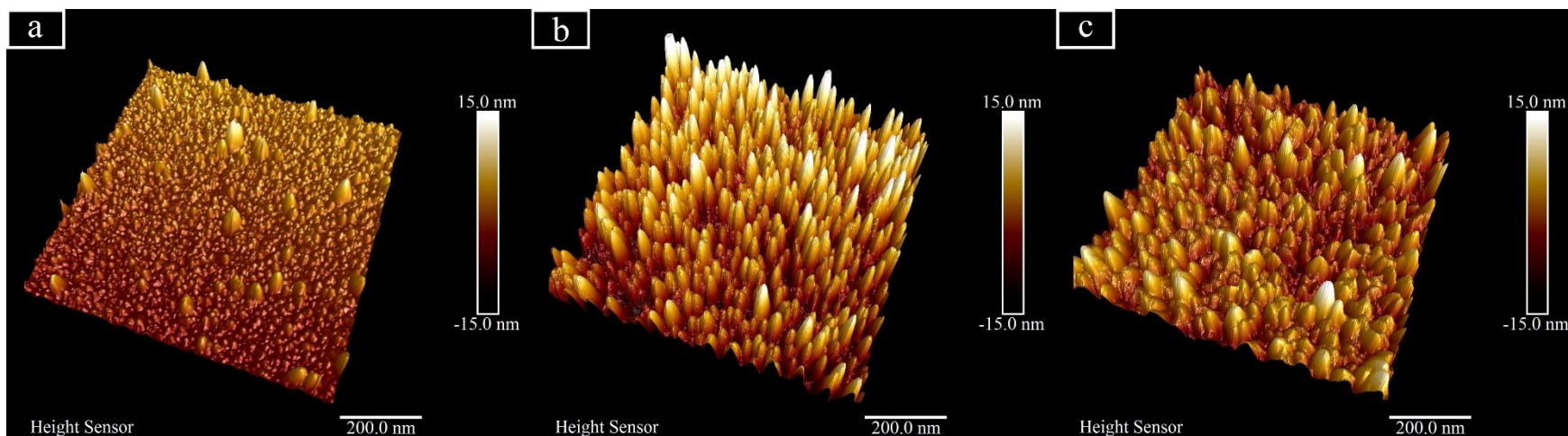


Figure 5.10: AFM images of 1000 cycle-grown GaN films with the substrate temperature of a) 150°C b) 325°C c) 425°C.

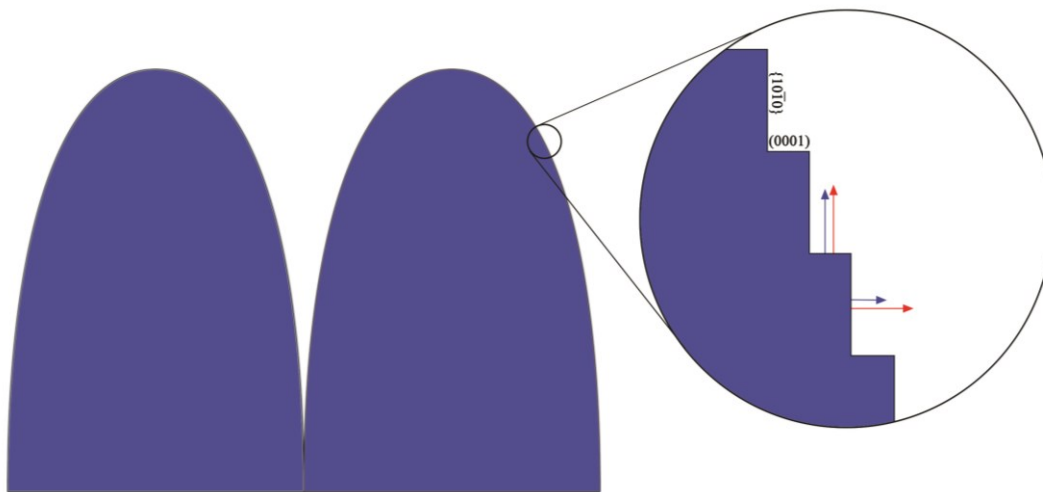


Figure 5.11: Schematic illustrating the effect of substrate temperature on lateral and longitudinal growth rates of GaN hillocks; blue and red arrows indicate lower and higher temperature, respectively.

5.3.4 Structure and normalized density

X-ray reflectometry (XRR) is a characterization technique used to probe the structure of the thin films. Fig. 5.12 shows XRR curves of GaN ALD thin films deposited at various temperatures. For samples deposited at lower temperatures Kiessig fringes can be clearly observed. While the distance between the two consecutive peaks is indicative of the film thickness, while roughness and density mainly affect the rate of drop in the mean intensity and the intensity fluctuation amplitude.

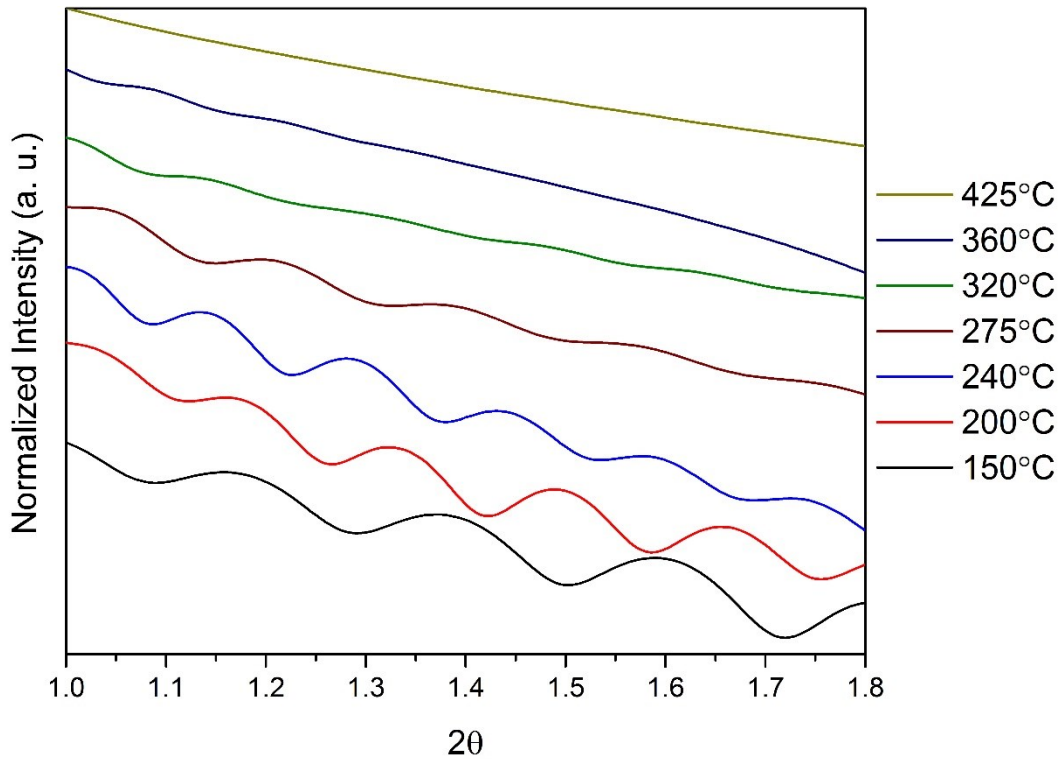


Figure 5.12: X-ray reflectometry spectra of GaN films deposited at various temperatures.

The gradual disappearance of Kiessig fringes might be the result of the rising roughness. This trend agrees with variation of roughness, as shown in Fig. 5.9 up to 360°C. It can be seen that even at 360°C traces of Kiessig fringes are detectable at lower angles, but the 425° sample shows a completely flat curve, in spite of the fact that the roughness actually decreases after 360°, as shown previously in Fig. 5.9.

If surface roughness were the sole cause of waning Kiessig fringes, the faint intensity fluctuations at lower 2θ angles observed at deposition temperature of 360° would amplify when the substrate temperature is further heated to 425°C, as the surface roughness drops. However, the sample deposited at 425° shows the absence of any such fluctuations. The simultaneous occurrence of the two seemingly contradictory observations necessitates the presence of a rival mechanism.

It has been repeatedly demonstrated that exposure of sapphire (001) surface to nitrogen plasma leads to formation of a nitride layer. The formation of this layer has been demonstrated using XPS⁴⁵⁻⁴⁷, RHEED⁴⁸, and AFM^{45,49}. The existence of such a layer means a gradual transition from Al₂O₃ to GaN, and the absence of a sharp interface. Kiessig fringes emerge after reflection of X-rays from a well-defined interface, whose absence disallows their existence. Since all the films were exposed to N₂/H₂ plasma for one minute prior to the start of deposition, formation of this transition AlN layer seems to be a likely contributor to the waning of the Kiessig fringes.

Due to the rapid attenuation of the Kiessig fringes, a reliable simulation could not be performed for the films deposited at higher temperatures, and the extraction of mass density from the XRR data requires another method. It is known that with increasing X-ray angle of incidence, there is a critical angle, at which the X-rays start penetrating the surface of the sample, and this angle is proportional to the square root of mass density of the film. Using the variations of the critical angle, the relative density of the films was derived and plotted in Fig. 5.13.

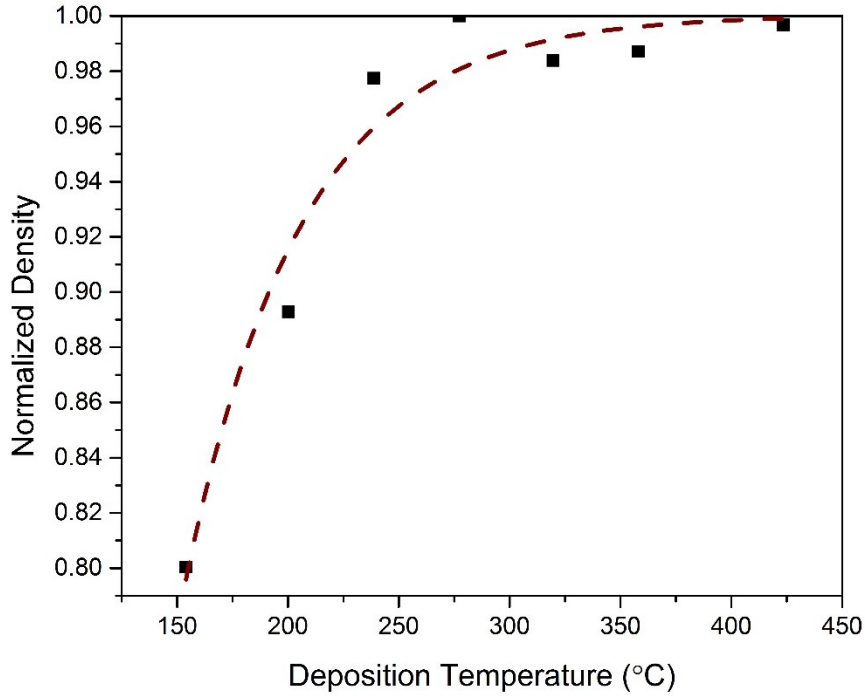


Figure 5.13: Variations of the mass density as a function of the growth temperature. The numbers are normalized to the maximum observed density.

The first minimum in the second derivative of intensity was regarded as the threshold of X-ray penetration. The unit relative density in Fig. 5.13 corresponds to 5.96 gcm^{-3} , which is 97% of the bulk density. It is observed that at the deposition temperature of 240°C , the mass density reaches the relative value of 0.98, and no meaningful change occurs above that.

5.3.5 Electrical and optical properties

Hall mobility measurements were conducted on the samples, and the results are shown in Fig. 5.14, where increasing the deposition temperature results in a decrease in resistivity and an increase in Hall mobility, respectively. Increasing the deposition temperature from 150°C to 425°C elevates Hall mobility from 2.2 to $575 \text{ cm}^2/\text{Vs}$, and decreases the resistivity from 3.7 to $7 \times 10^{-3} \Omega\text{-cm}$. The

Hall mobility measured at 425°C is higher than what has been reported in several studies for thicker films deposited using CVD⁵⁰⁻⁵³ and MBE⁵⁴ at considerably higher temperatures.

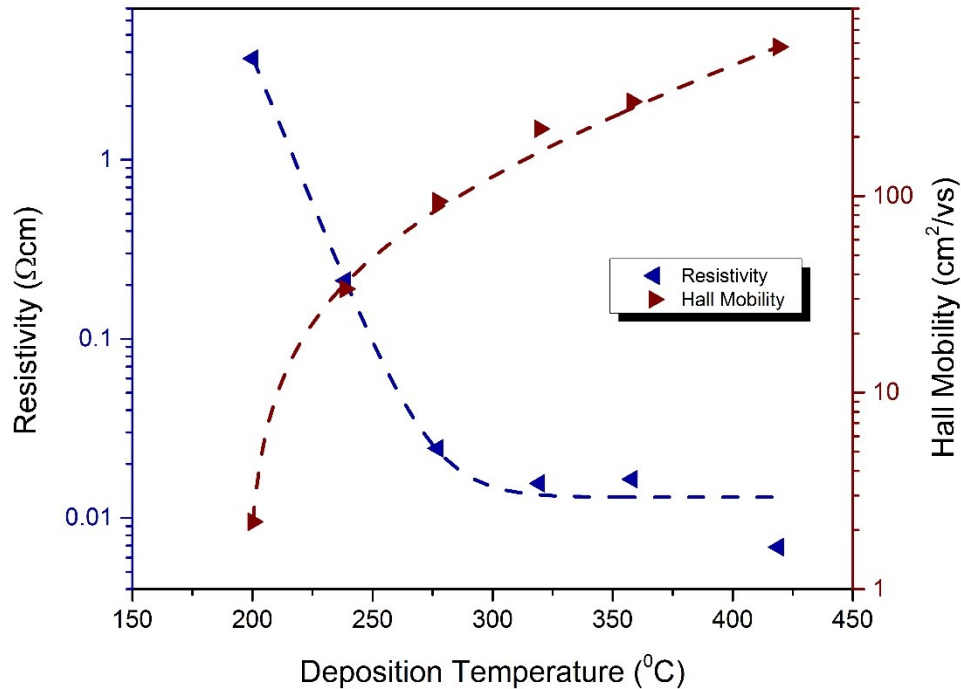


Figure 5.14: The dependence of resistivity and carrier mobility on the substrate temperature.

The increasing mobility versus substrate temperature, which has also been reported for CVD-grown GaN at temperatures above 1000°C⁵³, could be attributed to the rising density, increasing crystallite size, and improving crystal quality, as discussed earlier. Crystal defects are known to adversely affect both mobility and conductivity, as they scatter the charge carriers⁵³. Similar relationships between crystal structure and carrier mobility has also been reported by other researchers^{25,55}. Cheng et al.²¹ reported that increasing the substrate temperature from 300° to 500°C during the atomic layer deposition of TiN results in a drop in resistivity by two orders of

magnitude. A simultaneous increase in crystal order has also been reported by the authors. It is noteworthy that the films registered as p-type in our measurements.

In-situ ellipsometry was employed to study the variations of refractive index of the films as they grow at different temperatures. A similar trend was observed for the changes of refractive index as a function of thickness in all temperatures: a sharp drop was observed during the first initial ~100 cycles, before it starts increasing again (Fig. 15). This behavior has been reported earlier by the authors, and analyzed in view of TEM studies. In short, the layers close to the interface are made up of higher quality crystal, and this phenomenon is reflected in the optical performance of the films.

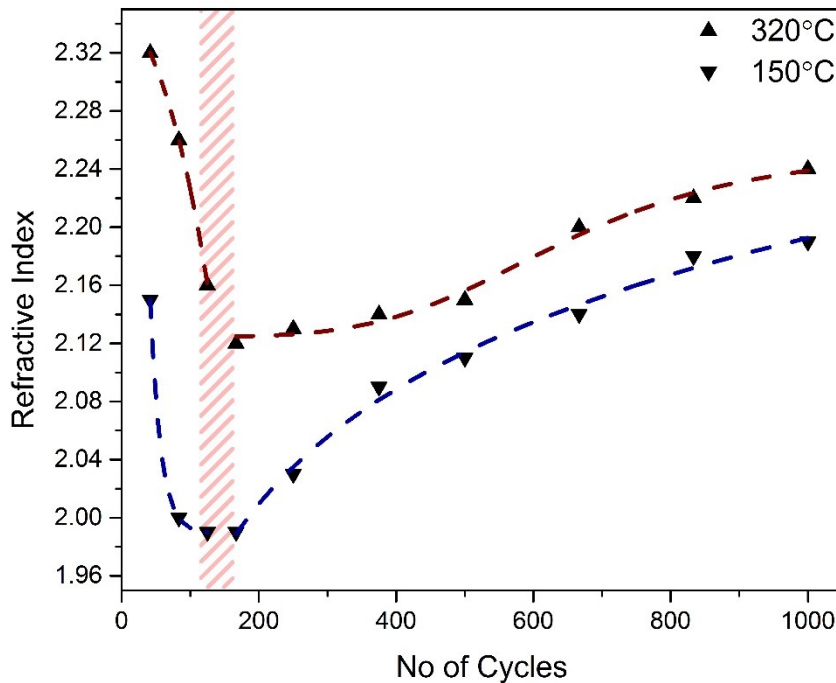


Figure 5.15: The in-situ observation of the evolution of refractive index at 632 nm, plotted at two representative temperatures.

The variations of the refractive index of the films after 1000 cycles of deposition at various temperatures are shown in Fig. 5.16.

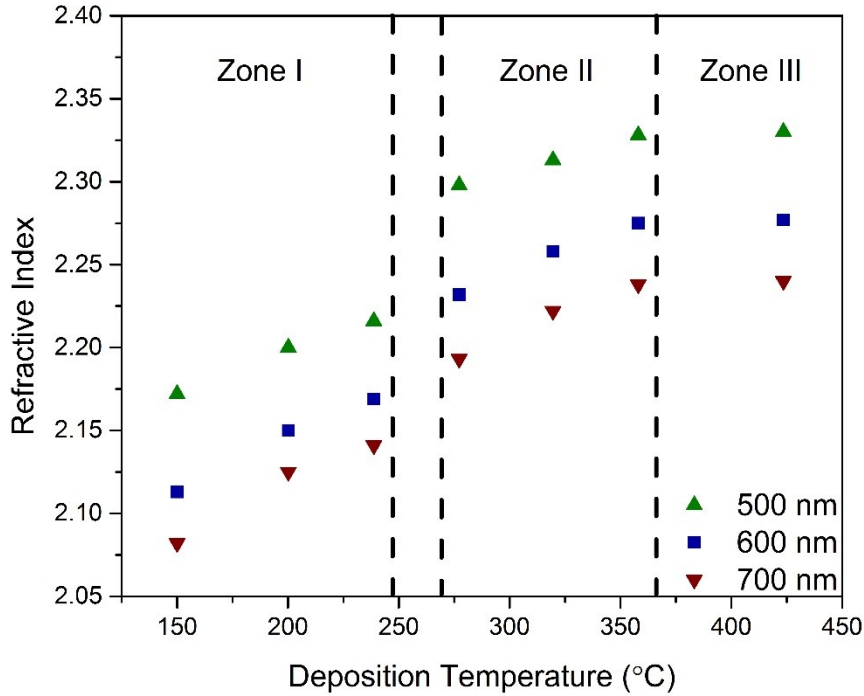


Figure 5.16: The in-situ observation of the evolution of refractive index at 632 nm, plotted at two representative temperatures b) The dependence of refractive index on the growth temperature, plotted at three different representative wavelengths; three different zone have been designated based on the behavior of the refractive index.

The data are the results of ex-situ measurements at room temperature. Three temperature zones are identified on the graph. In zones I and II the refractive index increases with increasing temperature, while a sudden jump is observed between the two. In zone III, the index reaches a plateau, and is no longer dependent on the temperature. The variations in the refractive index can be analyzed for the three different temperature zones. In Zone I, below 240°C, the refractive index shows a steady increase. In this zone, the rise of refractive index is due to the increase in mass density (Fig.

5.13). Between 240°C and 275°C a sudden jump is observed. Fig. 5.3 shows that 275°C is the onset of crystallinity. Therefore this jump can be attributed to the difference between the optical properties of amorphous and crystalline GaN. Reports on the effect of crystallinity on the refractive index of semiconductors have been published before^{56–58}. It has been shown that larger grain size and higher quality crystallites, as manifested in XRD patterns, leads to higher refractive index. As Fig. 5.3 shows, the diffraction patterns of the crystals are more pronounced, as the deposition temperature rises. This leads to an increase in the refractive index up until the deposition temperature of 360°C, as shown in Fig. 5.16. The range of temperature spanning from 275° to 360°C has therefore been designated as zone II, in which crystal quality determines the refractive index. Further increase of the temperature does not raise the index, and a saturation behavior is observed. Therefore temperatures above 360°C have been designated as zone III, where the increase of temperature does not affect the refractive index of GaN.

5.4 Conclusions

Substrate temperature was found to have a crucial role in all aspects of growth, structural evolution, electrical and optical properties of GaN films grown by atomic layer deposition. The films were found to be amorphous at temperatures of 240°C and below. XRD indicated that crystal quality improves at higher temperatures, owing to larger grain size and the optimal (002) orientation which occurs at 275°C and above. Nevertheless, clear proof of crystallographic relationship between the substrate and the films was observed for all the crystalline films. The combination of spectroscopic ellipsometry and AFM results strongly implies that a secondary growth mechanism is activated at 425°C. This leads to a substantial increase in growth rate, and a lower surface roughness. XRR

analyses show that the characteristic Kiessig fringes gradually disappear at higher temperatures, regardless of the trends in variation of roughness. This is likely due to the formation of a thin AlN interlayer at the interface of the substrate and the film. Variation of the refractive index is a function of both film density and crystal structure, with a clear jump at the onset of crystallinity. Significant improvements of more than two orders of magnitude were observed in film conductivity and Hall mobility, when the substrate temperature was increased from 150°C to 425°C.

References

- (1) Hardy, M. T.; Feezell, D. F.; DenBaars, S. P.; Nakamura, S. Group III-Nitride Lasers: A Materials Perspective. *Mater. Today* 2011, 14, 408–415.
- (2) Khan, A.; Balakrishnan, K.; Katona, T. Ultraviolet Light-Emitting Diodes Based on Group Three Nitrides. *Nat. Photonics* 2008, 2, 77–84.
- (3) Orton, J. w; Foxon, C. T. Group III Nitride Semiconductors for Short Wavelength Light-Emitting Devices. *Reports Prog. Phys.* 1998, 61, 1–75.
- (4) Ponce, F. A.; Bour, D. P. Nitride-Based Semiconductors for Blue and Green Light-Emitting Devices. *Nature* 1997, 386, 351–359.
- (5) Pearton, S. J.; Kang, B. S.; Kim, S.; Ren, F.; Gila, B. P.; Abernathy, C. R.; Lin, J.; Chu, S. N. G. GaN-Based Diodes and Transistors for Chemical, Gas, Biological and Pressure Sensing. *J. Phys. Condens. Matter* 2004, 16, R961–R994.
- (6) Stutzmann, M.; Steinhoff, G.; Eickhoff, M.; Ambacher, O.; Nebel, C. E.; Schalwig, J.; Neuberger, R.; Müller, G. GaN-Based Heterostructures for Sensor Applications. *Diam. Relat. Mater.* 2002, 11, 886–891.
- (7) Cimalla, V.; Pezoldt, J.; Ambacher, O. Group III Nitride and SiC Based MEMS and NEMS: Materials Properties, Technology and Applications. *J. Phys. D. Appl. Phys.* 2007, 40, 6386–6434.
- (8) Ambacher, O.; Eickhoff, M.; Link, a.; Hermann, M.; Stutzmann, M.; Bernardini, F.; Fiorentini, V.; Smorchkova, Y.; Speck, J.; Mishra, U.; et al. Electronics and Sensors Based on Pyroelectric AlGaIn/GaN Heterostructures. *Phys. Status Solidi* 2003, 1907, 1878–1907.
- (9) Chattopadhyay, S.; Ganguly, A.; Chen, K.-H.; Chen, L.-C. One-Dimensional Group III-Nitrides: Growth, Properties, and Applications in Nanosensing and Nano-Optoelectronics. *Crit. Rev. Solid State Mater. Sci.* 2009, 34, 224–279.
- (10) Ni, X.; Fu, Y.; Moon, Y. T.; Biyikli, N.; Morkoç, H. Optimization of a-Plane GaN Growth by MOCVD on R-Plane Sapphire. *J. Cryst. Growth* 2006, 290, 166–170.

- (11) Arslan, E.; Ozturk, M. K.; Teke, A.; Ozcelik, S.; Ozbay, E. Buffer Optimization for Crack-Free GaN Epitaxial Layers Grown on Si(1 1 1) Substrate by MOCVD. *J. Phys. D. Appl. Phys.* 2008, 41, 155317.
- (12) Imer, B.; Wu, F.; Craven, M. D.; Speck, J. S.; DenBaars, S. P. Stability of (1\bar{1}00) M - Plane GaN Films Grown by Metalorganic Chemical Vapor Deposition. *Jpn. J. Appl. Phys.* 2006, 45, 8644–8647.
- (13) Knox-Davies, E. C.; Shannon, J. M.; Silva, S. R. P. The Properties and Deposition Process of GaN Films Grown by Reactive Sputtering at Low Temperatures. *J. Appl. Phys.* 2006, 99, 073503.
- (14) Junaid, M.; Hsiao, C.-L.; Palisaitis, J.; Jensen, J.; Persson, P. O. Å.; Hultman, L.; Birch, J. Electronic-Grade GaN(0001)/Al₂O₃(0001) Grown by Reactive DC-Magnetron Sputter Epitaxy Using a Liquid Ga Target. *Appl. Phys. Lett.* 2011, 98, 141915.
- (15) Calarco, R.; Meijers, R. J.; Debnath, R. K.; Stoica, T.; Sutter, E.; Lu, H. Nucleation and Growth of GaN Nanowires on Si (1 1 1) Performed by Molecular Beam Epitaxy. *Nano Lett.* 2007, 7, 2248–2251.
- (16) Debnath, R. K.; Meijers, R.; Richter, T.; Stoica, T.; Calarco, R.; Lüth, H. Mechanism of Molecular Beam Epitaxy Growth of GaN Nanowires on Si(111). *Appl. Phys. Lett.* 2007, 90, 123117.
- (17) Li, G.; Ohta, J.; Okamoto, K.; Kobayashi, A.; Fujioka, H. Room-Temperature Epitaxial Growth of GaN on Atomically Flat MgAl₂O₄ Substrates by Pulsed-Laser Deposition. *Jpn. J. Appl. Phys.* 2006, 45, L457–L459.
- (18) Kawaguchi, Y.; Ohta, J.; Kobayashi, a.; Fujioka, H. Room-Temperature Epitaxial Growth of GaN on Lattice-Matched ZrB[sub 2] Substrates by Pulsed-Laser Deposition. *Appl. Phys. Lett.* 2005, 87, 221907.
- (19) Johnson, R. W.; Hultqvist, A.; Bent, S. F. A Brief Review of Atomic Layer Deposition: From Fundamentals to Applications. *Mater. Today* 2014, 17, 236–246.
- (20) George, S. M. Atomic Layer Deposition: An Overview. *Chem. Rev.* 2010, 110, 111–131.

- (21) Cheng, H.-E.; Lee, W.-J.; Hsu, C.-M. The Effect of Deposition Temperature on the Properties of TiN Diffusion Barriers Prepared by Atomic Layer Chemical Vapor Deposition. *Thin Solid Films* 2005, 485, 59–65.
- (22) King, P. J.; Werner, M.; Chalker, P. R.; Jones, a. C.; Aspinall, H. C.; Basca, J.; Wrench, J. S.; Black, K.; Davies, H. O.; Heys, P. N. Effect of Deposition Temperature on the Properties of CeO₂ Films Grown by Atomic Layer Deposition. *Thin Solid Films* 2011, 519, 4192–4195.
- (23) Kukli, K.; Ritala, M.; Aarik, J.; Uustare, T.; Leskelä, M. Influence of Growth Temperature on Properties of Zirconium Dioxide Films Grown by Atomic Layer Deposition. *J. Appl. Phys.* 2002, 92, 1833.
- (24) Lee, J.; Lee, S. J.; Han, W. B.; Jeon, H.; Park, J.; Jang, W.; Yoon, C. S.; Jeon, H. Deposition Temperature Dependence of Titanium Oxide Thin Films Grown by Remote-Plasma Atomic Layer Deposition. *Phys. Status Solidi* 2013, 210, 276–284.
- (25) Makino, H.; Miyake, A.; Yamada, T.; Yamamoto, N.; Yamamoto, T. Influence of Substrate Temperature and Zn-Precursors on Atomic Layer Deposition of Polycrystalline ZnO Films on Glass. *Thin Solid Films* 2009, 517, 3138–3142.
- (26) Yuan, N. Y.; Wang, S. Y.; Tan, C. B.; Wang, X. Q.; Chen, G. G.; Ding, J. N. The Influence of Deposition Temperature on Growth Mode, Optical and Mechanical Properties of ZnO Films Prepared by the ALD Method. *J. Cryst. Growth* 2013, 366, 43–46.
- (27) Särkijärvi, S.; Sintonen, S.; Tuomisto, F.; Bosund, M.; Suihkonen, S.; Lipsanen, H. Effect of Growth Temperature on the Epitaxial Growth of ZnO on GaN by ALD. *J. Cryst. Growth* 2014, 398, 18–22.
- (28) Ozgit, C.; Donmez, I.; Alevli, M.; Biyikli, N. Atomic Layer Deposition of GaN at Low Temperatures. *J. Vac. Sci. Technol. A Vacuum, Surfaces, Film.* 2012, 30, 01A124.
- (29) Kim, O. H.; Kim, D.; Anderson, T. Atomic Layer Deposition of GaN Using GaCl₃ and NH₃. *J. Vac. Sci. Technol. A Vacuum, Surfaces, Film.* 2009, 27, 923.

- (30) Ozgit-Akgun, C.; Goldenberg, E.; Okyay, A. K.; Biyikli, N. Hollow Cathode Plasma-Assisted Atomic Layer Deposition of Crystalline AlN, GaN and Al_xGa_{1-x}N Thin Films at Low Temperatures. *J. Mater. Chem. C* 2014, 2, 2123.
- (31) Foroughi-Abari, A.; Cadien, K. C. In Situ Spectroscopic Ellipsometry Study of Plasma-Enhanced ALD of Al₂O₃ on Chromium Substrates. *J. Electrochem. Soc.* 2012, 159, D59.
- (32) Birkholz, M. *Thin Film Analysis by X-Ray Scattering*; Wiley, 2006; p. 378.
- (33) Sayed, S. Y.; Buriak, J. M. Epitaxial Growth of Nanostructured Gold Films on Germanium via Galvanic Displacement. *ACS Appl. Mater. Interfaces* 2010, 2, 3515–3524.
- (34) Nagata, T.; Volk, J.; Haemori, M.; Yamashita, Y.; Yoshikawa, H.; Hayakawa, R.; Yoshitake, M.; Ueda, S.; Kobayashi, K.; Chikyow, T. Schottky Barrier Height Behavior of Pt–Ru Alloy Contacts on Single-Crystal N-ZnO. *J. Appl. Phys.* 2010, 107, 103714.
- (35) Lim, J.; Lee, C. Effects of Substrate Temperature on the Microstructure and Photoluminescence Properties of ZnO Thin Films Prepared by Atomic Layer Deposition. *Thin Solid Films* 2007, 515, 3335–3338.
- (36) Scarel, G.; Ferrari, S.; Spiga, S.; Wiemer, C.; Tallarida, G.; Fanciulli, M. Effects of Growth Temperature on the Properties of Atomic Layer Deposition Grown ZrO₂ Films. *J. Vac. Sci. Technol. A Vacuum, Surfaces, Film.* 2003, 21, 1359.
- (37) Brinks, P.; Heijmerikx, H.; Hendriks, T. a.; Rijnders, G.; Huijben, M. Achieving Chemical Stability in Thermoelectric Na_xCoO₂ Thin Films. *RSC Adv.* 2012, 2, 6023.
- (38) Pitzer, K. S.; Brewer, L. Mass Spectrometric Study of Ga(CH₃)₃ and Ga(C₂H₅)₃ Decomposition Reaction in H₂ and. *J. Electrochem. Soc. Solid-State Sci. Technol.* 1975, 132, 677–679.
- (39) Oikawa, S.; Tsuda, M.; Morishita, M.; MASHITA, M.; Kuniya, Y. Elementary Process of the Thermal Decomposition of Alkyl Gallium. *J. Cryst. Growth* 1988, 91, 471–480.
- (40) Donnelly, V. M.; McCaulley, J. A. Products of Thermal and Trimethylgallium Decomposition of Triethylgallium Adsorbed on Ga-Stabilized. *Surf. Sci.* 1990, 238, 34–52.

- (41) McCaulley, J. a.; Shu, R. J.; Donnelly, V. M. Kinetics of Thermal Decomposition of Triethylgallium, Trimethylgallium, and Trimethylindium Adsorbed on GaAs(100). *J. Vac. Sci. Technol. A Vacuum, Surfaces, Film.* 1991, 9, 2872.
- (42) Gu, S.; Zhang, R.; Shi, Y.; Zheng, Y. Epitaxial Lateral Overgrowth of GaN on Molecular Beam Epitaxy GaN Buffer Layers on Si Substrates by Hydride Vapour Phase Epitaxy. *J. Phys. D. Appl. Phys.* 2001, 34, 1951–1954.
- (43) Kapolnek, D.; Keller, S.; Vetry, R.; Underwood, R. D.; Kozodoy, P.; Den Baars, S. P.; Mishra, U. K. Anisotropic Epitaxial Lateral Growth in GaN Selective Area Epitaxy. *Appl. Phys. Lett.* 1997, 71, 1204.
- (44) Roskowski, a. M.; Miraglia, P. Q.; Preble, E. a.; Einfeldt, S.; Davis, R. F. Surface Instability and Associated Roughness during Conventional and Pendeo-Epitaxial Growth of GaN(0001) Films via MOVPE. *J. Cryst. Growth* 2002, 241, 141–150.
- (45) Paek, J.-S.; Kim, K.-K.; Lee, J.-M.; Kim, D.-J.; Yi, M.-S.; Noh, D. Y.; Kim, H.-G.; Park, S.-J. Nitridation of Sapphire Substrate and Its Effect on the Growth of GaN Layer at Low Temperature. *J. Cryst. Growth* 1999, 200, 55–62.
- (46) Losurdo, M.; Capezzuto, P.; Bruno, G. Plasma Cleaning and Nitridation of Sapphire (α -Al₂O₃) Surfaces: New Evidence from in Situ Real Time Ellipsometry. *J. Appl. Phys.* 2000, 88, 2138.
- (47) Losurdo, M.; Capezzuto, P.; Bruno, G.; Namkoong, G.; Doolittle, W. A.; Brown, A. S. Role of Sapphire Nitridation Temperature on GaN Growth by Plasma Assisted Molecular Beam Epitaxy: Part II . Interplay between Chemistry and Structure of Layers Role of Sapphire Nitridation Temperature on GaN Growth by Plasma Assisted Molecular Beam Epita. *J. Appl. Phys.* 2002, 91, 2508–2518.
- (48) Widmann, F.; Feuillet, G.; Daudin, B.; Rouvière, J. L. Low Temperature Sapphire Nitridation: A Clue to Optimize GaN Layers Grown by Molecular Beam Epitaxy. *J. Appl. Phys.* 1999, 85, 1550.

- (49) Grandjean, N.; Massies, J.; Leroux, M. Nitridation of Sapphire. Effect on the Optical Properties of GaN Epitaxial Overlayers. *Appl. Phys. Lett.* 1996, 69, 2071.
- (50) Meister, D.; Böhm, M.; Topf, M.; Kriegseis, W.; Burkhardt, W.; Dirnstorfer, I.; Rösel, S.; Farangis, B.; Meyer, B. K.; Hoffmann, a.; et al. A Comparison of the Hall-Effect and Secondary Ion Mass Spectroscopy on the Shallow Oxygen Donor in Unintentionally Doped GaN Films. *J. Appl. Phys.* 2000, 88, 1811.
- (51) Ko, C.-H.; Chang, S.-J.; Su, Y.-K.; Lan, W.-H.; Chen, J. F.; Kuan, T.-M.; Huang, Y.-C.; Chiang, C.-I.; Webb, J.; Lin, W.-J. On the Carrier Concentration and Hall Mobility in GaN Epilayers. *Jpn. J. Appl. Phys.* 2002, 41, L226–L228.
- (52) Hwang, C. Y.; Schurman, M. J.; Mayo, W. E.; Lu, Y. C.; Stall, R. a.; Salagaj, T. Effect of Structural Defects and Chemical Impurities on Hall Mobilities in Low Pressure MOCVD Grown GaN. *J. Electron. Mater.* 1997, 26, 243–251.
- (53) Wang, T.; Shirahama, T.; Sun, H. B.; Wang, H. X.; Bai, J.; Sakai, S.; Misawa, H. Influence of Buffer Layer and Growth Temperature on the Properties of an Undoped GaN Layer Grown on Sapphire Substrate by Metalorganic Chemical Vapor Deposition. *Appl. Phys. Lett.* 2000, 76, 2220.
- (54) Kordoš, P.; Javorka, P.; Morvic, M.; Betko, J.; Van Hove, J. M.; Wowchak, a. M.; Chow, P. P. Conductivity and Hall-Effect in Highly Resistive GaN Layers. *Appl. Phys. Lett.* 2000, 76, 3762.
- (55) Ahn, C. H.; Lee, S. Y.; Cho, H. K. Influence of Growth Temperature on the Electrical and Structural Characteristics of Conductive Al-Doped ZnO Thin Films Grown by Atomic Layer Deposition. *Thin Solid Films* 2013, 545, 106–110.
- (56) Jakhar, A.; Jamdagni, A.; Bakshi, A.; Verma, T.; Shukla, V.; Jain, P.; Sinha, N.; Arun, P. Refractive Index of SnS Thin Nano-Crystalline Films. *Solid State Commun.* 2013, 168, 31–35.
- (57) Fang, Z. B.; Yan, Z. J.; Tan, Y. S.; Liu, X. Q.; Wang, Y. Y. Influence of Post-Annealing Treatment on the Structure Properties of ZnO Films. *Appl. Surf. Sci.* 2005, 241, 303–308.

(58) Moustaghfir, A.; Tomasella, E.; Ben Amor, S.; Jacquet, M.; Cellier, J.; Sauvage, T. Structural and Optical Studies of ZnO Thin Films Deposited by R.f. Magnetron Sputtering: Influence of Annealing. *Surf. Coatings Technol.* 2003, 174-175, 193–196.

Chapter Six

Conclusions, Contributions to Knowledge, and Future Work

6.1 Conclusions and Contribution to Knowledge

The main conclusions of this research are discussed in the form of two groups, those related to AlN and those involving GaN:

6.1.1 ALD of AlN

The successful deposition of AlN via plasma-enhanced ALD was achieved through using N_2/H_2 plasma and trimethylaluminum at 250°C. The key structural characteristic of the deposited films match or surpass those of the films deposited at higher temperatures using mainstream deposition methods. Crystalline films could be deposited at low growth temperatures. The films have a high mass density, equal to 91% of the bulk density.

In addition to the deposition of AlN, studies were conducted to understand how the optical properties of the films evolve during the growth process. It was found that the optical properties stabilize, after a critical film thickness is reached. This critical number is ~30 nm and ~15 nm for refractive index and optical band gap, respectively.

One of the most noteworthy complications on the way of atomic layer deposition of AlN was the inevitable oxygen contamination. In spite of the systematic and extremely time consuming experiments designed and carried out to investigate this problem's every potential root cause, the oxygen content registered at the XPS reading never went below ~9 at%. The positive side of these investigations was that a comprehensive amount of knowledge was gathered on the problem of oxygen contamination in AlN thin films.

A survey of the literature shows that oxygen contamination is a major problem for deposition of nitrides. Important questions regarding the chemical nature of the oxygen impurity and how it

affects the chemistry and crystallography of the host material were answered, as a result of these investigations. More importantly, the experimental methods employed here could be used as a guideline for similar studies in other thin film materials.

6.1.2 ALD of GaN

Nitrogen plasma-enhanced ALD proved to be a suitable choice for low-temperature deposition of GaN. The resulting films have low carbon and oxygen impurity levels, and a Ga:N atomic ratio close to unity. The mass density is about 95% of the bulk value. In addition, the films show preferential orientation, and the (002) surface normal is the dominant growth direction, and both in-plane and out-of-plane misorientations were low. The resistivity and carrier mobility of the films are on par with the values reported for growth temperatures close to 1000°C.

The GaN deposition research led to observation and investigation of several interesting scientific phenomena. High-resolution transmission electron micrographs show an epitaxial layer at the interface of sapphire and GaN. This epitaxial layer is only 4-5 nm thick, and a transition from the two-dimensional to the three-dimensional growth mechanism is observed afterwards. Further study of the root cause of this phenomenon may lead to practical measures to inhibit or postpone it. This could potentially lead to the first hetero-epitaxial deposition of GaN at low temperatures. Interestingly, the in-situ studies of variations of refractive index during the film growth also agrees with the notion that the crystal quality is higher during the first hundred cycles of growth.

Another interesting observation was the fact that growth rate shows a steep increase, when the growth temperature is taken beyond 360°C. AFM studies indicate that this increase is accompanied by a drop in surface roughness, and radial growth of the surface hillocks. Such effects could be due to the accelerated growth along $\langle 10\bar{1}0 \rangle$ crystallographic directions, compared to the [001]

direction. This phenomenon has been observed and reported at higher temperatures, in CVD reactions. One more noteworthy observation is the gradual disappearance of the Kiessig fringes in the XRR spectra, when the growth temperature increases. This could be an indication of in-situ nitridation of the sapphire surface, caused by prolonged exposure to nitrogen plasma at elevated temperatures. This phenomenon and its effect on the crystal structure of GaN should be studied further.

6.2 Future Work

Now that the deposition of crystalline AlN and GaN at low temperatures through ALD has been accomplished, there are several research ideas that can be pursued as the next steps. In addition, this research has raised a few questions, which have remained unanswered, and are worth pursuing.

The following are a list of complementary steps I would have taken, had the time allowed:

- One potential source of oxygen that could not be checked for was the plasma tube. It is conceivable that oxygen atoms are knocked out of the quartz tube, and are later embedded in the film, due to their very high reactivity. Replacing the quartz tube with one made out of an oxygen-free ceramic material will put this hypothesis to test.
- Despite the attempts made, the desired (001) preferential orientation could not be achieved for AlN. Achieving this orientation has several technological benefits, and would be a worthy goal to pursue. It is possible that the high amount of oxygen in the lattice makes a hetero-epitaxial growth impossible, as it disrupts the lattice match between the substrate and the film. SIMS analysis will be useful in determining the amount of possible hydrogen impurity that may also disrupt hetero-epitaxial growth.

- Piezoelectricity is one of the most important properties of AlN. Our plans to measure piezoelectric constants of the films, and observe the effect of the deposition parameters on them never realized, due to lack of proper equipment. The existing AFM equipment at UofA campus can be equipped to specialized tips to conduct such measurements.
- One of the original reasons behind pursuing AlN deposition was to create a buffer layer for GaN-on-sapphire deposition. If (001)-oriented AlN can be deposited, using it as a buffer layer is likely to decrease the concentration of mismatch dislocations in GaN. This will improve the crystal structure of GaN, and might lead to enhancement of several optical and electrical properties. It might also increase the critical epitaxial thickness.
- The transition from the two-dimensional to the three-dimensional growth regime was one notable observation made in this study, and deserves further investigation. It is recommended that TEM and HRTEM studies be conducted on films with thicknesses lower and slightly higher than the critical epitaxial thickness, to watch the onset of hillock formation, and study the causes of this phenomenon.
- Based on the several studies that have reported plasma nitridization of sapphire at temperatures accessible to ALD systems, it is recommended that extensive studies be performed on this phenomenon, as it leads to an in-situ buffer layer for GaN.
- A comprehensive study of the ratio of lateral to vertical growth for (001) GaN at different temperatures will be very interesting, and could lead to a possible route to lateral overgrowth of GaN single crystals using ALD.

- Considerable research has been recently done on deposition of AlN and GaN nanowires. Controlling the directional growth of these materials will make it possible to deposit their nanowires through ALD at low temperatures.
- Simultaneous deposition of AlN and GaN will lead to deposition of ternary alloys with fine-tuned band gaps. In addition, deposition of compositionally graded materials and superlattices will be possible.

Bibliography

- Aaltonen, T., P. Alén, M. Ritala, and M. Leskelä, “Ruthenium Thin Films Grown by Atomic Layer Deposition,” *Chemical Vapor Deposition*, 9 (2003), 45–49 <doi:10.1002/cvde.200290007>
- Aaltonen, Titta, Mikko Ritala, Timo Sajavaara, Juhani Keinonen, and Markku Leskelä, “Atomic Layer Deposition of Platinum Thin Films,” *Chemistry of Materials*, 15 (2003), 1924–1928 <doi:10.1021/cm021333t>
- Aarik, Lauri, Tõnis Arroval, Raul Rammula, Hugo Mändar, Väino Sammelselg, Boris Hudec, and others, “Atomic Layer Deposition of High-Quality Al₂O₃ and Al-Doped TiO₂ Thin Films from Hydrogen-Free Precursors,” *Thin Solid Films*, 565 (2014), 19–24 <doi:10.1016/j.tsf.2014.06.038>
- Abernathy, C R, M E Overberg, G T Thaler, A H Onstine, B P Gila, F Ren, and others, “New Applications for Gallium Nitride,” *Review Literature And Arts Of The Americas*, 2002, 24–31
- Adams, I., T. R. AuCoin, and G. A. Wolff, “Luminescence in the System Al₂O₃-AlN,” *Journal of The Electrochemical Society*, 1962, 1050–1054
- Ahn, Cheol Hyoun, Sang Yeol Lee, and Hyung Koun Cho, “Influence of Growth Temperature on the Electrical and Structural Characteristics of Conductive Al-Doped ZnO Thin Films Grown by Atomic Layer Deposition,” *Thin Solid Films*, 545 (2013), 106–110 <doi:10.1016/j.tsf.2013.07.045>
- Akaltun, Yunus, M. Ali Yıldırım, Aytunç Ateş, and Muhammet Yıldırım, “The Relationship between Refractive Index-Energy Gap and the Film Thickness Effect on the Characteristic Parameters of CdSe Thin Films,” *Optics Communications*, 284 (2011), 2307–2311 <doi:10.1016/j.optcom.2010.12.094>
- Alevli, Mustafa, Cagla Ozgit, Inci Donmez, and Necmi Biyikli, “Structural Properties of AlN Films Deposited by Plasma-Enhanced Atomic Layer Deposition at Different Growth Temperatures,” *Physica Status Solidi (a)*, 209 (2012), 266–271 <doi:10.1002/pssa.201127430>
- Alevli, Mustafa, Cagla Ozgit, Inci Donmez, and Necmi Biyikli, “The Influence of N₂/H₂ and Ammonia N Source Materials on Optical and Structural Properties of AlN Films Grown by Plasma Enhanced Atomic Layer Deposition,” *Journal of Crystal Growth*, 335 (2011), 51–57 <doi:10.1016/j.jcrysgro.2011.09.003>

- Ambacher, O., M. Eickhoff, a. Link, M. Hermann, M. Stutzmann, F. Bernardini, and others, "Electronics and Sensors Based on Pyroelectric AlGaN/GaN Heterostructures," *Physica Status Solidi (C)*, 1907 (2003), 1878–1907 <doi:10.1002/pssc.200303138>
- Arslan, Engin, Mustafa K Ozturk, Ali Teke, Suleyman Ozcelik, and Ekmel Ozbay, "Buffer Optimization for Crack-Free GaN Epitaxial Layers Grown on Si(1 1 1) Substrate by MOCVD," *Journal of Physics D: Applied Physics*, 41 (2008), 155317 <doi:10.1088/0022-3727/41/15/155317>
- Asif Khan, M., M. Shatalov, H. P. Maruska, H. M. Wang, and E. Kuokstis, "III–Nitride UV Devices," *Japanese Journal of Applied Physics*, 44 (2005), 7191–7206 <doi:10.1143/JJAP.44.7191>
- Ates, Aytunc, M. Ali Yıldırım, Mutlu Kundakçı, and Aykut Astam, "Annealing and Light Effect on Optical and Electrical Properties of ZnS Thin Films Grown with the SILAR Method," *Materials Science in Semiconductor Processing*, 10 (2007), 281–286 <doi:10.1016/j.mssp.2008.04.003>
- Aubert, T., M. B. Assouar, O. Legrani, O. Elmazria, C. Tiusan, and S. Robert, "Highly Textured Growth of AlN Films on Sapphire by Magnetron Sputtering for High Temperature Surface Acoustic Wave Applications," *Journal of Vacuum Science & Technology A: Vacuum, Surfaces, and Films*, 29 (2011), 021010 <doi:10.1116/1.3551604>
- Aubert, Thierry, Omar Elmazria, Badreddine Assouar, Eloi Blampain, Ahmad Hamdan, Damien Genève, and others, "Investigations on AlN/sapphire Piezoelectric Bilayer Structure for High-Temperature SAW Applications.," *IEEE transactions on ultrasonics, ferroelectrics, and frequency control*, 59 (2012), 999–1005 <doi:10.1109/TUFFC.2012.2285>
- Aubert, Thierry, Omar Elmazria, Badreddine Assouar, Laurent Bouvot, and Mourad Oudich, "Surface Acoustic Wave Devices Based on AlN/sapphire Structure for High Temperature Applications," *Applied Physics Letters*, 96 (2010), 203503 <doi:10.1063/1.3430042>
- Aumann, C. E., G. L. Skofronick, and J. A. Martin, "Oxidation Behavior of Aluminum Nanopowders," *Journal of Vacuum Science & Technology B: Microelectronics and Nanometer Structures*, 13 (1995), 1178 <doi:10.1116/1.588232>
- Balasubramanian, C, S Bellucci, G Cinque, a Marcelli, M Cestelli Guidi, M Piccinini, and others, "Characterization of Aluminium Nitride Nanostructures by XANES and FTIR Spectroscopies with Synchrotron Radiation," *Journal of Physics: Condensed Matter*, 18 (2006), S2095–S2104 <doi:10.1088/0953-8984/18/33/S25>
- Baltrusaitis, Jonas, Pradeep M Jayaweera, and Vicki H Grassian, "XPS Study of Nitrogen Dioxide Adsorption on Metal Oxide Particle Surfaces under Different Environmental Conditions.," *Physical chemistry chemical physics : PCCP*, 11 (2009), 8295–305 <doi:10.1039/b907584d>

- Bao, Dinghua, Xi Yao, Naoki Wakiya, Kazuo Shinozaki, and Nobuyasu Mizutani, "Band-Gap Energies of Sol-Gel-Derived SrTiO₃ Thin Films," *Applied Physics Letters*, 79 (2001), 3767 <doi:10.1063/1.1423788>
- Bass, Michael, Casimer DeCusatis, Jay Enoch, Vasudevan Lakshminarayanan, Guifang Li, Carolyn MacDonald, and others, *Handbook of Optics, Third Edition Volume IV: Optical Properties of Materials, Nonlinear Optics, Quantum Optics* (McGraw Hill Professional, 2009), p. 1152 <<http://books.google.com/books?id=1CES2tOBwikC&pgis=1>> [accessed 8 April 2014]
- Bermudez, V.M, D.D Koleske, and a.E Wickenden, "The Dependence of the Structure and Electronic Properties of Wurtzite GaN Surfaces on the Method of Preparation," *Applied Surface Science*, 126 (1998), 69–82 <doi:10.1016/S0169-4332(97)00582-5>
- Birkholz, Mario, *Thin Film Analysis by X-Ray Scattering* (Wiley, 2006), p. 378 <http://books.google.ca/books/about/Thin_Film_Analysis_by_X-Ray_Scattering.html?id=GLf5m7-1CHkC&pgis=1>
- Bjurström, Johan, Gunilla Wingqvist, and Iliia Katardjiev, "Synthesis of Textured Thin Piezoelectric AlN Films with a Nonzero c-Axis Mean Tilt for the Fabrication of Shear Mode Resonators.," *IEEE transactions on ultrasonics, ferroelectrics, and frequency control*, 53 (2006), 2095–100 <<http://www.ncbi.nlm.nih.gov/pubmed/17091844>>
- Bosund, Markus, Timo Sajavaara, Mikko Laitinen, Teppo Huhtio, Matti Putkonen, Veli-Matti Airaksinen, and others, "Properties of AlN Grown by Plasma Enhanced Atomic Layer Deposition," *Applied Surface Science*, 257 (2011), 7827–7830 <doi:10.1016/j.apsusc.2011.04.037>
- Brien, V., and P. Pigeat, "Correlation between the Oxygen Content and the Morphology of AlN Films Grown by R.f. Magnetron Sputtering," *Journal of Crystal Growth*, 310 (2008), 3890–3895 <doi:10.1016/j.jcrysgro.2008.06.021>
- Brinks, P., H. Heijmerikx, T. a. Hendriks, G. Rijnders, and M. Huijben, "Achieving Chemical Stability in Thermoelectric Na_xCoO₂ Thin Films," *RSC Advances*, 2 (2012), 6023 <doi:10.1039/c2ra20734f>
- Bruker AXS, *General Area Detector Diffraction System (GADDS) User Manual*, 4.1 edn (Madison, WI)
- Calarco, Raffaella, Ralph J Meijers, Ratan K Debnath, Toma Stoica, Eli Sutter, and Hans Lu, "Nucleation and Growth of GaN Nanowires on Si (111) Performed by Molecular Beam Epitaxy," *Nano Letters*, 7 (2007), 2248–2251

- Callaghan, L A, V Lugh, M V Requa, N C Macdonald, D R Clarke, and K L Turner, “Fabrication and Testing of Beam Supported AlN FBARs,” in *IEEE International Ultrasonics, Ferroelectrics, and Frequency Control Joint 50th Anniversary Conference*, 2004, 00, 18–21
- Chambouleyron, I., S. D. Ventura, E. G. Birgin, and J. M. Martínez, “Optical Constants and Thickness Determination of Very Thin Amorphous Semiconductor Films,” *Journal of Applied Physics*, 92 (2002), 3093 <doi:10.1063/1.1500785>
- Chason, E, and T M Mayer, “Thin Film and Surface Characterization by Specular X-Ray Reflectivity,” *Critical Reviews in Solid State and Materials Sciences*, 22 (1997), 1–67
- Chattopadhyay, Surojit, Abhijit Ganguly, Kuei-Hsien Chen, and Li-Chyong Chen, “One-Dimensional Group III-Nitrides: Growth, Properties, and Applications in Nanosensing and Nano-Optoelectronics,” *Critical Reviews in Solid State and Materials Sciences*, 34 (2009), 224–279 <doi:10.1080/10408430903352082>
- Chen, Da, Dong Xu, Jingjing Wang, and Yafei Zhang, “Investigation of Chemical Etching of AlN Film with Different Textures by X-Ray Photoelectron Spectroscopy,” *Journal of Physics D: Applied Physics*, 41 (2008), 235303 <doi:10.1088/0022-3727/41/23/235303>
- Cheng, Hsyi-En, Wen-Jen Lee, and C.-M. Hsu, “The Effect of Deposition Temperature on the Properties of TiN Diffusion Barriers Prepared by Atomic Layer Chemical Vapor Deposition,” *Thin Solid Films*, 485 (2005), 59–65 <doi:10.1016/j.tsf.2005.03.049>
- Chiu, Shao-Yen, Hsuan-Wei Huang, Tze-Hsuan Huang, Kun-Chieh Liang, Kang-Ping Liu, Jung-Hui Tsai, and others, “Comprehensive Investigation on Planar Type of Pd–GaN Hydrogen Sensors,” *International Journal of Hydrogen Energy*, 34 (2009), 5604–5615 <doi:10.1016/j.ijhydene.2009.04.073>
- Chong, Yuen Tung, Eric Man Yan Yau, Kornelius Nielsch, and Julien Bachmann, “Direct Atomic Layer Deposition of Ternary Ferrites with Various Magnetic Properties,” *Chemistry of Materials*, 22 (2010), 6506–6508 <doi:10.1021/cm102600m>
- Cimalla, V, J Pezoldt, and O Ambacher, “Group III Nitride and SiC Based MEMS and NEMS: Materials Properties, Technology and Applications,” *Journal of Physics D: Applied Physics*, 40 (2007), 6386–6434 <doi:10.1088/0022-3727/40/20/S19>
- Clement, M, L Vergara, J Sangrador, E Iborra, and a Sanz-Hervás, “SAW Characteristics of AlN Films Sputtered on Silicon Substrates,” *Ultrasonics*, 42 (2004), 403–7 <doi:10.1016/j.ultras.2004.01.034>
- Collins, A. T., E. C. Lightowers, and P. J. Dean, “Lattice Vibration Spectra of Aluminum Nitride,” *Physical Review*, 158 (1967), 833–838

- Colomban, Ph., “Structure of Oxide Gels and Glasses by Infrared and Raman Scattering,” *Journal of Materials Science*, 24 (1989), 3002–3010
- Coq Germanicus, R., E. Picard, B. Domenges, K. Danilo, and R. Rogel, “Microstructure and Electrical Characterization Based on AFM of Very High-Doped Polysilicon Grains,” *Applied Surface Science*, 253 (2007), 6006–6012 <doi:10.1016/j.apsusc.2006.12.114>
- Das, N.S., P.K. Ghosh, M.K. Mitra, and K.K. Chattopadhyay, “Effect of Film Thickness on the Energy Band Gap of Nanocrystalline CdS Thin Films Analyzed by Spectroscopic Ellipsometry,” *Physica E: Low-dimensional Systems and Nanostructures*, 42 (2010), 2097–2102 <doi:10.1016/j.physe.2010.03.035>
- Daudin, B, G. Feuillet, Guido Mula, H. Mariette, J. L. Rouviere, N. Pelekanos, and others, “Epitaxial Growth of GaN , AlN and InN : 2D / 3D Transition and Surfactant Effects,” *Physica Status Solidi (a)*, 621 (1999), 621–628
- Daudin, B, F Widmann, G Feuillet, Y Samson, M Arlery, and J L Rouvie, “Stranski-Krastanov Growth Mode during the Molecular Beam Epitaxy of Highly Strained GaN,” *PHYSICAL REVIEW B*, 56 (1997), 7069–7072
- Davydov, V Yu, A A Klochikhin, R P Seisyan, and V V Emtsev, “Absorption and Emission of Hexagonal InN . Evidence of Narrow Fundamental Band Gap,” *Physica Status Solidi (B)*, 3 (2002), 1972–1974
- Debnath, R. K., R. Meijers, T. Richter, T. Stoica, R. Calarco, and H. Lüth, “Mechanism of Molecular Beam Epitaxy Growth of GaN Nanowires on Si(111),” *Applied Physics Letters*, 90 (2007), 123117 <doi:10.1063/1.2715119>
- Dendooven, J., D. Deduytsche, J. Musschoot, R. L. Vanmeirhaeghe, and C. Detavernier, “Conformality of Al₂O₃ and AlN Deposited by Plasma-Enhanced Atomic Layer Deposition,” *Journal of The Electrochemical Society*, 157 (2010), G111–G116 <doi:10.1149/1.3301664>
- Dezelah, Charles L., Jaakko Niinistö, Kaupo Kukli, Frans Munnik, Jun Lu, Mikko Ritala, and others, “The Atomic Layer Deposition of HfO₂ and ZrO₂ Using Advanced Metallocene Precursors and H₂O as the Oxygen Source,” *Chemical Vapor Deposition*, 14 (2008), 358–365 <doi:10.1002/cvde.200806716>
- Djurišić, Aleksandra B., and E. Herbert Li, “Modeling the Optical Constants of Hexagonal GaN, InN, and AlN,” *Journal of Applied Physics*, 85 (1999), 2848 <doi:10.1063/1.369604>
- Dobrzański, Leszek A., Marek Szindler, Aleksandra Drygała, and Magdalena M. Szindler, “Silicon Solar Cells with Al₂O₃ Antireflection Coating,” *Central European Journal of Physics*, 12 (2014), 666–670 <doi:10.2478/s11534-014-0500-9>

- Donnelly, V M, and J.A. McCaulley, “Products of Thermal and Trimethylgallium Decomposition of Triethylgallium Adsorbed on Ga-Stabilized,” *Surface Science*, 238 (1990), 34–52
- Eaglesham, D J, H Gossmann, and M Cerullo, “Limiting Thickness H Epi for Epitaxial Growth and Room-Temperature Si Growth on Si(100),” *PHYSICAL REVIEW LETTERS*, 65 (1990), 1227–1230
- Ealet, B., M.H. Elyakhloufi, E. Gillet, and M. Ricci, “Electronic and Crystallographic Structure of Γ -Alumina Thin Films,” *Thin Solid Films*, 250 (1994), 92–100 <doi:10.1016/0040-6090(94)90171-6>
- Eigenfeld, Nathan T, Jason M Gray, Joseph J Brown, George D Skidmore, Steven M George, and Victor M Bright, “Ultra-Thin 3D Nano-Devices from Atomic Layer Deposition on Polyimide.,” *Advanced materials*, 26 (2014), 3962–7 <doi:10.1002/adma.201400410>
- Elam, J.W., C.E. Nelson, R.K. Grubbs, and S.M. George, “Nucleation and Growth during Tungsten Atomic Layer Deposition on SiO₂ Surfaces,” *Thin Solid Films*, 386 (2001), 41–52 <doi:10.1016/S0040-6090(01)00762-3>
- Elsner, J., R. Jones, M. Heggie, P. Sitch, M. Haugk, Th. Frauenheim, and others, “Deep Acceptors Trapped at Threading-Edge Dislocations in GaN,” *Physical Review B*, 58 (1998), 12571–12574 <doi:10.1103/PhysRevB.58.12571>
- Fang, Z.B., Z.J. Yan, Y.S. Tan, X.Q. Liu, and Y.Y. Wang, “Influence of Post-Annealing Treatment on the Structure Properties of ZnO Films,” *Applied Surface Science*, 241 (2005), 303–308 <doi:10.1016/j.apsusc.2004.07.056>
- Foroughi-Abari, Ali, and Kenneth C. Cadien, “In Situ Spectroscopic Ellipsometry Study of Plasma-Enhanced ALD of Al₂O₃ on Chromium Substrates,” *Journal of The Electrochemical Society*, 159 (2012), D59 <doi:10.1149/2.035202jes>
- Foxon, C, “The Growth and Properties of Group III Nitrides,” *Journal of Crystal Growth*, 150 (1995), 892–896 <doi:10.1016/0022-0248(95)80068-N>
- Fu, Jenna L., Roozbeh Tabrizian, and Farrokh Ayazi, “Dual-Mode AlN-on-Silicon Micromechanical Resonators for Temperature Sensing,” *IEEE Transactions on Electron Devices*, 61 (2014), 591–597 <doi:10.1109/TED.2013.2295613>
- Gaponenko, S. V., *Optical Properties of Semiconductor Nanocrystals* (Cambridge University Press, 1998), p. 245 <<http://books.google.com/books?id=1Y1zvul3kbQC&pgis=1>> [accessed 8 April 2014]
- García Molleja, Javier, Bernardo José Gómez, Julio Ferrón, Eric Gautron, Juan Bürgi, Bassam Abdallah, and others, “AlN Thin Films Deposited by DC Reactive Magnetron Sputtering:

- Effect of Oxygen on Film Growth,” *The European Physical Journal Applied Physics*, 64 (2013), 20302 <doi:10.1051/epjap/2013130445>
- García-Méndez, Manuel, Santos Morales-Rodríguez, Sadasivan Shaji, Bindu Krishnan, and Pascual Bartolo-Pérez, “Structural Properties of AlN Films with Oxygen Content Deposited by Reactive Magnetron Sputtering: XRD and XPS Characterization,” *Surface Review and Letters*, 18 (2011), 23–31 <doi:10.1142/S0218625X1101445X>
- Geng, Huijuan, Tingjui Lin, Ayra Jagadhamma Letha, Huey-Liang Hwang, Fedor a. Kyznetsov, Tamara P. Smirnova, and others, “Advanced Passivation Techniques for Si Solar Cells with High-K Dielectric Materials,” *Applied Physics Letters*, 105 (2014), 123905 <doi:10.1063/1.4896619>
- George, Steven M, “Atomic Layer Deposition: An Overview,” *Chemical reviews*, 110 (2010), 111–31 <doi:10.1021/cr900056b>
- Gogotsi, Y., *Nanomaterials Handbook* (CRC Press, 2006)
- Goh, Eunice S. M., T. P. Chen, C. Q. Sun, and Y. C. Liu, “Thickness Effect on the Band Gap and Optical Properties of Germanium Thin Films,” *Journal of Applied Physics*, 107 (2010), 024305 <doi:10.1063/1.3291103>
- Grandjean, N., B. Damilano, S. Dalmaso, M. Leroux, M. Laügt, and J. Massies, “Built-in Electric-Field Effects in Wurtzite AlGaIn/GaN Quantum Wells,” *Journal of Applied Physics*, 86 (1999), 3714 <doi:10.1063/1.371241>
- Grandjean, N., J. Massies, and M. Leroux, “Nitridation of Sapphire. Effect on the Optical Properties of GaN Epitaxial Overlayers,” *Applied Physics Letters*, 69 (1996), 2071 <doi:10.1063/1.116883>
- Gredelj, Sabina, Andrea R Gerson, Sunil Kumar, and Giuseppe P Cavallaro, “Characterization of Aluminium Surfaces with and without Plasma Nitriding by X-Ray Photoelectron Spectroscopy,” *Applied Surface Science*, 174 (2001), 240–250 <doi:10.1016/S0169-4332(01)00169-6>
- Gu, Shulin, Rong Zhang, Yi Shi, and Youdou Zheng, “Epitaxial Lateral Overgrowth of GaN on Molecular Beam Epitaxy GaN Buffer Layers on Si Substrates by Hydride Vapour Phase Epitaxy,” *Journal of Physics D: Applied Physics*, 34 (2001), 1951–1954 <doi:10.1088/0022-3727/34/13/304>
- Guziewicz, E., I. A. Kowalik, M. Godlewski, K. Kopalko, V. Osinniy, A. Wójcik, and others, “Extremely Low Temperature Growth of ZnO by Atomic Layer Deposition,” *Journal of Applied Physics*, 103 (2008), 033515 <doi:10.1063/1.2836819>

- H.M. Manasevit, F.M. Erdman, And W.I. Simpson, "The Use of Metalorganics in the Preparation of Semiconductor Materials," *Journal of electrochemistry Society*, 118 (1971), 1864
- Hanada, T., M. Kobayashi, S. Tanabe, and N. Soga, "Preparation and Physical Properties of Rf-Sputtered Amorphous Films in the Al₂O₃-AlN System," *Journal of Non-Crystalline Solids*, 135 (1991), 227–235
- Hao, M., H. Ishikawa, and T. Egawa, "Formation Chemistry of High-Density Nanocraters on the Surface of Sapphire Substrates with an in Situ Etching and Growth Mechanism of Device-Quality GaN Films on the Etched Substrates," *Applied Physics Letters*, 84 (2004), 4041 <doi:10.1063/1.1751607>
- Hardy, Matthew T., Daniel F. Feezell, Steven P. DenBaars, and Shuji Nakamura, "Group III-Nitride Lasers: A Materials Perspective," *Materials Today*, 14 (2011), 408–415 <doi:10.1016/S1369-7021(11)70185-7>
- Harris, J H, R A Youngman, and R G Teller, "On the Nature of the Oxygen-Related Defect in Aluminum Nitride," *Journal of Materials Research*, 44128 (1990), 1763–1773
- Herzinger, C. M., B. Johs, W. a. McGahan, J. a. Woollam, and W. Paulson, "Ellipsometric Determination of Optical Constants for Silicon and Thermally Grown Silicon Dioxide via a Multi-Sample, Multi-Wavelength, Multi-Angle Investigation," *Journal of Applied Physics*, 83 (1998), 3323 <doi:10.1063/1.367101>
- Herzinger, Craig M., and Blaine D. Johs, "Dielectric Function Parametric Model, And Method Of Use" (United States of America, 1998)
- Hobert, H., H.H. Dunken, J. Meinschien, and H. Stafast, "Infrared and Raman Spectroscopic Investigation of Thin Films of AlN and SiC on Si Substrates," *Vibrational Spectroscopy*, 19 (1999), 205–211 <doi:10.1016/S0924-2031(98)00076-9>
- Huganen, Juha, and Taplo Kannlaln, "United States Patent U-S- PATENT DOCUMENTS," 2004
- Hwang, C. Y., M. J. Schurman, W. E. Mayo, Y. C. Lu, R. a. Stall, and T. Salagaj, "Effect of Structural Defects and Chemical Impurities on Hall Mobilities in Low Pressure MOCVD Grown GaN," *Journal of Electronic Materials*, 26 (1997), 243–251 <doi:10.1007/s11664-997-0158-9>
- Ihn, Y.S., T.J. Kim, T.H. Ghong, Y.D. Kim, D.E. Aspnes, and J. Kossut, "Parametric Modeling of the Dielectric Functions of Cd_{1-x}Mg_xTe Alloy Films," *Thin Solid Films*, 455-456 (2004), 222–227 <doi:10.1016/j.tsf.2004.01.015>

- Imer, Bilge, Feng Wu, Michael D. Craven, James S. Speck, and Steven P. DenBaars, "Stability of (1\bar{1}00) M -Plane GaN Films Grown by Metalorganic Chemical Vapor Deposition," *Japanese Journal of Applied Physics*, 45 (2006), 8644–8647 <doi:10.1143/JJAP.45.8644>
- Iriarte, G.F., D.F. Reyes, D. González, J.G. Rodríguez, R. García, and F. Calle, "Influence of Substrate Crystallography on the Room Temperature Synthesis of AlN Thin Films by Reactive Sputtering," *Applied Surface Science*, 257 (2011), 9306–9313 <doi:10.1016/j.apsusc.2011.05.025>
- Ishihara, M, S.J Li, H Yumoto, K Akashi, and Y Ide, "Control of Preferential Orientation of AlN Films Prepared by the Reactive Sputtering Method," *Thin Solid Films*, 316 (1998), 152–157 <doi:10.1016/S0040-6090(98)00406-4>
- Jain, S. C., M. Willander, J. Narayan, and R. Van Overstraeten, "III-Nitrides: Growth, Characterization and Properties," *Applied Physics Reviews*, 87 (2000), 965–1006
- Jakhar, Amit, Ashu Jamdagni, Ayushi Bakshi, Taruna Verma, Vibhav Shukla, Priyal Jain, and others, "Refractive Index of SnS Thin Nano-Crystalline Films," *Solid State Communications*, 168 (2013), 31–35 <doi:10.1016/j.ssc.2013.06.013>
- Jin, H., J. Zhou, S.R. Dong, B. Feng, J.K. Luo, D.M. Wang, and others, "Deposition of c-Axis Orientation Aluminum Nitride Films on Flexible Polymer Substrates by Reactive Direct-Current Magnetron Sputtering," *Thin Solid Films*, 520 (2012), 4863–4870 <doi:10.1016/j.tsf.2012.03.015>
- Johnson, Richard W., Adam Hultqvist, and Stacey F. Bent, "A Brief Review of Atomic Layer Deposition: From Fundamentals to Applications," *Materials Today*, 17 (2014), 236–246 <doi:10.1016/j.mattod.2014.04.026>
- Johs, B, C M Herzinger, J H Dinan, A Cornfeld, and J D Benson, "Development of a Parametric Optical Constant Model for Hg_{1-x}Cd_xTe for Control of Composition by Spectroscopic Ellipsometry during MBE Growth," *Thin Solid Films*, 313-314 (1998), 137–142
- Jorke, H, H Kibbel, and F Sch, "LOW TEMPERATURE KINETICS OF Si(100) MBE GROWTH," *Thin Solid Films*, 183 (1989), 307–313
- Jose, Feby, R Ramaseshan, S Dash, S Bera, a K Tyagi, and Baldev Raj, "Response of Magnetron Sputtered AlN Films to Controlled Atmosphere Annealing," *Journal of Physics D: Applied Physics*, 43 (2010), 075304 <doi:10.1088/0022-3727/43/7/075304>
- Junaid, M., C.-L. Hsiao, J. Palisaitis, J. Jensen, P. O. å. Persson, L. Hultman, and others, "Electronic-Grade GaN(0001)/Al₂O₃(0001) Grown by Reactive DC-Magnetron Sputter Epitaxy Using a Liquid Ga Target," *Applied Physics Letters*, 98 (2011), 141915 <doi:10.1063/1.3576912>

- Kalisch, Holger, Michael Heuken, Andrei Vescan, and Achim Trampert, "Formation of a Monocrystalline, M-Plane AlN Layer by the Nitridation of Γ -LiAlO₂(100)," *Applied Physics Express*, 105501 (2012)
- Kapolnek, D., S. Keller, R. Vetury, R. D. Underwood, P. Kozodoy, S. P. Den Baars, and others, "Anisotropic Epitaxial Lateral Growth in GaN Selective Area Epitaxy," *Applied Physics Letters*, 71 (1997), 1204 <doi:10.1063/1.119626>
- Kapolnek, D., X. H. Wu, B. Heying, S. Keller, B. P. Keller, U. K. Mishra, and others, "Structural Evolution in Epitaxial Metalorganic Chemical Vapor Deposition Grown GaN Films on Sapphire," *Applied Physics Letters*, 67 (1995), 1541 <doi:10.1063/1.114486>
- Kar, J.P., G. Bose, and S. Tuli, "Influence of Rapid Thermal Annealing on Morphological and Electrical Properties of RF Sputtered AlN Films," *Materials Science in Semiconductor Processing*, 8 (2005), 646–651 <doi:10.1016/j.mssp.2006.04.001>
- Karam, N. H., T. Parodos, P. Colter, D. McNulty, W. Rowland, J. Schetzina, and others, "Growth of Device Quality GaN at 550 °C by Atomic Layer Epitaxy," *Applied Physics Letters*, 67 (1995), 94 <doi:10.1063/1.115519>
- Katamreddy, Rajesh, Ronald Inman, Gregory Jursich, Axel Soulet, Alan Nicholls, and Christos Takoudis, "Post Deposition Annealing of Aluminum Oxide Deposited by Atomic Layer Deposition Using Tris(diethylamino)aluminum and Water Vapor on Si(100)," *Thin Solid Films*, 515 (2007), 6931–6937 <doi:10.1016/j.tsf.2007.02.001>
- Kawaguchi, Y., J. Ohta, a. Kobayashi, and H. Fujioka, "Room-Temperature Epitaxial Growth of GaN on Lattice-Matched ZrB₂ Substrates by Pulsed-Laser Deposition," *Applied Physics Letters*, 87 (2005), 221907 <doi:10.1063/1.2137876>
- Kazan, M., B. Rufflé, Ch. Zgheib, and P. Masri, "Oxygen Behavior in Aluminum Nitride," *Journal of Applied Physics*, 98 (2005), 103529 <doi:10.1063/1.2137461>
- , "Oxygen Behavior in Aluminum Nitride," *Journal of Applied Physics*, 98 (2005), 103529 <doi:10.1063/1.2137461>
- Khan, Asif, Krishnan Balakrishnan, and Tom Katona, "Ultraviolet Light-Emitting Diodes Based on Group Three Nitrides," *Nature Photonics*, 2 (2008), 77–84 <doi:10.1038/nphoton.2007.293>
- Kim, Hyun-Jeong, Dongjin Byun, Gyeungho Kim, and Dong-Wha Kum, "Effects of Reactive Ion Beam Treatment of a Sapphire Surface to Optimize the Deposition of GaN Films," *Journal of Applied Physics*, 87 (2000), 7940 <doi:10.1063/1.373478>

- Kim, Kwang-Ho, No-Won Kwak, and Soo Hong Lee, "Fabrication and Properties of AlN Film on GaN Substrate by Using Remote Plasma Atomic Layer Deposition Method," *Electronic Materials Letters*, 5 (2009), 83–86 <doi:10.3365/eml.2009.06.083>
- Kim, Oh Hyun, Dojun Kim, and Tim Anderson, "Atomic Layer Deposition of GaN Using GaCl₃ and NH₃," *Journal of Vacuum Science & Technology A: Vacuum, Surfaces, and Films*, 27 (2009), 923 <doi:10.1116/1.3106619>
- King, David M, Xiaohua Du, Andrew S Cavanagh, and Alan W Weimer, "Quantum Confinement in Amorphous TiO₂ Films Studied via Atomic Layer Deposition.," *Nanotechnology*, 19 (2008), 445401 <doi:10.1088/0957-4484/19/44/445401>
- King, P.J., M. Werner, P.R. Chalker, a.C. Jones, H.C. Aspinall, J. Basca, and others, "Effect of Deposition Temperature on the Properties of CeO₂ Films Grown by Atomic Layer Deposition," *Thin Solid Films*, 519 (2011), 4192–4195 <doi:10.1016/j.tsf.2011.02.025>
- King, S. W., J. P. Barnak, M. D. Bremser, K. M. Tracy, C. Ronning, R. F. Davis, and others, "Cleaning of AlN and GaN Surfaces," *Journal of Applied Physics*, 84 (1998), 5248 <doi:10.1063/1.368814>
- Kirsch, P. D., M. A. Quevedo-Lopez, H. -J. Li, Y. Senzaki, J. J. Peterson, S. C. Song, and others, "Nucleation and Growth Study of Atomic Layer Deposited HfO₂ Gate Dielectrics Resulting in Improved Scaling and Electron Mobility," *Journal of Applied Physics*, 99 (2006), 023508 <doi:10.1063/1.2161819>
- Klingshirn, Claus F., *Semiconductor Optics*, Graduate Texts in Physics (Berlin, Heidelberg: Springer Berlin Heidelberg, 2012) <doi:10.1007/978-3-642-28362-8>
- Knoops, H. C. M., L. Baggetto, E. Langereis, M. C. M. van de Sanden, J. H. Klootwijk, F. Roozeboom, and others, "Deposition of TiN and TaN by Remote Plasma ALD for Cu and Li Diffusion Barrier Applications," *Journal of The Electrochemical Society*, 155 (2008), G287 <doi:10.1149/1.2988651>
- Knox-Davies, E. C., J. M. Shannon, and S. R. P. Silva, "The Properties and Deposition Process of GaN Films Grown by Reactive Sputtering at Low Temperatures," *Journal of Applied Physics*, 99 (2006), 073503 <doi:10.1063/1.2186380>
- Ko, Chih-Hsin, Shoou-Jinn Chang, Yan-Kuin Su, Wen-How Lan, Jone F. Chen, Ta-Ming Kuan, and others, "On the Carrier Concentration and Hall Mobility in GaN Epilayers," *Japanese Journal of Applied Physics*, 41 (2002), L226–L228 <doi:10.1143/JJAP.41.L226>
- Kordoš, P., P. Javorka, M. Morvic, J. Betko, J. M. Van Hove, a. M. Wowchak, and others, "Conductivity and Hall-Effect in Highly Resistive GaN Layers," *Applied Physics Letters*, 76 (2000), 3762 <doi:10.1063/1.126773>

- Kuang, Xu-Ping, Hua-Yu Zhang, Gui-Gen Wang, Lin Cui, Can Zhu, Lei Jin, and others, "AlN Films Prepared on 6H-SiC Substrates under Various Sputtering Pressures by RF Reactive Magnetron Sputtering," *Applied Surface Science*, 263 (2012), 62–68 <doi:10.1016/j.apsusc.2012.08.121>
- Kuchibhatla, S., L.E. Rodak, and D. Korakakis, "Fourier Transform Infrared Spectroscopy Characterization of AlN Thin Films Grown on Sacrificial Silicon Oxide Layers via Metal Organic Vapor Phase Epitaxy," *Thin Solid Films*, 519 (2010), 117–121 <doi:10.1016/j.tsf.2010.07.076>
- Kukli, Kaupo, Mikko Ritala, Jaan Aarik, Teet Uustare, and Markku Leskelä, "Influence of Growth Temperature on Properties of Zirconium Dioxide Films Grown by Atomic Layer Deposition," *Journal of Applied Physics*, 92 (2002), 1833 <doi:10.1063/1.1493657>
- Kumar, Suresh, Santosh Kumar, Pankaj Sharma, Vineet Sharma, and S. C. Katyal, "CdS Nanofilms: Effect of Film Thickness on Morphology and Optical Band Gap," *Journal of Applied Physics*, 112 (2012), 123512 <doi:10.1063/1.4769799>
- Kung, Patrick, Xiaolong Zhang, Erwan Bigan, and Manijeh Razeghi, "Low Pressure Metalorganic Chemical Vapor Deposition of High Quality AlN and GaN Thin Films on Sapphire and Silicon Substrates Patrick," in *Proc. SPIE 2397, Optoelectronic Integrated Circuit Materials, Physics, and Devices*, 1995, MMCCCXCVII, 311–320
- Kushi, Kouichi, Hajime Sasamoto, Daisuke Sugihara, Shinichi Nakamura, Akihiko Kikuchi, and Katsumi Kishino, "High Speed Growth of Device Quality GaN and InGaN by RF-MBE," *Materials Science and Engineering: B*, 59 (1999), 65–68 <doi:10.1016/S0921-5107(98)00365-1>
- Lee, Jaesang, Seung Jae Lee, Won Bae Han, Heeyoung Jeon, Jingyu Park, Woochool Jang, and others, "Deposition Temperature Dependence of Titanium Oxide Thin Films Grown by Remote-Plasma Atomic Layer Deposition," *Physica Status Solidi (a)*, 210 (2013), 276–284 <doi:10.1002/pssa.201228671>
- Lee, Yong Ju, and Sang-won Kang, "Growth of Aluminum Nitride Thin Films Prepared by Plasma-Enhanced Atomic Layer Deposition," *Thin Solid Films*, 446 (2004), 227–231 <doi:10.1016/j.tsf.2003.10.004>
- Lei, Wenwen, and Qiang Chen, "Crystal AlN Deposited at Low Temperature by Magnetic Field Enhanced Plasma Assisted Atomic Layer Deposition," *Journal of Vacuum Science & Technology A: Vacuum, Surfaces, and Films*, 31 (2013), 01A114 <doi:10.1116/1.4764112>
- Li, Guoqiang, Jitsuo Ohta, Koichiro Okamoto, Atsushi Kobayashi, and Hiroshi Fujioka, "Room-Temperature Epitaxial Growth of GaN on Atomically Flat MgAl₂O₄ Substrates by Pulsed-Laser Deposition," *Japanese Journal of Applied Physics*, 45 (2006), L457–L459 <doi:10.1143/JJAP.45.L457>

- Li, J., K. B. Nam, M. L. Nakarmi, J. Y. Lin, H. X. Jiang, Pierre Carrier, and others, “Band Structure and Fundamental Optical Transitions in Wurtzite AlN,” *Applied Physics Letters*, 83 (2003), 5163 <doi:10.1063/1.1633965>
- Liao, H. M., “Surface Composition of AlN Powders Studied by X-Ray Photoelectron Spectroscopy and Bremsstrahlung-Excited Auger Electron Spectroscopy,” *Journal of Vacuum Science & Technology A: Vacuum, Surfaces, and Films*, 11 (1993), 2681 <doi:10.1116/1.578626>
- Liliental-Weber, Z., “Derivation of Growth Mechanism of Nano-Defects in GaN from TEM Data,” *Journal of electron microscopy*, 49 (2000), 339–48
- Lim, Jongmin, and Chongmu Lee, “Effects of Substrate Temperature on the Microstructure and Photoluminescence Properties of ZnO Thin Films Prepared by Atomic Layer Deposition,” *Thin Solid Films*, 515 (2007), 3335–3338 <doi:10.1016/j.tsf.2006.09.007>
- Lin, Chih-Ming, Yung-Yu Chen, Valery V Felmetzger, Wei-Cheng Lien, Tommi Riekkinen, Debbie G Senesky, and others, “Surface Acoustic Wave Devices on AlN/3C–SiC/Si Multilayer Structures,” *Journal of Micromechanics and Microengineering*, 23 (2013), 025019 <doi:10.1088/0960-1317/23/2/025019>
- Liu, B.L, M Lachab, a Jia, a Yoshikawaa, and K Takahashi, “MOCVD Growth of Device-Quality GaN on Sapphire Using a Three-Step Approach,” *Journal of Crystal Growth*, 234 (2002), 637–645 <doi:10.1016/S0022-0248(01)01755-9>
- Liu, G., E. W. Deguns, L. Lecordier, G. Sundaram, and J. S. Becker, “Atomic Layer Deposition of AlN with Tris(Dimethylamido)aluminum and NH₃,” *ECS Transactions*, 41 (2011), 219–225
- Liu, Xinye, Sasangan Ramanathan, Eddie Lee, and Thomas E Seidel, “Atomic Layer Deposition of Aluminum Nitride Thin Films from Trimethyl Aluminum (TMA) and Ammonia,” in *Materials Research Society Symposium*, 2004, DCCCXI, 1–6
- Longrie, Delphine, Davy Deduytsche, Jo Haemers, Kris Driesen, and Christophe Detavernier, “A Rotary Reactor for Thermal and Plasma-Enhanced Atomic Layer Deposition on Powders and Small Objects,” *Surface and Coatings Technology*, 213 (2012), 183–191 <doi:10.1016/j.surfcoat.2012.10.045>
- Losurdo, M., P. Capezzuto, and G. Bruno, “Plasma Cleaning and Nitridation of Sapphire (α -Al₂O₃) Surfaces: New Evidence from in Situ Real Time Ellipsometry,” *Journal of Applied Physics*, 88 (2000), 2138 <doi:10.1063/1.1305926>
- Losurdo, Maria, Pio Capezzuto, Giovanni Bruno, Gon Namkoong, W Alan Doolittle, and April S Brown, “Role of Sapphire Nitridation Temperature on GaN Growth by Plasma Assisted Molecular Beam Epitaxy : Part II . Interplay between Chemistry and Structure of Layers Role

- of Sapphire Nitridation Temperature on GaN Growth by Plasma Assisted Molecular Beam Epita,” *Journal Of Applied Physics*, 91 (2002), 2508–2518 <doi:10.1063/1.1435835>
- Makino, Hisao, Aki Miyake, Takahiro Yamada, Naoki Yamamoto, and Tetsuya Yamamoto, “Influence of Substrate Temperature and Zn-Precursors on Atomic Layer Deposition of Polycrystalline ZnO Films on Glass,” *Thin Solid Films*, 517 (2009), 3138–3142 <doi:10.1016/j.tsf.2008.11.088>
- Manova, D, V Dimitrova, W Fukarek, and D Karpuzovc, “Investigation of D . c . -Reactive Magnetron-Sputtered AlN Thin Films by Electron Microprobe Analysis , X-Ray Photoelectron Spectroscopy and Polarised Infra-Red Reflection,” *Surface and Coatings Technology*, 106 (1998), 205–208
- Mazza, Daniele, Mario Vallino, Guido Busca, Istituto Chimica, and Facolta Ingegneria, “Mullite-Type Structures in the Systems Al₂O₃-Me₂O (Me = Na, K) and Al₂O₃-B₂O₃,” *Journal of American Ceramic Society*, 34 (1992), 1929–1934
- Mccauley, James W, K. M. Krishnan, R.S. Rai, and G. Thomas, “Anion-Controlled Microstructures in the AlN-Al₂O₃ System,” in *Ceramic Microstructures '86*, ed. by Pask and Evans (Plenum Publishing Corporation, 1988), pp. 577–590
- McCaulley, J. a., R. J. Shu, and V. M. Donnelly, “Kinetics of Thermal Decomposition of Triethylgallium, Trimethylgallium, and Trimethylindium Adsorbed on GaAs(100),” *Journal of Vacuum Science & Technology A: Vacuum, Surfaces, and Films*, 9 (1991), 2872 <doi:10.1116/1.577146>
- McMillan, Paul, and Bernard Piriou, “The Structures and Vibrational Spectra of Crystals and Glasses in the Silica-Alumina System,” *Journal of Non-Crystalline Solids*, 53 (1982), 279–298
- Meeder, A, D. Fuertes Marrón, A. Rumberg, M. Ch. Lux-Steiner, V. Chu, and J. P. Conde, “Direct Measurement of Urbach Tail and Gap State Absorption in CuGaSe₂ Thin Films by Photothermal Deflection Spectroscopy and the Constant Photocurrent Method,” *Journal of Applied Physics*, 92 (2002), 3016 <doi:10.1063/1.1501745>
- Meister, D., M. Böhm, M. Topf, W. Kriegseis, W. Burkhardt, I. Dirnstorfer, and others, “A Comparison of the Hall-Effect and Secondary Ion Mass Spectroscopy on the Shallow Oxygen Donor in Unintentionally Doped GaN Films,” *Journal of Applied Physics*, 88 (2000), 1811 <doi:10.1063/1.1305549>
- Min, Jae-sik, Sang-won Kang, and Young-ung Ha, “Heater of Inkjet Printhead, Inkjet Printhead Having the Heater and Method of Manufacturing the Inkjet Printhead,” 2007 <<http://www.google.com/patents/US20070030313>>

- Mohammad, S.N., and H. Morkoc, "Progress and Prospects of Group-III Semiconductors," *Progress in Quantum Electronics*, 20 (1996), 361–525
- Morkoç, H, "Comprehensive Characterization of Hydride VPE Grown GaN Layers and Templates," *Materials Science and Engineering: R: Reports*, 33 (2001), 135–207 <doi:10.1016/S0927-796X(01)00031-6>
- Morkoç, Hadis, *Nitride Semiconductor Device: Principles and Simulation Properties of Group-IV, III-V and II-VI Semiconductors Nitride Semiconductors, US Patent*, 2009 <http://www.google.com/patents?hl=en&lr=&vid=USPAT7365369&id=D-WqAAAAEBAJ&oi=fnd&dq=Nitride+semiconductor+device&printsec=abstract>
- Motamedi, P., and K. Cadien, "XPS Analysis of AlN Thin Films Deposited by Plasma Enhanced Atomic Layer Deposition," *Applied Surface Science*, 315 (2014), 104–109 <doi:10.1016/j.apsusc.2014.07.105>
- Moustaghfir, A., E. Tomasella, S. Ben Amor, M. Jacquet, J. Cellier, and T. Sauvage, "Structural and Optical Studies of ZnO Thin Films Deposited by R.f. Magnetron Sputtering: Influence of Annealing," *Surface and Coatings Technology*, 174-175 (2003), 193–196 <doi:10.1016/S0257-8972(03)00417-1>
- Muralt, Paul, "Recent Progress in Materials Issues for Piezoelectric MEMS," *Journal of the American Ceramic Society*, 91 (2008), 1385–1396 <doi:10.1111/j.1551-2916.2008.02421.x>
- Nagata, T., J. Volk, M. Haemori, Y. Yamashita, H. Yoshikawa, R. Hayakawa, and others, "Schottky Barrier Height Behavior of Pt–Ru Alloy Contacts on Single-Crystal N-ZnO," *Journal of Applied Physics*, 107 (2010), 103714 <doi:10.1063/1.3427562>
- Naik, R S, R Reif, J J Lutsky, and C G Sodini, "Low-Temperature Deposition of Highly Textured Aluminum Nitride by Direct Current Magnetron Sputtering for Applications in Thin-Film Resonators," *Journal of The Electrochemical Society*, 146 (1999), 691–696
- Nair, M.T.S, Laura Guerrero, Olga L Arenas, and P.K Nair, "Chemically Deposited Copper Oxide Thin Films: Structural, Optical and Electrical Characteristics," *Applied Surface Science*, 150 (1999), 143–151 <doi:10.1016/S0169-4332(99)00239-1>
- Nepal, N., K. B. Nam, M. L. Nakarmi, J. Y. Lin, H. X. Jiang, J. M. Zavada, and others, "Optical Properties of the Nitrogen Vacancy in AlN Epilayers," *Applied Physics Letters*, 84 (2004), 1090 <doi:10.1063/1.1648137>
- Ni, X., Y. Fu, Y.T. Moon, N. Biyikli, and H. Morkoç, "Optimization of a-Plane GaN Growth by MOCVD on R-Plane Sapphire," *Journal of Crystal Growth*, 290 (2006), 166–170 <doi:10.1016/j.jcrysgro.2006.01.008>

- Oikawa, Setsuko, Minoru Tsuda, Mutsuo Morishita, Masao MASHITA, and Yasuo Kuniya, "Elementary Process of the Thermal Decomposition of Alkyl Gallium," *Journal of Crystal Growth*, 91 (1988), 471–480
- Oila, J., J. Kivioja, V. Ranki, K. Saarinen, D. C. Look, R. J. Molnar, and others, "Ga Vacancies as Dominant Intrinsic Acceptors in GaN Grown by Hydride Vapor Phase Epitaxy," *Applied Physics Letters*, 82 (2003), 3433 <doi:10.1063/1.1569414>
- Orton, J w, and C T Foxon, "Group III Nitride Semiconductors for Short Wavelength Light-Emitting Devices," *Reports on Progress in Physics*, 61 (1998), 1–75 <http://iopscience.iop.org/0034-4885/61/1/001/>
- Ozgit, Cagla, Inci Donmez, Mustafa Alevli, and Necmi Biyikli, "Atomic Layer Deposition of GaN at Low Temperatures," *Journal of Vacuum Science & Technology A: Vacuum, Surfaces, and Films*, 30 (2012), 01A124 <doi:10.1116/1.3664102>
- , "Self-Limiting Low-Temperature Growth of Crystalline AlN Thin Films by Plasma-Enhanced Atomic Layer Deposition," *Thin Solid Films*, 520 (2012), 2750–2755 <doi:10.1016/j.tsf.2011.11.081>
- Ozgit-Akgun, Cagla, Eda Goldenberg, Ali Kemal Okyay, and Necmi Biyikli, "Hollow Cathode Plasma-Assisted Atomic Layer Deposition of Crystalline AlN, GaN and Al_xGa_{1-x}N Thin Films at Low Temperatures," *Journal of Materials Chemistry C*, 2 (2014), 2123 <doi:10.1039/c3tc32418d>
- Padmaja, P, G.M Anilkumar, P Mukundan, G Aruldhas, and K.G.K Warriar, "Characterisation of Stoichiometric Sol–gel Mullite by Fourier Transform Infrared Spectroscopy," *International Journal of Inorganic Materials*, 3 (2001), 693–698 <doi:10.1016/S1466-6049(01)00189-1>
- Paek, Jong-Sik, Kyoung-Kook Kim, Ji-Myon Lee, Dong-Joon Kim, Min-Su Yi, Do Young Noh, and others, "Nitridation of Sapphire Substrate and Its Effect on the Growth of GaN Layer at Low Temperature," *Journal of Crystal Growth*, 200 (1999), 55–62 <doi:10.1016/S0022-0248(98)01253-6>
- Pang, C. H., P. Hing, and a. See, "Application of Phase-Imaging Tapping-Mode Atomic-Force Microscopy to Investigate the Grain Growth and Surface Morphology of TiSi₂," *Journal of Vacuum Science & Technology B: Microelectronics and Nanometer Structures*, 20 (2002), 1866 <doi:10.1116/1.1501580>
- Park, Minseo, J.-P. Maria, J. J. Cuomo, Y. C. Chang, J. F. Muth, R. M. Kolbas, and others, "X-Ray and Raman Analyses of GaN Produced by Ultrahigh-Rate Magnetron Sputter Epitaxy," *Applied Physics Letters*, 81 (2002), 1797 <doi:10.1063/1.1506781>

- Park, Seoung-Hwan, and Shun-Lien Chuang, "Comparison of Zinc-Blende and Wurtzite GaN Semiconductors with Spontaneous Polarization and Piezoelectric Field Effects," *Journal of Applied Physics*, 87 (2000), 353 <doi:10.1063/1.371915>
- Pearton, S J, B S Kang, Suku Kim, F Ren, B P Gila, C R Abernathy, and others, "GaN-Based Diodes and Transistors for Chemical, Gas, Biological and Pressure Sensing," *Journal of Physics: Condensed Matter*, 16 (2004), R961–R994 <doi:10.1088/0953-8984/16/29/R02>
- Pitzer, K S, and L Brewer, "Mass Spectrometric Study of Ga(CH₃)₃ and Ga(C₂H₅)₃ Decomposition Reaction in H₂ and," *Journal of electrochemistry Society: Solid-State Science and Technology*, 132 (1975), 677–679
- Pobedinskas, P., B. Ruttens, J. D'Haen, and K. Haenen, "Optical Phonon Lifetimes in Sputtered AlN Thin Films," *Applied Physics Letters*, 100 (2012), 191906 <doi:10.1063/1.4711773>
- Polyanskiy, M. N., "Refractive Index Database" <<http://refractiveindex.info>>
- Ponce, F. A., and D. P. Bour, "Nitride-Based Semiconductors for Blue and Green Light-Emitting Devices," *Nature*, 386 (1997), 351–359 <<http://www.nature.com/nature/journal/v386/n6623/abs/386351a0.html>>
- Ponce, F. a., D. P. Bour, W. T. Young, M. Saunders, and J. W. Steeds, "Determination of Lattice Polarity for Growth of GaN Bulk Single Crystals and Epitaxial Layers," *Applied Physics Letters*, 69 (1996), 337 <doi:10.1063/1.118052>
- "Powder Diffraction File 03-065-3409, International Center for Diffraction Data, PDF-2/Release 2007"
- Powell, C. J., and A. Jablonski, *NIST Electron Effective-Attenuation-Length Database - Version 1.3* (Gaithersburg, MD: National Institute of Standards and Technology, 2011)
- Power GaN-2012 Edition*, 2012
- Profijt, H. B., S. E. Potts, M. C. M. van de Sanden, and W. M. M. Kessels, "Plasma-Assisted Atomic Layer Deposition: Basics, Opportunities, and Challenges," *Journal of Vacuum Science & Technology A: Vacuum, Surfaces, and Films*, 29 (2011), 050801 <doi:10.1116/1.3609974>
- Puurunen, Riikka L., "Surface Chemistry of Atomic Layer Deposition: A Case Study for the Trimethylaluminum/water Process," *Journal of Applied Physics*, 97 (2005), 121301 <doi:10.1063/1.1940727>
- Qin, Lifeng, Qingming Chen, Hongbin Cheng, Qian Chen, Jing-Feng Li, and Qing-Ming Wang, "Viscosity Sensor Using ZnO and AlN Thin Film Bulk Acoustic Resonators with Tilted Polar

- c-Axis Orientations,” *Journal of Applied Physics*, 110 (2011), 094511 <doi:10.1063/1.3657781>
- Rabeh, M. Ben, N. Khedmi, M.a. Fodha, and M. Kanzari, “The Effect of Thickness on Optical Band Gap and N-Type Conductivity of CuInS₂ Thin Films Annealed in Air Atmosphere,” *Energy Procedia*, 44 (2014), 52–60 <doi:10.1016/j.egypro.2013.12.009>
- Rahal, Achour, Said Benramache, and Boubaker Benhaoua, “The Effect of the Film Thickness and Doping Content of SnO₂:F Thin Films Prepared by the Ultrasonic Spray Method,” *Journal of Semiconductors*, 34 (2013), 093003 <doi:10.1088/1674-4926/34/9/093003>
- Razeghi, M., and M. Henini, *Optoelectronics Devices: III-Nitrides*, 2005
- Red’kin, a. N., V. I. Tatsii, Z. I. Makovei, a. N. Gruzintsev, and E. E. Yakimov, “Chemical Vapor Deposition of GaN from Gallium and Ammonium Chloride,” *Inorganic Materials*, 40 (2004), 1049–1053 <doi:10.1023/B:INMA.0000046466.62619.e9>
- Reddy, R. Subba, “Effect of Film Thickness on the Structural Morphological and Optical Properties of Nanocrystalline ZnO Films Formed by RF Magnetron Sputtering,” *Advanced Materials Letters*, 3 (2012), 239–245 <doi:10.5185/amlett.2012.3329>
- Rosenberger, Leland, Ronald Baird, Erik McCullen, Gregory Auner, and Gina Shreve, “XPS Analysis of Aluminum Nitride Films Deposited by Plasma Source Molecular Beam Epitax,” *Surface and Interface Analysis*, 40 (2008), 1254–1261
- Roskowski, a.M., P.Q. Miraglia, E.a. Preble, S. Einfeldt, and R.F. Davis, “Surface Instability and Associated Roughness during Conventional and Pendeo-Epitaxial Growth of GaN(0001) Films via MOVPE,” *Journal of Crystal Growth*, 241 (2002), 141–150 <doi:10.1016/S0022-0248(02)00943-0>
- Rothenberger, J.B., D.E. Montenegro, M.a. Prelas, T.K. Ghosh, R.V. Tompson, and S.K. Loyalka, “An Aluminum Nitride-Based Chemical Sensor Using Q-DLTS,” *Diamond and Related Materials*, 23 (2012), 72–75 <doi:10.1016/j.diamond.2012.01.010>
- Rummukainen, M., J. Oila, a. Laakso, K. Saarinen, a. J. Ptak, and T. H. Myers, “Vacancy Defects in O-Doped GaN Grown by Molecular-Beam Epitaxy: The Role of Growth Polarity and Stoichiometry,” *Applied Physics Letters*, 84 (2004), 4887 <doi:10.1063/1.1762984>
- S. J. Pearton, C. R. Abernathy, M. E. Overberg, G. T. Thaler, A. H. Onstine, B. P. Gila, and others, “New Applications Advisable for Gallium Nitride,” *Materials Today*, 5 (2002), 24–31 <doi:10.1016/S1369-7021(02)00636-3>
- Saarinen, K, V Ranki, T Suski, M Bockowski, and I Grzegory, “Vacancies as Compensating Centers in Bulk GaN: Doping Effects,” *Journal of Crystal Growth*, 246 (2002), 281–286 <doi:10.1016/S0022-0248(02)01752-9>

- Sahyoun, Walaa, and Jean-marc Duchamp, "Nonlinearities of AlN in Coupled Resonator Filters for High RF Power Levels," *IEEE TRANSACTIONS ON ULTRASONICS, FERROELECTRICS, AND FREQUENCY CONTROL*, 58 (2011), 2162–2170
- Sakai, Tosikazu, "Hot-Pressing of the AlN-Al₂O₃ System," *Journal of the Ceramic Association of Japan*, 86 (1978), 125–130
- Sanchez-Garcia, M.a., E. Calleja, E. Monroy, F.J. Sanchez, F. Calle, E. Muñoz, and others, "The Effect of the III/V Ratio and Substrate Temperature on the Morphology and Properties of GaN- and AlN-Layers Grown by Molecular Beam Epitaxy on Si(1 1 1)," *Journal of Crystal Growth*, 183 (1998), 23–30 <doi:10.1016/S0022-0248(97)00386-2>
- Särkijärvi, Suvi, Sakari Sintonen, Filip Tuomisto, Markus Bosund, Sami Suihkonen, and Harri Lipsanen, "Effect of Growth Temperature on the Epitaxial Growth of ZnO on GaN by ALD," *Journal of Crystal Growth*, 398 (2014), 18–22 <doi:10.1016/j.jcrysgro.2014.04.006>
- Sayed, Sayed Y, and Jillian M Buriak, "Epitaxial Growth of Nanostructured Gold Films on Germanium via Galvanic Displacement.," *ACS applied materials & interfaces*, 2 (2010), 3515–24 <doi:10.1021/am100698w>
- Scarel, G., S. Ferrari, S. Spiga, C. Wiemer, G. Tallarida, and M. Fanciulli, "Effects of Growth Temperature on the Properties of Atomic Layer Deposition Grown ZrO₂ Films," *Journal of Vacuum Science & Technology A: Vacuum, Surfaces, and Films*, 21 (2003), 1359 <doi:10.1116/1.1564032>
- Schiaber, Ziani S., Douglas M. G. Leite, José R. R. Bortoleto, Paulo N. Lisboa-Filho, and José H. D. da Silva, "Effects of Substrate Temperature, Substrate Orientation, and Energetic Atomic Collisions on the Structure of GaN Films Grown by Reactive Sputtering," *Journal of Applied Physics*, 114 (2013), 183515 <doi:10.1063/1.4828873>
- Schoser, S, G Bräuchle, J Forget, K Kohlhof, T Weber, J Voigt, and others, "XPS Investigation of AlN Formation in Aluminum Alloys Using Plasma Source Ion Implantation," *Surface and Coatings Technology*, 103-104 (1998), 222–226 <doi:10.1016/S0257-8972(98)00397-1>
- Search, Home, Collections Journals, About Contact, My Iopscience, and I P Address, "Group III Nitride Semiconductors for Short Wavelength Light-Emitting Devices," 1
- Shen, L., S. Heikman, B. Moran, R. Coffie, N.-Q. Zhang, D. Buttari, and others, "AlGaIn/AlN/GaN High-Power Microwave HEMT," *IEEE Electron Device Letters*, 22 (2001), 457–459 <doi:10.1109/55.954910>
- Slack, G. A., "Nonmetallic Crystals with High Thermal Conductivity," *Journal of Physics and Chemistry of Solids*, 34 (1973), 321–335

- Steranka, F.M., J. Bhat, D. Collins, L. Cook, M.G. Craford, R. Fletcher, and others, "High Power LEDs - Technology Status and Market Applications," *Physica Status Solidi (a)*, 194 (2002), 380–388 <doi:10.1002/1521-396X(200212)194:2<380::AID-PSSA380>3.0.CO;2-N>
- Strittmatter, A., A. Krost, M. Straßburg, V. Türek, D. Bimberg, J. Bläsing, and others, "Low-Pressure Metal Organic Chemical Vapor Deposition of GaN on silicon(111) Substrates Using an AlAs Nucleation Layer," *Applied Physics Letters*, 74 (1999), 1242 <doi:10.1063/1.123512>
- Stuart, Barbara, *Infrared Spectroscopy: Fundamentals and Application* (Wiley, 2004)
- Stutzmann, M., G. Steinhoff, M. Eickhoff, O. Ambacher, C.E. Nebel, J. Schalwig, and others, "GaN-Based Heterostructures for Sensor Applications," *Diamond and Related Materials*, 11 (2002), 886–891 <doi:10.1016/S0925-9635(02)00026-2>
- Suntola, Tuomo, and Jorma Antson, "Method for Producing Compound Thin Films," 1977 <<http://www.google.com/patents/US4058430>> [accessed 4 November 2014]
- Tabary, P., and C. Servant, "Crystalline and Microstructure Study of the AlN–Al₂O₃ Section in the Al–N–O System. I. Polytypes and Γ -AlON Spinel Phase," *Journal of Applied Crystallography*, 32 (1999), 241–252 <doi:10.1107/S0021889898012485>
- Takikawa, Hirofumi, Keisaku Kimura, Ryuichi Miyano, Tateki Sakakibara, Avi Bendavid, Philip J. Martin, and others, "Effect of Substrate Bias on AlN Thin Film Preparation in Shielded Reactive Vacuum Arc Deposition," *Thin Solid Films*, 386 (2001), 276–280 <doi:10.1016/S0040-6090(00)01673-4>
- Tansley, T. L., and C. P. Foley, "Optical Band Gap of Indium Nitride," *Journal of Applied Physics*, 59 (1986), 3241 <doi:10.1063/1.336906>
- Tendeloo, G. Van, K. T. Faber, and G. Thomas, "Characterization of AlN Ceramics Containing Long-Period Polytypes," *Journal of Materials Science*, 18 (1983), 525–532
- Tian, Ruhai, Oliver Seitz, Meng Li, Wenchuang Walter Hu, Yves J Chabal, and Jinming Gao, "Infrared Characterization of Interfacial Si-O Bond Formation on Silanized Flat SiO₂/Si Surfaces," *Langmuir: the ACS journal of surfaces and colloids*, 26 (2010), 4563–6 <doi:10.1021/la904597c>
- Tolstoy, Valeri P., and Irina V. Chernyshova Valeri A. Skryshevsky, *Handbook of Infrared Spectroscopy of Ultrathin Films* (Wiley-Interscience Publication, 2003)
- Tonisch, K., V. Cimalla, Ch. Foerster, H. Romanus, O. Ambacher, and D. Dontsov, "Piezoelectric Properties of Polycrystalline AlN Thin Films for MEMS Application," *Sensors and Actuators A: Physical*, 132 (2006), 658–663 <doi:10.1016/j.sna.2006.03.001>

- Toth, M, K Fleischer, and M R Phillips, "Direct Experimental Evidence for the Role of Oxygen in the Luminescent Properties of GaN," *Physical Review B*, 59 (2007), 1575–1578
- Tsubouchi, KAZUO, and NOBUO Mikoshiba, "Zero-Temperature-Coefficient SAW Devices on AlN Epitaxial Films," *IEEE Transactions on Sonics and Ultrasonics*, SU-32 (1985), 634–644
- Venkataraj, S., D. Severin, R. Drese, F. Koerfer, and M. Wuttig, "Structural, Optical and Mechanical Properties of Aluminium Nitride Films Prepared by Reactive DC Magnetron Sputtering," *Thin Solid Films*, 502 (2006), 235–239 <doi:10.1016/j.tsf.2005.07.281>
- Vispute, R. D., J. Narayan, Hong Wu, and K. Jagannadham, "Epitaxial Growth of AlN Thin Films on Silicon (111) Substrates by Pulsed Laser Deposition," *Journal of Applied Physics*, 77 (1995), 4724 <doi:10.1063/1.359441>
- Wang, C. C., M. C. Chiu, M. H. Shiao, and F. S. Shieu, "Characterization of AlN Thin Films Prepared by Unbalanced Magnetron Sputtering," *Journal of The Electrochemical Society*, 151 (2004), F252 <doi:10.1149/1.1790531>
- Wang, Jingjing, Da Chen, Yan Xu, Qixin Liu, and Luyin Zhang, "Influence of the Crystal Texture on Raman Spectroscopy of the AlN Films Prepared by Pulse Laser Deposition," *Journal of Spectroscopy*, 2013 (2013), 1–6
- Wang, L., Y. Pu, Y.F. Chen, C.L. Mo, W.Q. Fang, C.B. Xiong, and others, "MOCVD Growth of ZnO Films on Si(111) Substrate Using a Thin AlN Buffer Layer," *Journal of Crystal Growth*, 284 (2005), 459–463 <doi:10.1016/j.jcrysgro.2005.06.058>
- Wang, T., T. Shirahama, H. B. Sun, H. X. Wang, J. Bai, S. Sakai, and others, "Influence of Buffer Layer and Growth Temperature on the Properties of an Undoped GaN Layer Grown on Sapphire Substrate by Metalorganic Chemical Vapor Deposition," *Applied Physics Letters*, 76 (2000), 2220 <doi:10.1063/1.126302>
- Wang, X, and a Yoshikawa, "Molecular Beam Epitaxy Growth of GaN, AlN and InN," *Progress in Crystal Growth and Characterization of Materials*, 48-49 (2004), 42–103 <doi:10.1016/j.pcrysgrow.2005.03.002>
- Watanabe, Naoki, Tsunenobu Kimoto, and Jun Suda, "The Temperature Dependence of the Refractive Indices of GaN and AlN from Room Temperature up to 515 °C," *Journal of Applied Physics*, 104 (2008), 106101 <doi:10.1063/1.3021148>
- Wetzel, C., T. Suski, J. Ager III, E. Weber, E. Haller, S. Fischer, and others, "Pressure Induced Deep Gap State of Oxygen in GaN," *Physical Review Letters*, 78 (1997), 3923–3926 <doi:10.1103/PhysRevLett.78.3923>

- Widmann, F., G. Feuillet, B. Daudin, and J. L. Rouvière, “Low Temperature Sapphire Nitridation: A Clue to Optimize GaN Layers Grown by Molecular Beam Epitaxy,” *Journal of Applied Physics*, 85 (1999), 1550 <doi:10.1063/1.369286>
- Wormington, Matthew, Charles Panaccione, Kevin M. Matney, and D. Keith Bowen, “Characterization of Structures from X-Ray Scattering Data Using Genetic Algorithms,” *Philosophical Transactions of The Royal Society A: Mathematical Physical and Engineering Sciences*, 1999, 2827–2848
- Wu, J., and W. Walukiewicz, “Band Gaps of InN and Group III Nitride Alloys,” *Superlattices and Microstructures*, 34 (2003), 63–75 <doi:10.1016/j.spmi.2004.03.069>
- Wu, X. H., D. Kapolnek, E. J. Tarsa, B. Heying, S. Keller, B. P. Keller, and others, “Nucleation Layer Evolution in Metal-Organic Chemical Vapor Deposition Grown GaN,” *Applied Physics Letters*, 68 (1996), 1371 <doi:10.1063/1.116083>
- Würfl, J, “Reliability Considerations of III-Nitride Microelectronic Devices,” *Microelectronics Reliability*, 39 (1999), 1737–1757 <doi:10.1016/S0026-2714(99)00181-X>
- Xie, Qi, Yu-Long Jiang, Christophe Detavernier, Davy Deduytsche, Roland L. Van Meirhaeghe, Guo-Ping Ru, and others, “Atomic Layer Deposition of TiO₂ from Tetrakis-Dimethyl-Amido Titanium or Ti Isopropoxide Precursors and H₂O,” *Journal of Applied Physics*, 102 (2007), 083521 <doi:10.1063/1.2798384>
- Yadav, Brajesh S., S. S. Major, and R. S. Srinivasa, “Growth and Structure of Sputtered Gallium Nitride Films,” *Journal of Applied Physics*, 102 (2007), 073516 <doi:10.1063/1.2786100>
- Yadav, Brajesh S., Sukhvinder Singh, Tapas Ganguli, Ravi Kumar, S.S. Major, and R.S. Srinivasa, “Highly Oriented GaN Films Grown on ZnO Buffer Layer over Quartz Substrates by Reactive Sputtering of GaAs Target,” *Thin Solid Films*, 517 (2008), 488–493 <doi:10.1016/j.tsf.2008.06.085>
- Yao, Z.Q., Y.Q. Li, J.X. Tang, W.J. Zhang, and S.T. Lee, “Growth and Photoluminescence Studies of AlN Thin Films with Different Orientation Degrees,” *Diamond and Related Materials*, 17 (2008), 1785–1790 <doi:10.1016/j.diamond.2008.02.009>
- Yin, Zongyou, and Xiaohong Tang, “A Review of Energy Bandgap Engineering in III–V Semiconductor Alloys for Mid-Infrared Laser Applications,” *Solid-State Electronics*, 51 (2007), 6–15 <doi:10.1016/j.sse.2006.12.005>
- Yong, Ken-Tye, and Siu Fung Yu, “AlN Nanowires: Synthesis, Physical Properties, and Nanoelectronics Applications,” *Journal of Materials Science*, 47 (2012), 5341–5360 <doi:10.1007/s10853-012-6388-0>

- Youngman, Robert A, and Jonathan H Harris, “Luminescence Studies of Oxygen-Related Defects in Aluminum Nitride,” *Journal of American Ceramic Society*, 46 (1990), 3238–3246
- Yuan, Guangjie, Hideharu Shimizu, Takeshi Momose, and Yukihiro Shimogaki, “Kinetic Study on Hot-Wire-Assisted Atomic Layer Deposition of Nickel Thin Films,” *Journal of Vacuum Science & Technology A: Vacuum, Surfaces, and Films*, 32 (2014), 01A104 <doi:10.1116/1.4829361>
- Yuan, N.Y., S.Y. Wang, C.B. Tan, X.Q. Wang, G.G. Chen, and J.N. Ding, “The Influence of Deposition Temperature on Growth Mode, Optical and Mechanical Properties of ZnO Films Prepared by the ALD Method,” *Journal of Crystal Growth*, 366 (2013), 43–46 <doi:10.1016/j.jcrysgr.2012.12.024>
- Zhang, Yongheng, “Characterization of as-Received Hydrophobic Treated AlN Powder Using XPS,” *Journal of Materials Science Letters*, 21 (2002), 1603–1605
- Zhao, Jianqing, and Ying Wang, “Ultrathin Surface Coatings for Improved Electrochemical Performance of Lithium Ion Battery Electrodes at Elevated Temperature,” *The Journal of Physical Chemistry C*, 116 (2012), 11867–11876 <doi:10.1021/jp3010629>
- Zolper, J, “A Review of Junction Field Effect Transistors for High-Temperature and High-Power Electronics,” *Solid-State Electronics*, 42 (1998), 2153–2156 <doi:10.1016/S0038-1101(98)00210-X>